TAMPERE UNIVERSITY OF TECHNOLOGY

MIKKO MÄENPÄÄ

BLIND DETECTION OF INTERFERING CELL DATA CHANNEL POWER LEVEL IN 3GPP LTE/LTE-A DOWNLINK

Master of Science Thesis

Examiner:
Prof. Mikko Valkama
Instructor:
D.Sc. Tero Ihalainen
Examiners and topic approved by the Faculty Council meeting of Computing and Electrical Engineering on 12th of August 2015

TIIVISTELMÄ

TAMPEREEN TEKNILLINEN YLIOPISTO
Sähkötekniikan koulutusohjelma
MÄENPÄÄ, MIKKO: Häiritsevän solun datakanavan tehotason sokea estimointi 3GPP LTE/LTE-Advanced järjestelmän alalinkissä.
Diplomityö, 92 sivua
Toukokuu 2016
Pääaine: Langaton Tietoliikenne
Tarkastaja: Prof. Mikko Valkama
Ohjaaja: TkT Tero Ihalainen
Avainsanat LTE, LTE-Advanced, linkkitason simulaattori, häiriön vaimentaminen, naapurisolun häiriö, epälineaarinen vastaanotin, sokea estimointi, SLIC

Matkapuhelinverkkojen käytön ja siirretyn datan määrä jatkavat vahvasti kasvuaan. Syitä tähän ovat muun muassa uusien mobiililaitteiden ja -palveluiden suosion kasvu sekä se, että matkapuhelinverkkoja on alettu käyttää kiinteän laajakaistan tavoin pääasiallisena internetyhteytenä. Uusia teknologioita tarvitaan, jotta nämä kasvavat tarpeet kapasiteetille ja vasteajoille saadaan tyydytettyä. Long Term Evolution (LTE) ja LTE-Advanced ovat teknologioita, jotka Third Generation Partnership Project (3GPP) on kehittänyt ja standardoinut, koska niillä on potentiaalia täyttää tulevaisuuden matkapuhelinverkkojen kapasiteettivaatimukset.

LTE/LTE-Advanced mobiiliverkko on tyypillisesti häiriörajoitteinen, koska naapurisolut käyttävät samaa taajuusaluetta tiedonsiirtoon. Tästä syystä useat käyttäjät voivat kärsiä korkeasta häiriötasosta ja näin ollen ne eivät voi saavuttaa korkeita tiedonsiirtonopeuksia ilman vastatoimia. Siksi 3GPP tutkii kehittyneitä tekniikoita, joilla häiriötä voidaan hallita, tukahduttaa tai poistaa.

3GPP tutkii muun muassa verkkoavustettuja häiriön tukahduttamis- ja poistotekniikoita (Network Assisted Interference Cancellation and Suppression, NAICS). Yksi näistä tutkimuksista liittyy niin kutsuttuun häiritsevän solun parametrien sokeaan estimointiin mobiililaitteessa. Häiritsevän solun parametreja tarvitaan kehittyneissä epälineaarisissa vastaanottimissa, joilla on potentiaalia tukahduttaa tai poistaa häiriötä merkittävästi. Nämä parametrit pitää joko signaloida mobiililaitteelle tai vaihtoehtoisesti niitä voidaan sokeasti estimoida mobiililaitteessa suoraan vastaanotetusta häiriötä sisältävästä signaalista.

Tässä diplomityössä tutkitaan häiritsevän solun datakanavan tehotason sokean estimaattorin käyttökelpoisuutta. Epälineaariset vastaanottimet tarvitsevat tätä parametria toimiakseen tehokkaasti. Tutkimus suoritetaan linkkitasolla numeerisilla simulaatioilla, joissa mallinnetaan yksityiskohtaisesti lähettimen ja vastaanottimen signaalinkäsittelyalgoritmeja sekä radiokanavan aiheuttamia vääristymiä.

Tutkimuksen kohteena on Symbol Level Interference Cancellation -vastaanotin (SLIC), johon lisätään häiritsevän solun datakanavan tehotason sokea estimaattori. Tämän vastaanottimen suorituskykyä verrataan SLIC vastaanottimeen, jossa kaikki tarvittavat parametrit ovat tunnettuja ja näin ollen sitä voidaan pitää suorituskyvyn ylärajana. Suorituskyvyn alarajana toimii Linear Minimum Mean Squared Error - Interference Rejection Combiner -vastaanotin (LMMSE-IRC). Simulaatiotuloksien perusteella voidaan todeta, että tässä diplomityössä käytetyn sokean estimaattorin suorituskyky on hyvä. Näin ollen sillä voidaan helpottaa verkkoa kuormittavaa signalointia.

ABSTRACT

TAMPERE UNIVERSITY OF TECHNOLOGY
Master's Degree Programme in Electrical Engineering
MÄENPÄÄ, MIKKO: Blind detection of interfering cell data channel power level in 3GPP LTE/LTE-Advanced downlink
Master of Science Thesis, 92 pages
May 2016
Major: Wireless Communications
Examiner: Prof. Mikko Valkama
Instructor: D.Sc. Tero Ihalainen
Keywords: LTE, LTE-Advanced, link level simulation, interference cancellation, inter-cell interference, non-linear receiver, blind detection, SLIC

Nowadays wireless cellular networks can be seen as ubiquitous systems used by a majority of the world's population and their usage continues to grow in the future. Continuously higher data rates and shorter latencies are required due to the introduction of new mobile devices and services. In addition, mobile networks are more and more used as a primary connectivity solution in several places. Thus, new technologies are required to improve the capacity and latency of mobile networks. Long Term Evolution (LTE) and LTE-Advanced are technologies standardized by Third Generation Partnership Project (3GPP) with the potential to fulfill these requirements for future mobile networks.

LTE/LTE-Advanced cellular networks are usually interference limited, because neighbouring cells use the same frequency band for data transmission. Because of this, several users may experience high interference levels and thus cannot achieve high data rates without proper counteractions. Consequently, advanced techniques to control, suppress or cancel the interference are of interest to be studied for LTE and LTE-Advanced by 3GPP.

Network Assisted Interference Cancellation and Suppression (NAICS) techniques are currently been studied by 3GPP. One of the recent studies on NAICS is so called blind detection of interfering cell parameters in a user equipment for advanced non-linear receivers. Such receivers have the capability to suppress or cancel interference significantly but they require the knowledge of specific parameters of the interfering cell to perform efficiently. These parameters have to be either signaled by the network or blindly detected from the received signal in user equipment.

The topic of this thesis is to study the feasibility of blind detection of interfering cell's data channel power level, which is crucial knowledge to non-linear receivers. The study is performed at radio link level by using numerical simulations, in which the transmitter and receiver processing are modeled in detail. In addition, also the effects caused by the radio channel to the transmitted signals are modeled.

The performance of one non-linear receiver, namely Symbol Level Interference Cancellation (SLIC) receiver, with blind detection is compared to the performance of SLIC receiver which has the knowledge of all required parameters. While Linear Minimum Mean Squared Error - Interference Rejection Combiner (LMMSE-IRC) receiver operates as the baseline. From the simulation results it can be seen that the blind detector performs well. Consequently this blind detector can be one noteworthy option to avoid signaling of interfering cell's data channel power level.

PREFACE

This thesis has been carried out as a part of a larger cooperation activity with Nokia Networks. I have been developing LTE/LTE-Advanced link level simulator as a consultant for Nokia Networks in Tampere site and the topic of this thesis stems from one of the algorithms I developed in the simulator. As I have done also full-time work and carrying out studies during the writing of the thesis, the whole process has been quite stressful, but educational.

I would like to thank my friends, family and co-workers for the support while doing this thesis. Special thanks go also to Prof. Mikko Valkama from Tampere University of Technology, D.Sc. Tero Ihalainen and D.Sc. Mihai Enescu from Nokia Networks for their valuable comments during the process of writing the thesis. I would also like to extend my gratitude to D.Sc. Toni Huovinen from Magister Solutions for his helpful comments.

Contents

ABBREVIATIONS

AWGN	Additive White Gaussian Noise
CFI	Control Format Indicator
CP	Cyclic Prefix
CQI	Channel Quality Indicator
CRS	Cell-specific Reference Signal
CRS-IC	CRS Interference Cancellation
CSI	Channel-State Information
DIP	Dominant Interferer Proportion
EDGE	Echanced Data Rates for GSM Evolution
eNB	Basestation, eNodeB
EPRE	Energy Per Resource Element
FDD	Frequency Division Duplexing
FFD	Fast Fading Drop
FFT/IFFT	Fast Fourier Transform / Inverse FFT
GPRS	General Packet Radio Service
GSM	Global System for Mobile Communications
HSPA	High-Speed Packet Access
INR	Interference-to-Noise Ratio
IRC	Interference Rejection Combiner
ISI	Inter Symbol Interference
ITU	International Telecommunication Union
LMMSE	Linear Minimum Mean Square Error
LLR	Log-likelihood-ratio
LTE	Long Term Evolution
MBSFN	Multicast-broadcast single-frequency network
MCS	Modulation and Coding Scheme
MIMO	Multiple-Input and Multiple-Output
MRC	Maximum Ratio Combiner

MUST	Multiuser Superposition Transmission
NAICS	Network Assisted Interference Cancellation and Suppression
NOMA	Non-Orthogonal Multiple Access
OFDM	Orthogonal Frequency Division Multiplexing
OFDMA	Orthogonal Frequency Division Multiple Access
PDP	Power Delay Profile
PBCH	Physical Broadcast Channel
PCFICH	Physical Control Format Indicator Channel
PDCCH	Physical Downlink Control Channel
PDSCH	Physical Downlink Shared Channel, data channel
PHICH	Physical Hybrid-ARQ Indicator Channel
PMI	Precoder Matrix Indicator
PRB	Physical Resource Block
RAN	Radio Access Networks
RE	Resource Element
RF	Radio Frequency
RI	Rank Indicator
RS	Reference Signal
SLIC	Symbol Level Interference Cancellation
SINR	Signal-to-Interference-plus-Noise Ratio
SNR	Signal-to-Noise Ratio
TDD	Time Division Duplexing
TM	Transmission Mode
TP	Throughput
UE	User Equipment, Mobile Device
VoIP	Voice over Internet Protocol
WCDMA	Wideband Code Division Multiple Access
WG	Work Group
ZF	Zero-Forcing

2G	2nd Generation
3G	3rd Generation
3GPP	3rd Generation Partnership Project
4G	4th Generation

SYMBOLS

$\mathbf{B}$	Precoding matrix
$\mathbf{C_y}$	Covariance matrix of the received signal $\mathbf{y}$
$\mathbf{C}_\mathbf{y}^{(\mathrm{s})}$	Covariance matrix of the received signal $\mathbf{y}$ used for demodulation of desired signal
$\mathbf{C}_\mathbf{y}^{(\mathrm{d})}$	Covariance matrix of the received signal $\mathbf{y}$ used for demodulation of dominant interfering signal
$\mathbf{C_{ys}}$	Covariance of the received signal $\mathbf{y}$ and the original data symbol vector $\mathbf{s}$
$e(f,t)$	Raw estimate of interference plus noise variance at subcarrier f in OFDM symbol t.
$\triangle f$	Subcarrier spacing, i.e., the frequency separation between subcarriers
f_s	Sampling rate
$\hat{\mathbf{h}}_{\mathrm{raw}}$	Raw channel estimates, i.e., the measurements taken from pilot positions
$\hat{\mathbf{h}}$	Channel estimate vector generated by Wiener filter
$\mathbf{H}$	Physical channel matrix
$\mathbf{H}_{\mathrm{eff}}$	Effective channel matrix
$\mathbf{i}$	Transmitted interfering signal
$IoNo_{\mathrm{est}}$	Interference plus noise power estimate
$\mathbf{n}$	Noise vector
N_{c}	Number of active subcarriers
N_{l}	Number of layers
N_{t}	Number of transmit antennas
N_{r}	Number of receive antennas
$N_{r,idx}$	Receive antenna index
P_a	Parameter needed for defining the data to CRS power ratio
P_b	Parameter needed for defining an additional power level offset in OFDM symbols where CRS are present
P_d	Power of the dominant interferer
P_w	Power of the weaker interferer
$\mathbf{Q}$	Linear channel estimation matrix

$\mathbf{r}$	Total interference plus noise
$\mathbf{R_r}$	Interference plus noise covariance
$\mathbf{R}_{\mathbf{r}}^{(\mathbf{s})}$	Interference plus noise covariance estimate for the serving cell
$\mathbf{R}_{\mathbf{r}}^{(\mathrm{d})}$	Interference plus noise covariance estimate for the dominant interferer
$\mathbf{R}_{\hat{\mathrm{h}}_{\mathrm{raw}}\mathrm{h}}$	Cross-correlation matrix between raw channel estimate and the channel
$\mathbf{R}_{\mathrm{h}}$	Auto-correlation matrix of the channel
$\tilde{\mathbf{R}}(\rho_{a,n}^{(\mathrm{d})})$	Covariance matrix hypothesis of the reconstructed (or emulated) received signal for the case of using n-th $\rho_{\mathrm{a}}^{(\mathrm{d})}$ candidate
$\mathbf{s}$	Transmitted signal vector
$\mathbf{S}$	$r \times c$ rectangular matrix containing singular values
S	Number of streams
T_u	Subcarrier symbol period.
$\mathbf{U}$	$r \times r$ unitary matrix containing left-singular vectors
$\mathbf{V}$	$c \times c$ unitary matrix containing right-singular vectors
w	Receive filter tap
$\mathbf{W}$	Receive filter
$\mathbf{W}_{\mathrm{d}}$	Receive filter for the dominant interfering signal (from dominant interfering cell)
$\mathbf{W}_{\mathrm{s}}$	Receive filter for the desired signal (from serving cell)
$\mathbf{y}$	Received signal vector
$\mathbf{z}$	Residual interference plus noise, i.e., interference from the weaker interferer plus noise.
σ_{IoNo}	Interference plus noise variance
σ_{No}	Noise variance
$\sigma_{\mathbf{s}_{\mathrm{s}}}$	Variance of signal $\mathbf{s}_{\mathrm{s}}$
ρ_a	PDSCH to CRS power ratio in OFDM symbols where CRS are *not* present
ρ_b	PDSCH to CRS power ratio in OFDM symbols where CRS are present
$(.)_{\mathrm{s}}$	Denotes a symbol of serving cell
$(.)_{\mathrm{d}}$	Denotes a symbol of dominant interferer
$(.)_{\mathrm{w}}$	Denotes a symbol of weaker interferer

1 Introduction

Wireless cellular networks have evolved from being an expensive technology for a few selected individuals to today's ubiquitous systems used by a majority of the world's population. Nowadays there are more cellular subscribers than main telephone lines and thus it can be said that mobile communications is an everyday commodity [6]. Reasons for this are the introduction of new mobile devices such as smart phones and tablets, services such as video and music streaming as well as the fact that nowadays wireless cellular networks are also used as primary connectivity solution in several places. Current mobile-communication systems are very complex compared to their predecessors like analog mobile systems of the 1980s. These first mobile systems targeted "low-bandwidth" services such as voice whereas current mobile systems use relatively wide bandwidth in order to provide increasingly faster data services over the mobile-communication networks. However, the frequency bandwidth is a scarce resource and an expensive investment for the operators. This is one reason why the given bandwidth is tried to be utilized as efficiently as possible and why the research of mobile networks is ongoing.

1.1 Evolution of wireless cellular networks

People often classify mobile communication technologies as belonging to one of several generations. The first generation of mobile radio systems was analog and it was designed for voice-only communications. In the 90's 1G mobile systems were replaced by the digital 2G mobile systems, where the transmitted voice is compressed digitally and ciphered, giving better system capacity. The most notable 2G technology is *Global System for Mobile Communications* (GSM), which is designed mainly for the voice traffic. In order to support packet data services in a GSM network, extensions to the GSM standard have been developed. These extensions are named *General Packet Radio Service* (GPRS) and *Enhanced Data Rates for GSM Evolution* (EDGE), which allow better utilization of the GSM radio resource for data transmission. EDGE is often being labeled as 2.5G. [2]

The standards of the third generation mobile systems (3G) were completed at the beginning of the 2000s, and practically this meant that the cellular systems became real multiservice networks. 3G has been developed with more focus on the data transmission and it utilizes the new radio access scheme *Wideband Code Division Multiple Access* (WCDMA). This scheme allows wider system bandwidths and thus higher data throughput. An extension has been developed for WCDMA, called *High-Speed Packet Access* (HSPA), which is often called 3.5G. It is good to point out that the further development of HSPA is still ongoing and it is done parallel with the development of *Long Term Evolution* (LTE). [2]

LTE introduces a new radio access scheme based on *Orthogonal Frequency Division Multiplexing* (OFDM), which allows LTE technology to provide wider mobile broadband data connections as well as higher-speed internet access to the subscribers compared to WCDMA [2]. Therefore LTE technology is used nowadays by the majority of the network operators worldwide. The LTE technology is highly complex as it utilizes, among other things, advanced procedures on top of those that are existing in WCDMA or HSPA. One remarkable note in LTE technology compared to it's predecessors is the fact that LTE

does not support circuit-switched operation which means that normal phone calls need to be implemented via *Voice over Internet Protocol* (VoIP) [2]. Secondly, LTE and LTE-Advanced are techniques in which serving and neighbouring basestations are using the same frequency bands for transmission and thus they are interference limited.

LTE is standardized by the *3rd Generation Partnership Project* (3GPP). LTE technology is often misleadingly called 4G although it still belongs to the 3G-family because it does not meet the 4G-requirements set by *International Telecommunication Union* (ITU) [27]. LTE corresponds to the first release of LTE (release 8) and it is labeled as 3.9G. LTE release 10 and onwards, also referred to as *LTE-Advanced,* is the true 4G evolution step. The new LTE-Advanced -specific features concern mostly multi-antenna transmission and carrier aggregation [2]. Thus it is good to point out that LTE and LTE-Advanced are building on the same technology and the label "Advanced" highlights the release 10 of LTE. It is also good to bear in mind that LTE-Advanced is not in any way the final evolution step to be taken for LTE. An obvious example about this is actually the topic of this thesis, which is related to advanced interference cancellation and suppression studies which in turn are part of the release 12 of LTE [15].

1.2 Objectives and scope of the thesis

In this thesis, the downlink physical layer aspects of LTE and LTE-Advanced systems are studied. To be more exact, so called single-link-with-interference model is considered, meaning that only a single mobile terminal (or user equipment, UE) is connected to a single basestation and the mobile terminal utilizes the whole given bandwidth. Also interfering cells are modeled, meaning that also baseband time-domain waveform of interfering cells is truly generated similarly to serving cell and added to the overall received signal with predefined interference-to-noise-ratio (INR).

Using OFDM in the downlink transmission offers new possibilities of fine-tuning the transmission parameters. The ultimate goal is to adapt the parameters in a way that is most beneficial to the link performance in specific reference conditions. Secondly, as already mentioned, basestations utilizing LTE and LTE-Advanced technology are interference limited. Thus high data rates cannot be supported for users having high interference level without any counteractions. Consequently, techniques to control, suppress or cancel interference are of interest for LTE and LTE-Advanced.

The study, which is performed in this thesis, stems from the 3GPP standardization work on NAICS (Network Assisted Interference Cancellation and Suppression) at link-level, i.e., Radio Access Networks Work Group 4 (RAN WG4, RAN4). More detailed description about the 3GPP NAICS work item (WI) can be found in [15]. RAN4 defines performance requirements of diverse radio frequency (RF) system scenarios. Once these requirements are set, the group defines the test procedures that will be used to verify them. More detailed information about the scope of RAN4 can be found from [7].

Recent studies on NAICS is blind detection of interfering cell parameters for non-linear receivers, such as Symbol Level Interference Cancellation (SLIC), Reduced complexity Maximum Likelihood (R-ML) and Code Word Interference Cancellation (CWIC). In this thesis, only SLIC receiver is considered. SLIC receiver is a successive interference cancellation receiver which operates by successively applying linear detection, reconstruction and cancellation of interferer(s) signal at symbol level. Thus, the performance of the SLIC receiver is depending on how good estimate of the interfering signal can be reconstructed. More detailed description of SLIC receiver is provided in Section 3.5. In

order to reconstruct the interfering signal, SLIC needs the knowledge of specific parameters of the interfering cell. In this distinct RAN4 NAICS study, the goal is to answer to the following: which interfering cell transmission parameters need to be dynamically signaled and which could be blindly detected in NAICS UE. The goal is also to study if it is sufficient to signal only some restrictions and/or subsets instead of dynamic parameter signaling in order to help blind detectors to perform more efficiently.

The focus and objective of this thesis is to study feasibility of blind P_a detector in NAICS UE. P_a is a parameter which is signaled from higher layers by its serving base station and which defines the power level of downlink data channel, namely Physical Downlink Shared Channel (PDSCH). More detailed description of downlink power control and P_a is given is Section 2.8. The goal is to study whether is it possible to blindly detect interfering cell's P_a parameter in NAICS UE without significant loss in performance or would it be better to signal its P_a dynamically by network assistance. Also parameters, which affect to P_a detection performance, needs to be optimized. Such parameters are, for instance, bandwidth used for detection, and the set of possible P_a values used for quantization. Also interfering cell's modulation may have an impact on P_a detection performance.

1.3 Structure of the thesis

In Chapter 2, the basic physical layer structure of LTE/LTE-Advanced downlink is introduced. System model, signal model, Cell-specific reference Signal (CRS) based channel estimation, network assisted covariance estimation as well as receiver types, including the SLIC receiver, are described in Chapter 3. Then research methods are introduced in Chapter 4, including single-link principles and simulation assumptions. In Chapter 5, blind detection of interfering cell data channel power level is examined in detail, including sensitivity of SLIC receiver on incorrect power level assumptions and parameters that have an impact on blind P_a detector performance. Simulation results in terms of throughput are given in Chapter 6 and finally conclusions are drawn in Chapter 7.

2 Physical Layer of LTE/LTE-Advanced Downlink

In this chapter, a basic understanding of LTE/LTE-Advanced downlink is given. LTE/LTE-Advanced is a complex system, utilizing several more or less complex methods to achieve continuously higher data rates. Therefore, the purpose of this chapter is to introduce only those physical layer aspects, which are essential for this thesis. LTE/LTE-Advanced systems are based on OFDM, where resources are divided in frequency and time. More detailed description of OFDM is given in the next section. After describing the basic elements of LTE/LTE-Advanced, frame structure, physical resources and physical channels are introduced. Then reference signals, feedback methods and Multiple-Input and Multiple-Output (MIMO) system are examined. Finally, in the last section of this chapter, the downlink power allocation is explained in detail as it provides essential information in order to acquire better insight about the topic and the goal of this thesis.

2.1 Orthogonal Frequency Division Multiplexing

In this section, an overview of an OFDM system is given. It is essential to acquire a basic understanding of the OFDM system because it is utilized in the LTE downlink. Channel estimation methods as well as equalization methods are investigated from the OFDM system point of view. OFDM is a modulation scheme that suits for high-data-rate transmission in delay-dispersive environments [14], that is, in frequency selective channels.

OFDM transmission can be seen as a kind of multi-carrier transmission but it uses typically very large number of relatively narrow frequency bands, that is, subcarriers. In other words, it converts a high-rate data stream into low-rate streams that are transmitted in parallel over narrowband channels. Frequencies of subcarriers have to be chosen so that the subcarriers will be orthogonal. Orthogonal subcarriers are permitted to have overlapping spectra and thus it is possible to achieve higher spectral efficiency compared to conventional multi-carrier transmission [2]. The frequency separation, $\triangle f$, between subcarriers, i.e., subcarrier spacing is $\triangle f = 1/T_u$, where T_u is the subcarrier symbol period. Thus the subcarrier spacing is equal to the subcarrier modulation rate $1/T_u$[1]. OFDM system uses simple rectangular pulse shaping which is illustrated in Figure 1.

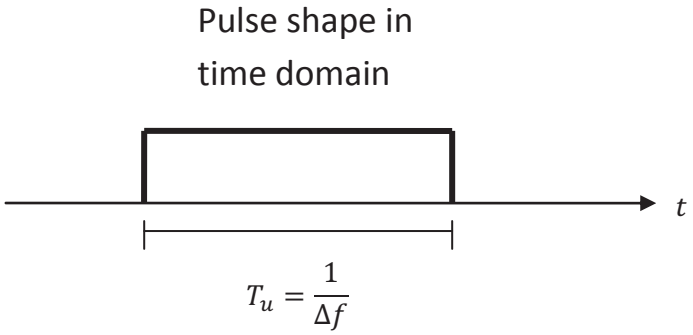

Figure 1: *Pulse shape of one subcarrier in time domain.*

Time domain rectangular pulse shape corresponds to a sinc function in the frequency domain, which can be seen in Figure 2. It can also be seen that although the spectrum is

[1]However, this ignores a possible cyclic prefix, which is described in the following subsection

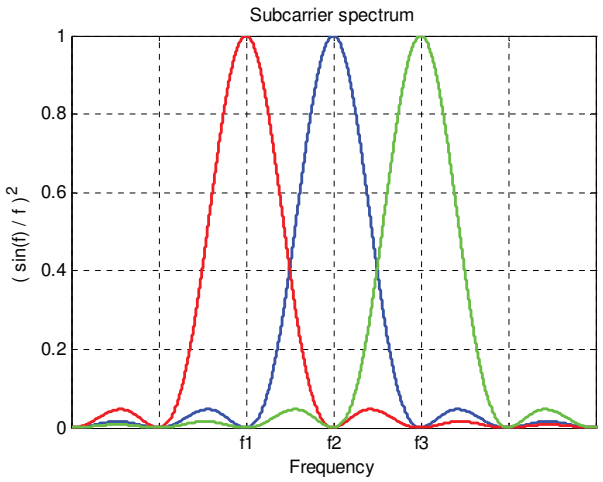

Figure 2: *OFDM subcarrier spacing in frequency domain. Orthogonality in an OFDM system occurs when at the peak of each subcarrier spectrum, the contribution from all other subcarriers is zero* [1, p. 5].

overlapping, it does not cause inter carrier interference at carrier locations due to orthogonal subcarriers.

In theory, a bank of modulators/correlators could be used for OFDM modulation and demodulation, that is, assigning an oscillator for each subcarrier, but this type of implementation is impractical as there can be even thousands of subcarriers. Practical low-complexity implementations use computationally efficient *Fast Fourier Transform* (FFT) processing. With this approach, data symbols are mapped to the input bins of an *Inverse Fast Fourier Transform* (IFFT) processing block which transforms the frequency domain symbols into one time domain OFDM symbol as illustrated in Figure 3.

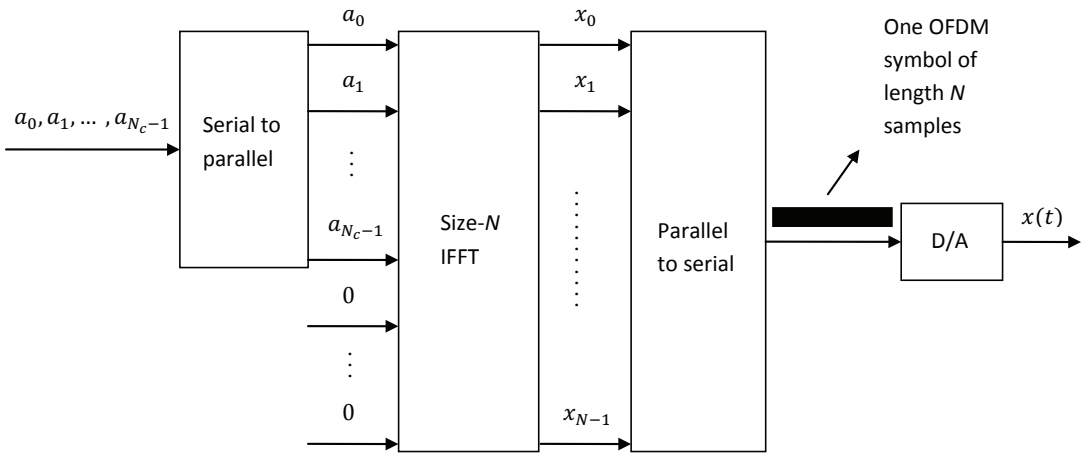

Figure 3: *Generation of the OFDM baseband waveform using IFFT processing. N_c denotes the number of data symbols or active subcarriers. Insertion of cyclic-prefix is ignored, but it will be described in the following subsection.*

In more detail, if $\triangle f$ is assumed to be the subcarrier spacing, the sampling rate f_s is a multiple of subcarrier spacing, that is, $f_s = N \times \triangle f$. Now N_c denotes the number of active subcarriers or data symbols so the nominal bandwidth of the OFDM signal can be seen as $N_c \times \triangle f$. Consequently, N should exceed N_c with a sufficient margin so that

Table 1: *Supported spectrum allocations and corresponding number of active subcarriers and FFT sizes in LTE/LTE-Advanced [28].*

Spectrum allocation (MHz)	**1.25**	**2.5**	**5**	**10**	**15**	**20**
FFT size, N	128	256	512	1024	1536	2048
Active subcarriers, N_c	75	150	300	600	900	1200
Sampling frequency, f_s (MHz)	1.92	3.84	7.68	15.36	23.04	30.72

the sampling theorem is fulfilled. If Figure 3 is considered, it can be seen that N_c data symbols are mapped to the input bins of an IFFT processing block and the rest $N - N_c$ bins are extended with zeros. The N output samples are parallel-to-serial converted and thus forming one OFDM symbol of length N samples. Then digital-to-analog conversion is carried out and a continuous time domain signal $x(t)$ is obtained. It should be noted that the selected IFFT-size, N, should equal to 2^n for some integer n in order to use IFFT/FFT processing.

As an example, if 10 MHz spectrum allocation is considered in the LTE system, the number of active subcarriers N_c is 600 and the IFFT size N should be chosen so that the sampling theorem is fulfilled and hence N = 1024 is suitable. This corresponds to a sampling rate $f_s = N \times \triangle f$ = 15.36 MHz, where $\triangle f$ = 15 kHz, i.e., the subcarrier spacing in LTE [2, p. 31]. Supported spectrum allocations and corresponding numbers of active subcarriers and FFT sizes in LTE/LTE-Advanced are shown in Table 1.

FFT processing can be also used for OFDM demodulation similarly to OFDM modulation. The demodulator samples the received signal with the sampling rate of $f_s = N \times \triangle f$, followed by a size-$N$ FFT. Outputs from unused FFT-bins[2] are discarded and the rest N_c data symbols are converted from parallel to serial and forwarded to further processing.

Cyclic prefix

In the case of a time dispersive channel, the orthogonality between the subcarriers will be lost without any countermeasures, at least to some extent. The reason for this is that the receiver sees multiple replicas of the transmitted signal due to multi-path propagation in the radio channel. Each of these replicas have some attenuation and delay. Time domain OFDM symbols are transmitted consecutively so some multi-path components of the previous symbol may be still received while the next symbol arrives. This overlapping of OFDM symbols is called inter-symbol interference (ISI) and is illustrated in Figure 4.

[2] i.e. those bins that were extended with zeros in the modulator

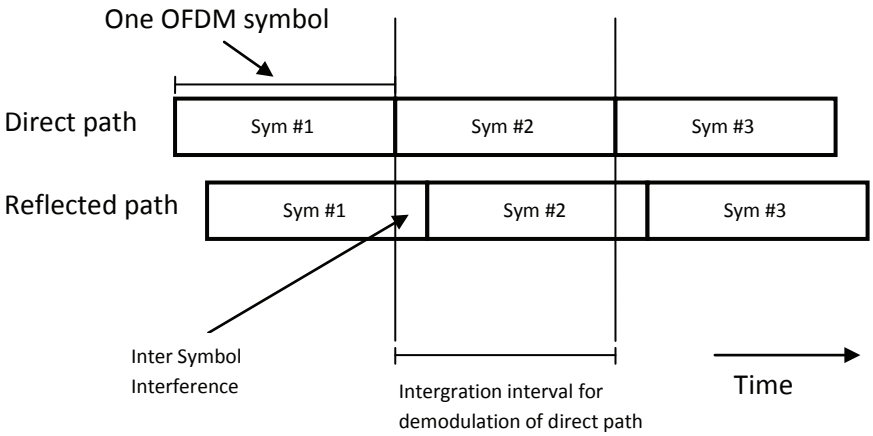

Figure 4: *Illustration of inter symbol interference in multi-path propagation environment.*

To deal with ISI and to make the OFDM signal truly insensitive to time dispersion, a so called *cyclic-prefix* (CP) is used in OFDM transmission. Cyclic-prefix insertion implies that the last part of the OFDM symbol is copied and inserted at the beginning of the OFDM symbol. To be more exact, this process is explained by the fact that an OFDM symbol is formed by sinusoidal basis functions, of which there are one for each subcarrier. Thus one OFDM symbol contains complete cycles of every sinusoid. Now that the last part of the OFDM symbol is copied and inserted at the beginning, the phases of the sinusoids match and the OFDM symbol is cyclically extended. [1, p. 6.]

In practice, cyclic-prefix insertion is implemented as follows. The last N_{CP} samples of the IFFT output block of length N are copied and inserted at the beginning of the block. This increases the block length from N to $N + N_{CP}$ and consequently it increases the relative overhead. At the receiver side, the corresponding samples are discarded before the demodulation, i.e., before the FFT processing. Cyclic-prefix insertion as well as a baseband-equivalent model of OFDM transmission and reception are shown in Figure 5.

The length of the cyclic-prefix should be at least as long as the significant part of the impulse response experienced by the transmitted signal. In other words, the length of the CP is suitable as long as the time span of the time dispersion does not exceed the length of the CP [14]. If we now assume that the cyclic-prefix is inserted into every OFDM symbol and it's length is appropriate, ISI can be avoided as the cyclic-prefix acts as a safe zone between consecutive OFDM symbols. An example of a reception in multi-path propagation environment with the use of the cyclic-prefix is illustrated in Figure 6.

The advantages of the cyclic-prefix are not without a cost. The drawback is that a part of the total transmission time and power is wasted on sending redundant information, implying a corresponding rate loss in the OFDM demodulator. In general, there is a trade-off between the rate loss due to the cyclic-prefix and the ISI due to time dispersion that is not covered by the cyclic-prefix.

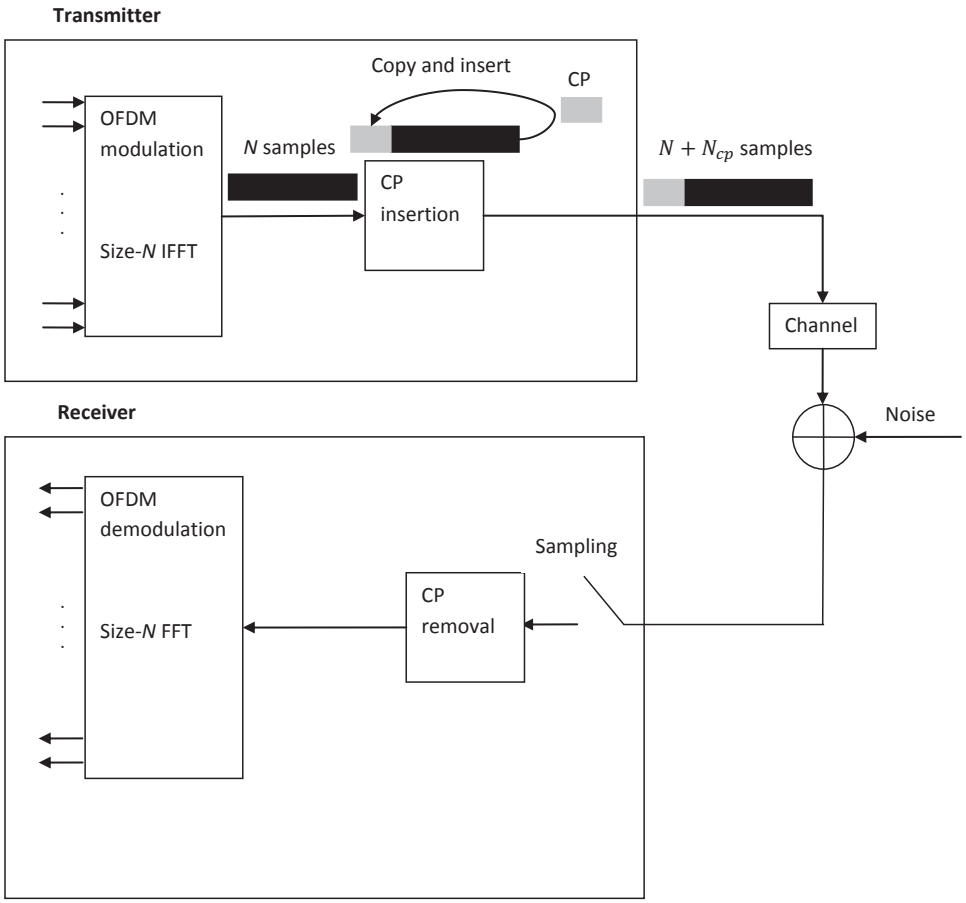

Figure 5: *Baseband-equivalent model of OFDM transmission and reception in time domain. Also cyclic-prefix insertion is shown.*

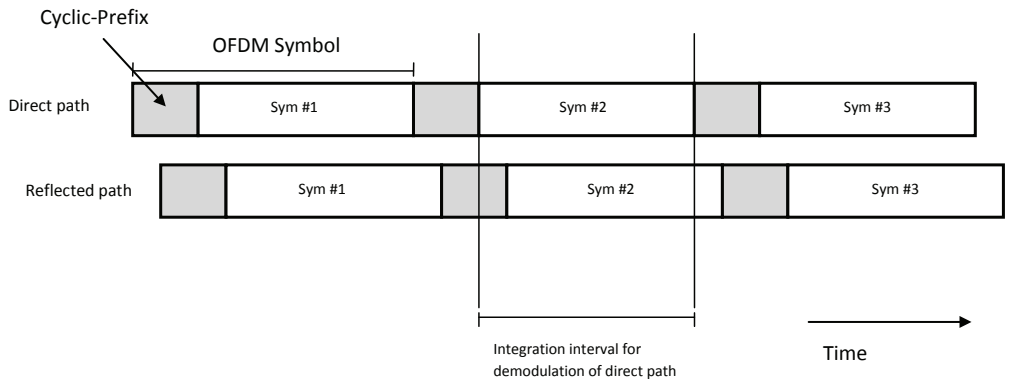

Figure 6: *Cyclic-prefix acts as a safe zone between consecutive OFDM symbols and thus prevents ISI.*

Frequency domain model of OFDM transmission

If the cyclic-prefix can be assumed to be long enough to prevent ISI, the OFDM system can handle multi-path propagation with fairly simple receiver design. In this case, the radio channel can be modeled as a simple frequency domain channel which means that the channel response of each subcarrier can be modeled by a single complex-valued scalar.

This single complex-valued scalar denotes an attenuation and a phase distortion caused by the channel to one subcarrier. Consequently algorithms, e.g., for channel estimation and equalization can be implemented more simply, i.e., the channel estimator needs to find only one complex channel coefficient for each subcarrier and the effects caused by the channel to each subcarrier can be compensated by a so called one-tap equalizer. One-tap equalization principle is illustrated in Figure 7, where only one transmit antenna and receive antenna is considered for convenience[3]. The transmitted symbol s_k[4] is scaled and phase rotated by the complex frequency-domain channel tap h_k and impaired by noise n_k. To properly compensate the effects caused by the channel to the transmitted symbol s_k, the receiver should multiply the received symbol y_k by one filter tap w_k to obtain an estimate $\hat{s}$ from the transmitted symbol:

$$\hat{s} = w_k y_k, \tag{2.1}$$

where

$$y_k = h_k s_k + n_k. \tag{2.2}$$

The filter tap w_k depends on the equalization method. Different equalization methods are described in Section 3.5. After this one-tap equalization, the estimate $\hat{s}_k$ can be forwarded to further processing, for example, to data demodulation and channel decoding.

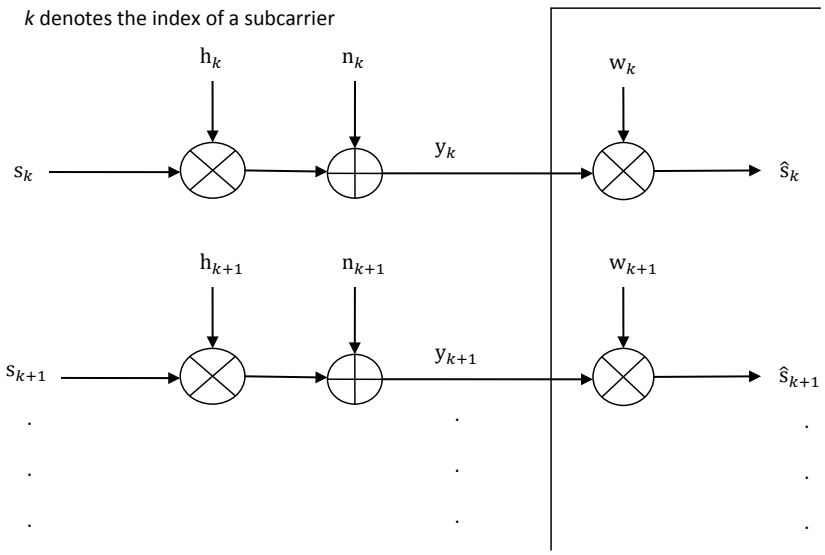

Figure 7: *Frequency-domain model of OFDM transmission and reception using one-tap equalization at the receiver.*

2.2 Physical resources and LTE frame structure

The parameters for OFDM based systems need to be carefully chosen. There are two main factors in radio propagation environment which need to be considered: the receiver mobility and the expected length of time-dispersion, that is, the length of the multi-path delays. The length of the cyclic-prefix should be as short as possible but still sufficiently

[3]MIMO will be described in Section 2.5.

[4]k denotes subcarrier index

long in order to avoid ISI. Also the subcarrier spacing should not be extremely narrow, as the receiver mobility causes Doppler shift. The more narrow the subcarrier spacing is, the more sensitive the OFDM system is to the effects of Doppler shift. Selecting 15 kHz for the LTE subcarrier spacing was found to meet these constraints [2, p. 127]. However, there is also a subcarrier spacing of 7.5 kHz defined in LTE but it is reserved for a special multicast configuration and therefore it is not considered in this thesis.

In LTE, the available physical resources can be seen as a resource grid, where the subcarrier spacing defines the frequency steps and the time dimension consist of consecutive OFDM symbols. A *resource element* (RE) is the smallest physical resource in LTE and it consist of one subcarrier during one OFDM symbol period and it can carry one complex-valued symbol. Resource elements are grouped into *resource blocks* (RB) and each resource block consists of 12 consecutive subcarriers in the frequency direction and seven OFDM symbols in the time direction in the case of normal cyclic-prefix. With extended cyclic-prefix, the number of OFDM symbols in time direction is six. However, only normal cyclic-prefix is considered in this thesis. When assuming normal cyclic-prefix, each resource block consist of $7 \times 12 = 84$ resource elements and the bandwidth of one resource block is $12 * 15\,\text{kHz} = 180\,\text{kHz}$. The LTE physical resource grid is illustrated in Figure 8. [2]

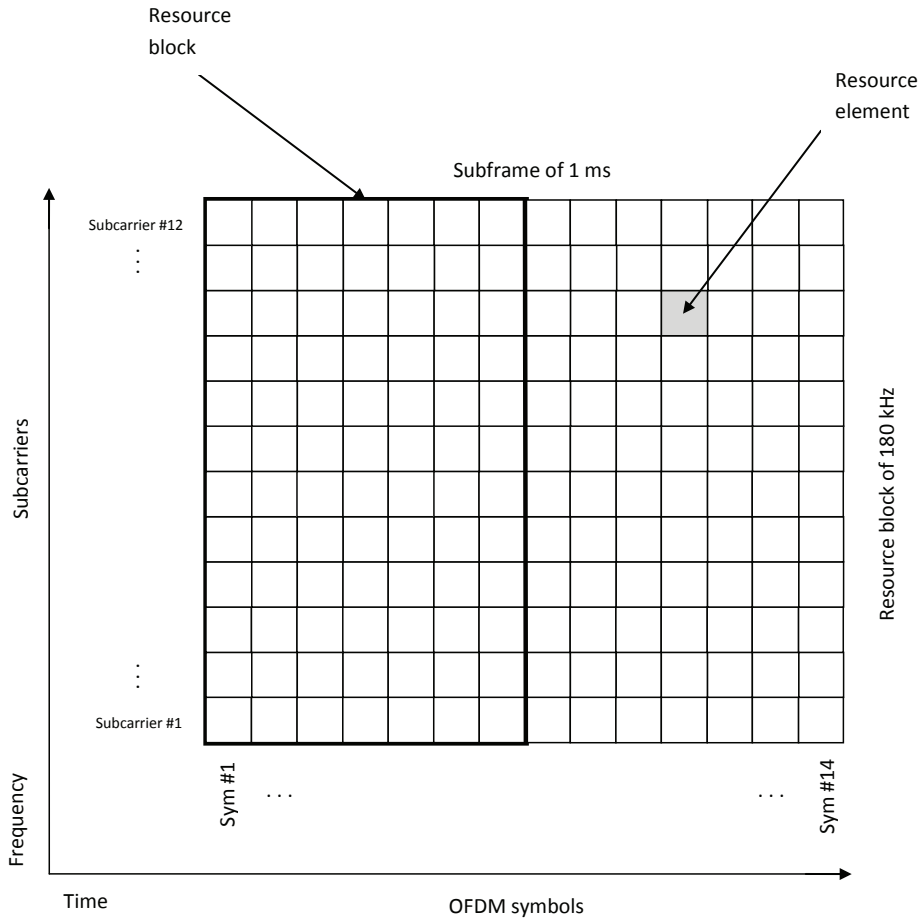

Figure 8: *Resource block pair consist of 14 OFDM symbols in time direction and 12 subcarriers in frequency direction. Thus, its duration is 1 ms and bandwidth is 180 kHz.*

Frequency division duplexing (FDD) means that the downlink and uplink have separate frequency bands. In LTE, frame structure type one is used with FDD. It should be noted here that throughout the whole thesis, normal CP and the frame structure type one are assumed to be used unless otherwise stated. So in the time domain and in the case of the frame structure type one, LTE transmissions are organized into *frames* of length 10 ms. Each frame consist of 10 equally sized *subframes* of length 1 ms, each of which consists of two equally sized *slots* of length 0.5 ms. Each slot consist of seven OFDM symbols when normal cyclic prefix is assumed. The LTE time-domain frame structure is illustrated in Figure 9. [2]

Also time division duplexing (TDD) has been defined for LTE. In TDD mode, uplink and downlink use the same frequency band and the transmissions are separated in time domain [2]. Thus also different frame structure has to be used in TDD operation. However, TDD operation is not considered in this thesis and thus it is not introduced in detail.

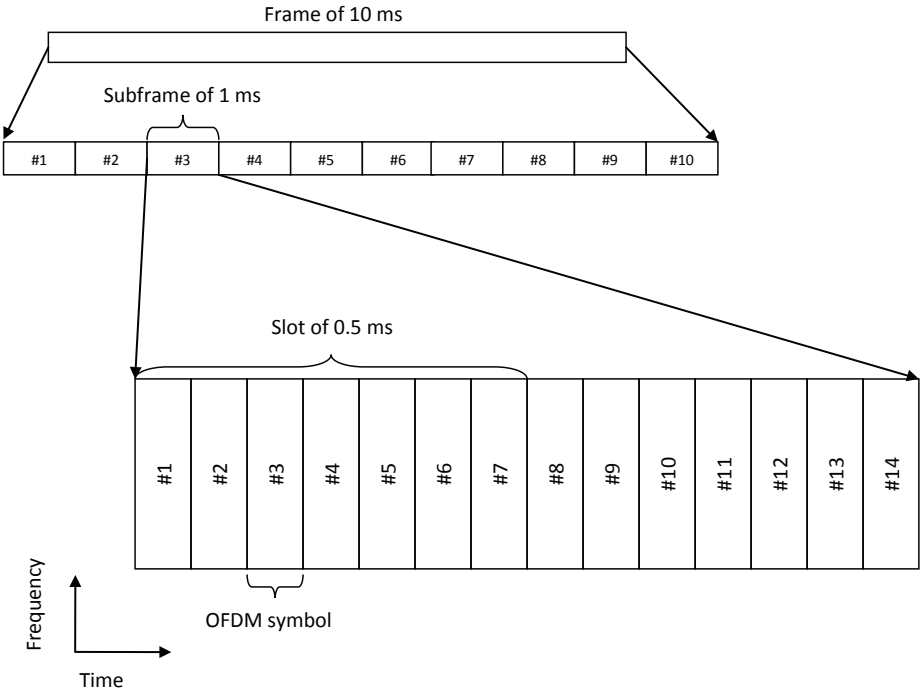

Figure 9: *LTE time-domain frame structure type 1.*

2.3 OFDM as a multiple access scheme

In previous sections, the discussion has assumed that all OFDM subcarriers are transmitted to a certain receiver, that is, to a single user equipment. However, user-multiplexing can be implemented straightforwardly in OFDM systems, allowing simultaneous frequency-separated transmission to multiple terminals. In the case of user-multiplexing in an OFDM system, the term Orthogonal Frequency Division Multiple Access (OFDMA) is also often used.

In LTE system, subframe is the smallest physical resource in time direction which can be allocated to different UEs. This means that without any frequency-separated trans-

mission schemes, user-multiplexing would be restricted to time direction, i.e., basestation should reserve the whole spectrum allocation to a single UE within one subframe. In many cases this would be too restrictive and inflexible. Hence simultaneous frequency-separated transmission are supported in LTE system.

In principle, different subsets of the overall set of available subcarriers could be used for transmission to different UEs. However, as there can be up to 1200 active subcarriers in 20 MHz spectrum allocation, a single subcarrier based frequency-separation would be too fine-grained, e.g., from signaling point of view. Therefore 12 consecutive subcarriers are grouped into a resource block as described in previous section. A single resource block is then the smallest physical resource in frequency direction which can be allocated to a single UE. Consequently basestation can allocate one or multiple resource blocks to different UEs simultaneously within one subframe.

2.4 Physical layer and channels

The LTE simulator, which is used to provide results for this study and which is described in more detail in Chapter 4.1, is a link level simulator and thus capable of modeling downlink transmission at physical layer. Furthermore, this thesis focuses mainly on physical layer performance and processing. Hence, an overview of physical layer and LTE physical channels is given in this section. However, a detailed description of the arrangement of all physical channels and physical layer processing is not needed for understanding the results in this thesis.

The physical layer is responsible for, among other things, channel coding, physical-layer retransmission processing, modulation, multi-antenna processing, and mapping of the signal to the appropriate physical time-frequency resources. Numerically this corresponds to mapping of the complex-valued symbols to the appropriate resource elements.

One physical channel corresponds to the set of time-frequency resources, which are used for transmission of a specific data. There are a total of five different downlink physical channels defined in LTE, namely Physical Broadcast Channel (PBCH), Physical Control Formal Indicator Channel (PCFICH), Physical Hybrid-ARQ Indicator Channel (PHICH), Physical Downlink Control Channel (PDCCH) and Physical Downlink Shared Channel (PDSCH). PDSCH is used for the data transmission and it can be said to be the main physical channel. The term "*shared*" in PDSCH stems from the possibility for simultaneous frequency-separated transmission to different UEs in LTE, as described in the previous section. Other physical channels are used for transmitting downlink control information, which provides the necessary information to the mobile terminal for proper reception and decoding of the downlink data transmission. Brief description of downlink physical channels can be found from Table 2.

Control information is separated from the actual data transmission in time direction as described in the following. In the case of normal CP, each subframe comprises 14 OFDM symbols. Within these 14 symbols, up to four OFDM symbols can be assigned for control information and the rest OFDM symbols are assigned for PDSCH transmission. However, this assigning is dynamic and it is signaled to the terminals as a part of the control information in the form of Control Format Indicator (CFI) carried by PCFICH. As an example, CFI of three maps to three control information and 11 PDSCH carrying symbols. This assigning of OFDM symbols for control signaling and PDSCH transmission is illustrated in Figure 10. It is good to mention here that performance results in this thesis are based only on the PDSCH transmission.

Table 2: LTE/LTE-Advanced physical channels.

Physical channel	**Description**
PBCH	Carries system information for UEs requiring to access the network
PCFICH	Carriers Control Format Indicators (CFI), i.e., it informs UE about the format of the subframe being received. To be more exact, it indicates the size of the control region used for the PDCCHs and consequently the number of OFDM symbols used for PDSCH.
PHICH	Used to report the Hybrid ARQ status, i.e., carriers ACK/NACK signal indicating whether a transport block has been correctly received. Transmitted within control region.
PDCCH	Carries scheduling information of different types, for instance: • Downlink resource scheduling • Uplink power control instructions • Uplink resource grants • Transmission scheme and MCS
PDSCH	Used for data transmission

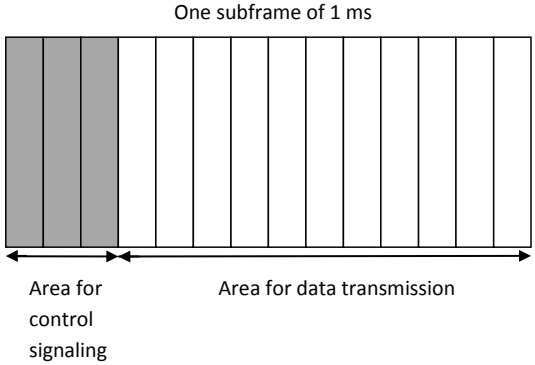

Figure 10: *There are own regions for control signalling and data transmission within a downlink subframe in LTE.*

2.5 Multi-antenna transmission

In this section, multi-antenna signal model is shortly discussed by assuming multiple antennas both in the transmitter and the receiver. Multi-antenna transmission or in other words, *multiple-input and multiple-output* (MIMO), has a crucial role in LTE systems because it can be utilized in different ways to achieve different goals, but mainly the data rate requirements set for both LTE and LTE-Advanced systems. In LTE/LTE-Advanced, multi-antenna transmission can be described as a mapping from the output of the data modulation to the different antenna ports. Thus, the input to the antenna mapping consists of the modulation symbols of QPSK, 16QAM or 64QAM alphabets. It is good to bear in mind that in general mapping of modulation symbols to antenna ports in MIMO systems include also precoding, which is described in the next subsection. In general, MIMO can be used to:

- Provide additional diversity against fading on the radio channel. In this case, the channel experienced by the different antennas should have low mutual correlation.
- Shape the overall antenna beam in a certain way. For example, to maximize the overall antenna gain in the direction of the target receiver.
- Create what can be seen as multiple parallel communication channels over the radio interface. Herein we will refer to this as *spatial multiplexing*. Spatial multiplexing allows more efficient utilization of high signal-to-noise ratios and significantly higher data rates over the radio interface. [2]
- Spatial multiplexing, i.e., multiple parallel communication channels can be used also for so-called *multi-user-MIMO,* where different parallel data streams are targeted to different mobile terminals. In other words, the same frequency and time resources are used to transmit data to multiple mobile terminals.

As described in Section 2.1, OFDM allows for the compensation of frequency-selective channel fading by a simple one-tap equalization. Thus, modeling of the channel frequency response is straightforward and this eases the formulation of the MIMO. All in all, MIMO is very suitable for LTE systems.

In the following, we start examining the MIMO system by a simple example. For simplicity and convenience, single-link model without interference is considered at start. In addition, precoding is not considered as it will be taken into account later in this section. In the general case of N_t transmit antennas and N_r receive antennas, the received vector $\mathbf{y}$ of length N_r at an arbitrary subcarrier can be defined as:

$$\mathbf{y} = \mathbf{H}\mathbf{s} + \mathbf{n}, \tag{2.3}$$

where $\mathbf{H}$ is the $N_\mathrm{r} \times N_\mathrm{t}$ dimensional channel matrix, $\mathbf{s}$ is the transmitted signal vector and $\mathbf{n}$ is a noise vector. If one subcarrier is examined, each element in matrix $\mathbf{H}$ is a channel coefficient, which characterizes the channel experienced between one pair of transmit and receive antennas at the considered subcarrier.

In this thesis, two transmit antennas and two receive antennas are used in simulations. Hence, in order to understand the basic principles how multiple parallel channels can be created, consider a 2×2 antenna configuration as outlined in Figure 11.

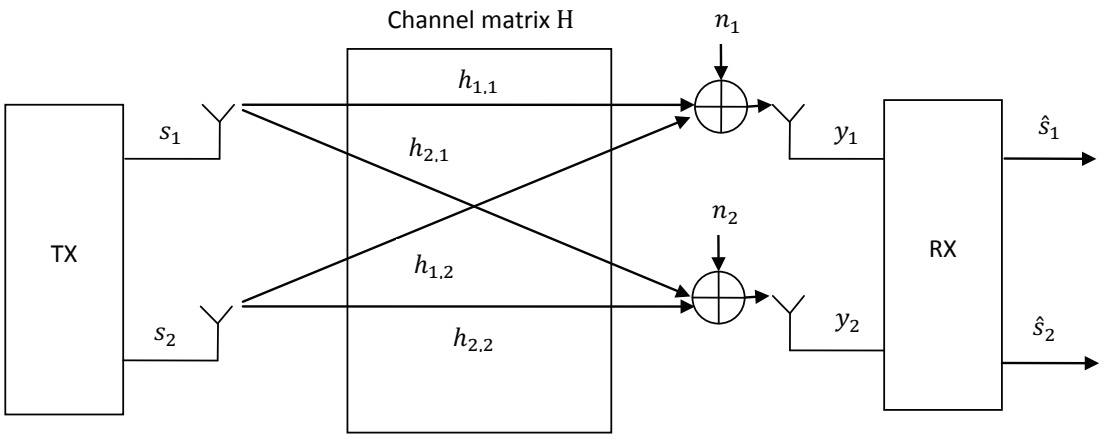

Figure 11: *2 x 2 antenna configuration.*

Based on Figure 11, the received signal can be expressed as:

$$\mathbf{y} = \begin{bmatrix} y_1 \\ y2 \end{bmatrix} = \begin{bmatrix} h_{1,1} & h_{1,2} \\ h_{2,1} & h_{2,2} \end{bmatrix} \times \begin{bmatrix} s_1 \\ s_2 \end{bmatrix} + \begin{bmatrix} n_1 \\ n_2 \end{bmatrix} = \mathbf{Hs} + \mathbf{n}, \tag{2.4}$$

where $\mathbf{H}$ is the 2×2 channel matrix. Assuming that the channel matrix is known in the receiver and it is invertible, an estimate $\hat{\mathbf{s}}$ of the transmitted symbol vector $\mathbf{s}$, and thus estimates of both signals s_1 and s_2 can be obtained at the receiver by multiplying the received vector $\mathbf{y}$ with receive filter $\mathbf{W}$, per subcarrier and receive antenna, as will be described in more detail in Section 3.5. Now an estimate of the transmitted symbol can be obtained as follows

$$\hat{\mathbf{s}} = \begin{bmatrix} \hat{s}_1 \\ \hat{s}_2 \end{bmatrix} = \mathbf{W}^{\mathrm{H}}\mathbf{y}, \tag{2.5}$$

where $(.)^{\mathrm{H}}$ denotes hermitian transpose. If the most simple equalization method is used, namely Zero-Forcing criterion, receive filter is of the form $\mathbf{W}^{\mathrm{H}} = \mathbf{H}^{-1}$, where $(.)^{-1}$ denotes inverse of $\mathbf{H}$. Thus the Equation (2.5) can be written, assuming $\mathbf{H}$ is invertible (full rank), as

$$\hat{\mathbf{s}} = \mathbf{H}^{-1}\mathbf{Hs} + \mathbf{H}^{-1}\mathbf{n} = \mathbf{s} + \mathbf{H}^{-1}\mathbf{n}. \tag{2.6}$$

In the case of no noise nor interference and when the channel matrix is invertible, the vector $\mathbf{s}$ can be perfectly recovered. However, in practice there is always noise and interference so the receiver can obtain only an estimate vector $\hat{\mathbf{s}}$ from the transmitted signals. One way to interpret the above model is that the signals transmitted from the two transmit antennas are two signals causing interference to each other. Then two receive antennas can be used to suppress the interference from signal transmitted on the second antenna while detecting the signal transmitted from the first antenna and vice versa. However, there are more sophisticated and complex equalization methods than Zero-Forcing criterion. Such methods provide better performance especially for NAICS systems, where two interfering eNBs are considered. In Section 3.5, some of these practical and better performing equalization methods will be introduced.

Precoding in MIMO systems

In the case of practical systems like LTE, linear precoding can be used with MIMO, that is, with spatial multiplexing. In general, precoding matrix $\mathbf{B}$ of size $N_\mathrm{t} \times N_\mathrm{l}$ is applied at the transmitter side, where N_l is the number of *layers* (or symbols) to be spatially multiplexed and N_t is the number of transmit antennas. Hence receive vector, given in the Equation (2.4), can be rewritten using the precoding assumption as

$$\mathbf{y} = \mathbf{HBs} + \mathbf{n}. \tag{2.7}$$

The receiver processing can be modeled by an $N_\mathrm{r} \times N_\mathrm{l}$ matrix $\mathbf{W}^\mathrm{H}$ that contains the reception weights for each symbol stream and where N_r is the number of receiver antennas. The multi-stream transmission chain can be written as

$$\hat{\mathbf{s}} = \mathbf{W}^\mathrm{H}\mathbf{HBs} + \mathbf{W}^\mathrm{H}\mathbf{n}. \tag{2.8}$$

This is illustrated in Figure 12.

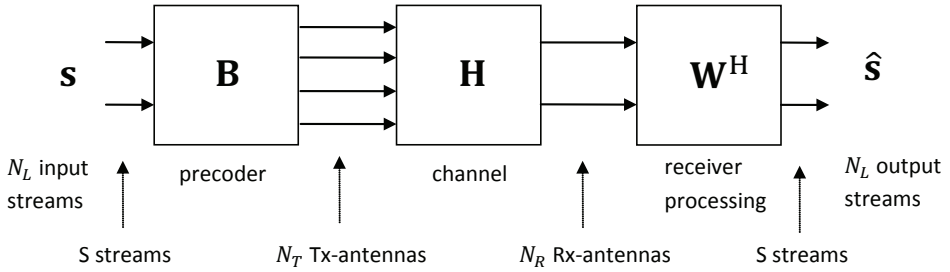

Figure 12: Multi-layer transmission chain.

Then the question is, how to determine the precoder matrix and the reception weights, that is, the matrix $\mathbf{W}^\mathrm{H}$. In order to find the answers, channel matrix $\mathbf{H}$ is examined in more detail in the following.

The channel matrix $\mathbf{H}$ can be expressed in multiple components by using its singular value decomposition defined as [1]:

$$\mathbf{H} = \mathbf{USV}^\mathrm{H}, \tag{2.9}$$

where matrices $\mathbf{U}$ and $\mathbf{V}$ are unitary and have dimensions of $N_\mathrm{r} \times N_\mathrm{r}$ and $N_\mathrm{t} \times N_\mathrm{t}$, respectively. $\mathbf{S}$ is a diagonal matrix of dimension $N_\mathrm{r} \times N_\mathrm{t}$ and its diagonal elements are the singular values of $\mathbf{H}$. By applying the matrix $\mathbf{V}$ as precoding matrix at the transmitter side and the matrix $\mathbf{U}$ as the reception weight matrix at the receiver side, $\mathbf{S}$ can be seen as an equivalent channel matrix $\mathbf{H}'$. Thus the precoding can improve the isolation between the spatially multiplexed signals. The Equation given in 2.8 can be now written

$$\hat{\mathbf{s}} = \mathbf{U}^\mathrm{H}\mathbf{HVs} + \mathbf{U}^\mathrm{H}\mathbf{n}. \tag{2.10}$$

However, the precoding matrix $\mathbf{V}$ will never perfectly match the channel matrix in practice and thus there will be always some residual interference between the spatially multiplexed signals [2]. One reason for this is the fact that to determine the precoding matrix, knowledge about the channel matrix $\mathbf{H}$ is needed and practical channel estimators

do not provide perfectly correct **H**. Other reason is the fact that in practice, the precoding matrix cannot be arbitrary and some predefined precoder matrices are used. The set of available precoding matrices are often called as precoder *code-book*. In this case, the receiver can feed back information about the preferred choice for the precoding matrix. Code-book based precoding in LTE is described in more detail in Section 2.7.

Transmission modes

In LTE, the different multi-antenna transmission schemes correspond to different so-called *transmission modes* (TM). For example, transmission mode 1 corresponds to single-antenna transmission while the rest transmission modes correspond to different multi-antenna transmission schemes like transmit diversity, beam-forming and spatial multiplexing. To be more exact, transmission modes differs in terms of the structure of the antenna mapping but also in terms of what reference signals are assumed to be used for channel estimation and demodulation, that is, either Cell-specific Reference Signals (also referred to as Common Reference Signals, CRS) or Demodulation Reference Signals (DM-RS). CRS based transmission modes were introduced already in the release 8 of LTE while DM-RS based transmission modes were introduced in the release 10 and onwards. However, DM-RS are not used nor introduced in detail as the transmission mode used in this thesis use CRS. In addition, it is good to point out that most of transmission modes are only applicable for PDSCH transmission, that is, for data transmission. Transmission modes using CRS are listed below. [2]

- Transmission mode 1: Single-antenna transmission.
- Transmission mode 2: Transmit diversity.
- Transmission mode 3: Open-loop codebook-based precoding in the case of more than one layer and transmit diversity in the case of rank-one transmission.
- Transmission mode 4: Closed-loop codebook-based precoding.
- Transmission mode 5: Multi-user-MIMO version of TM 4.
- Transmission mode 6: Special case of closed-loop codebook-based precoding limited to single-layer transmission.

Concepts of *open-loop* and *closed-loop* codebook-based precoding are explained in Section 2.7. In this thesis, simulations are carried out by using transmission mode 6 with 2×2 antenna configuration as described in more detail in Section 4.4. The main reason for this choice is the fact that the core techniques studied in this thesis are useful mainly for cell-edge users, who may suffer from strong inter-cell interference and hence single-layer transmission is more suitable for them.

It is good to point out that although DM-RS based TMs are not considered in this thesis, such TMs exists. The main difference between CRS and DM-RS based TMs is the precoding scheme. While CRS based TMs use either open-loop or closed-loop codebook based precoding supporting up to four layers, DM-RS based TMs use so called non-codebook-based precoding and can support up to eight layers. Detailed description of non-codebook-based precoding can be found from Section 10.3.4 in [2].

2.6 Reference signals

In this chapter, the usage of reference signals in the OFDM system is described, i.e., how the receiver can estimate the channel response based on the knowledge about reference signals. Then cell-specific reference signals in LTE/LTE-Advanced system are introduced in more detail.

In general, reference signals consist of reference symbols of predefined values inserted in predefined reference symbol positions, that is, in specific resource elements. Reference symbols, also referred to as pilot symbols, are needed to estimate frequency response of the propagation channel. Hence, reference symbols are inserted into the OFDM time-frequency grid at regular intervals. The receiver can use the knowledge about the reference symbol to estimate the frequency response around the location of the reference symbol. Therefore, the reference symbols should cover the whole OFDM time-frequency grid and they should also have a sufficiently high density, especially if the radio channel has high frequency and time selectivity [2]. However, the more there are reference symbols, the less there are resource elements left to transmit actual data. So defining the density and locations of reference symbols for different wireless systems is not straightforward.

Cell-specific Reference Signals - CRS

Cell-specific Reference Signals, also referred to as Common Reference Signals, are the most basic downlink reference signals in LTE and they cover the entire cell bandwidth. Thus, they are transmitted in every downlink subframe and in every resource block in the frequency domain. The terminal can use the cell-specific reference signals for channel estimation and also to acquire *channel-state information* (CSI) [2, p. 152].

In the case of the CRS, reference symbol values vary between different reference symbol positions and also between different cells. In the case of one transmit antenna or spatial multiplexing with one layer, these reference symbols are inserted within a resource block pair as follows:

- In time direction, *first, fifth, eighth* and *twelfth* OFDM symbol consist of reference symbols.
- In frequency direction, reference symbols of a given CRS port have a spacing of six subcarriers. Furthermore, within the *fifth* and *twelfth* OFDM symbol, there is a shift of three subcarriers in comparison to pilot positions of the *first* and *eighth* OFDM symbol.

Thus, in each recourse block pair which consists of twelve subcarriers and 14 OFDM symbols within one 1 ms subframe, there are a total of eight reference symbols [2, p. 153]. This is illustrated in Figure 13.

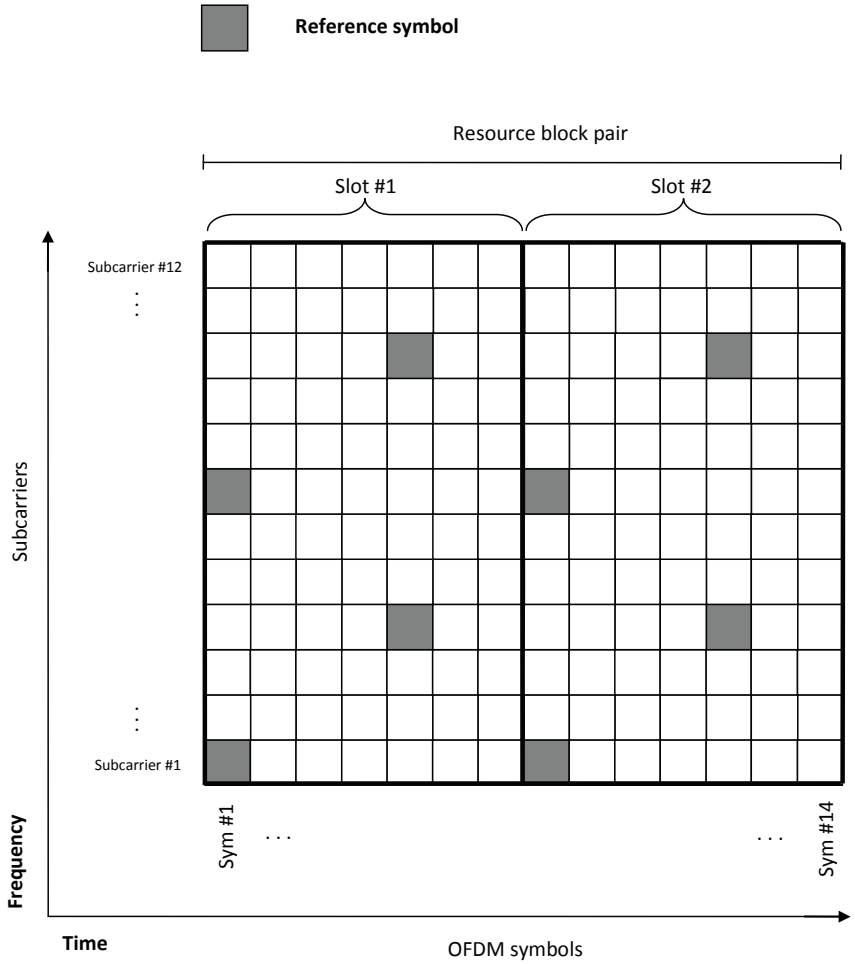

Figure 13: *Mapping of cell-specific reference symbols into the LTE resource grid* from CRS antenna port #0.

In the case of two and four transmit antennas or transmission layers, also two and four cell-specific reference signals are used within a cell, respectively. In the case of two transmission layers, the second reference signal transmitted from the second antenna is frequency multiplexed with the first reference signal, with a frequency-domain offset of three subcarriers [2, p. 155]. In the case of four transmission layers, the third and fourth reference signal are time multiplexed with the first and second reference signal, with a time-domain offset of one OFDM symbol. In other words, when a resource element carries a reference symbol for a certain antenna port, nothing is being transmitted on the antenna ports corresponding to the other reference signals. Therefore, the reference signals transmitted from the different antenna ports are orthogonal and do not interfere each other. Usage of four CRS is illustrated in Figure 14.

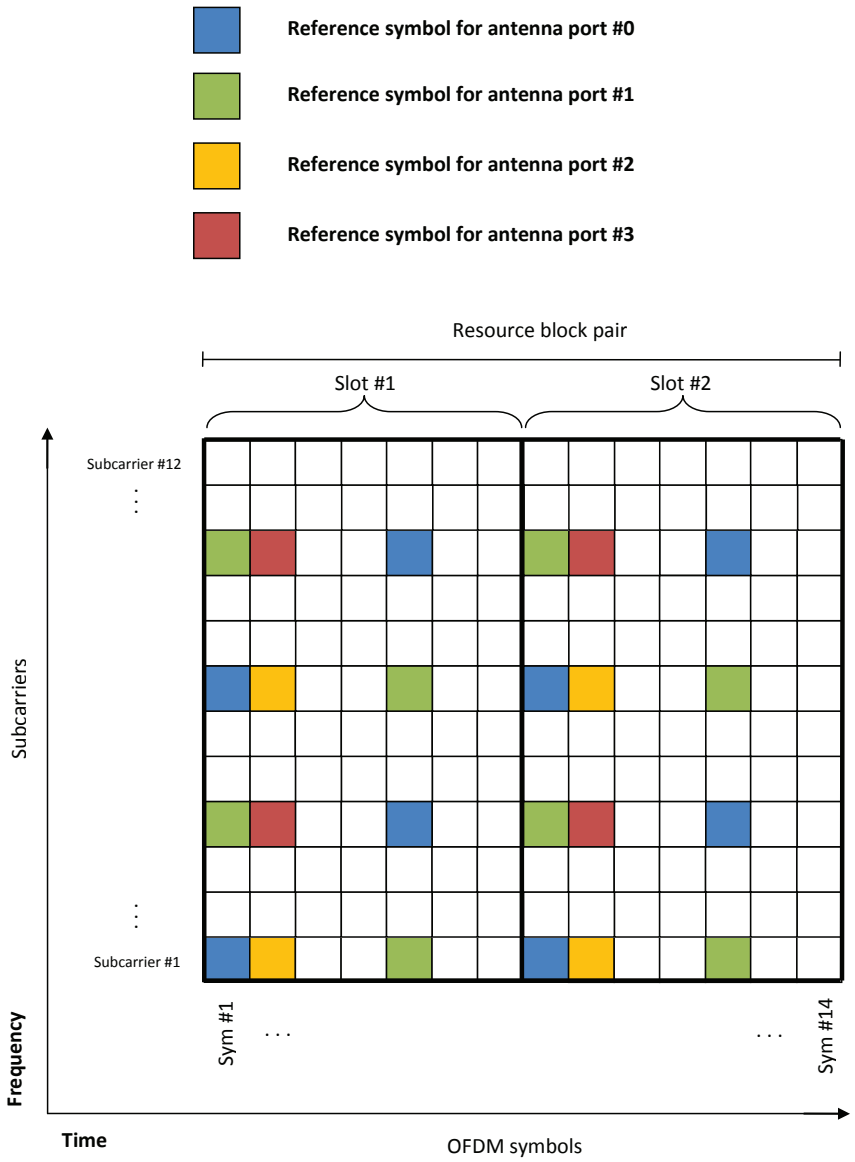

Figure 14: *Mapping of cell-specific reference signals in the case of four transmission layers or transmit antennas.*

When mobile terminals are at the border of the serving cell, signals from the neighboring cells start to interfere. Thus, there are also three possible frequency shifts for the set of reference symbol positions and for example in Figure 13, the frequency shift of zero is used. Different frequency shifts can be used in neighboring cells whereupon the reference signals are orthogonal, meaning that the reference signals transmitted from the different cells do not interfere with each other. This can be beneficial especially if the boosting of the reference signals is used within certain cell. Without the possibility of frequency shifts the boosted reference symbols of one cell would be interfered by equally boosted reference symbols of the neighboring cell. Consequently, there would be no gain in the reference signal signal-to-interference-ratio (SIR).

However, in the case of NAICS system, i.e., when interference is tried to be suppressed or canceled, it might be beneficial to have overlapping reference signals. The reason for this is the usage of reference signal interference cancellation (RS-IC) methods where it is

actually more beneficial that reference signals from the interfering cells collide with the reference signals of serving cell, compared to the situation where reference signals would interfere data channel REs, namely PDSCH REs. More detailed description of CRS-IC (CRS Interference Cancellation) is given in Section 3.2.

2.7 Channel state information feedback

As the environment, i.e, the channel between the UE and the basestation (eNB) and interference[5] are changing over time, the basestation (eNB) needs to adjust its transmission mode, transmission rank, modulation and coding scheme (MCS) and precoding matrix dynamically over time in order to provide optimized throughput for the UE. Therefore UE needs to perform a number of measurements in order to select the most optimal parameters for transmission. These measurements are based on so called post-detection SINR, that is, signal-to-interference-plus-noise ratio experienced by the UE after the equalization. Thus post-detection SINR depends on the performance of the receiver algorithm. For instance, if UE has an advanced interference suppressing receiver, it's post-detection SINR is most likely better compared to UE with non-interference-aware receiver.

Information about the UE selected parameters is then reported back to the eNB in the form of *Rank Indicator* (RI), *Precoder-Matrix Indicator* (PMI) and *Channel Quality Indicator* (CQI). It is good to point out that RI, PMI and CQI are only recommendations and the eNB does not need to follow these reports provided by the UE. When not following the UE recommendations, the eNB must explicitly inform what parameters are used. However, in this thesis the link adaptation is not used and thus rank, precoder matrix and MCS are fixed in all simulations. Nevertheless, RI and PMI as well as closed-loop and open-loop codebook-based precoding are introduced in the following.

RI and PMI

In downlink transmission, different number of streams/layers can be used depending on the used antenna configuration and channel state. Rank Indicator conveys the information about the number of layers that can be used with the current channel. In LTE/LTE-Advanced, the maximum number of codewords is two, that is, two independently modulated and coded data streams. In this case, the minimum number of layers is naturally two as well. However, in many cases one codeword is transmitted on several layers. The layers are then mapped to the antenna ports by means of the selected precoder. More detailed description of codeword-to-layer mapping in LTE can be found from Section 6.3.3 of [25].

Codebook-based precoding relies on the CRS for channel estimation and as discussed in Section 2.6, there are at most four CRSs in a cell. Thus, codebook-based precoding allows a maximum of four antenna ports and consequently a maximum of four layers. There are two operational modes for codebook-based precoding, closed-loop and open-loop operation. These two modes differ in terms of how precoding matrix is selected by the network and made known to the terminal. [2]

When closed-loop operation is used, the network selects the precoder matrix based on feedback from the UE. In order to limit signaling, only a limited set of precoder matrices are defined, that is, a *codebook* is defined for each transmission rank for a given number

[5]Both intra-cell interference and inter-cell interference.

of antenna ports. When using the codebook, only the index of the selected matrix needs to be signaled. [2]

As already mentioned in Section 2.5, transmission mode 6 is used in this thesis. TM 6 corresponds to a closed-loop codebook-based precoding strictly limited to single-layer (rank-1) transmission. The reason for defining such separate transmission mode is the fact that the signaling overhead on both downlink and uplink can be reduced. Furthermore, transmission mode 6 is suitable for UEs with low SINR for which multi-layer transmission would not apply anyway. This is indeed the case in this thesis.

When open-loop operation is used, the precoder matrix is selected in a predefined and deterministic way known to the UE in advance. This open-loop operation does not require any explicit network signaling and consequently it is suitable for high-mobility scenarios, where accurate feedback is difficult to achieve due to latency. Still similarly to closed-loop operation, open-loop precoding can also vary dynamically down to a minimum of two layers. [2]

2.8 Downlink power allocation

This section is essential as it gives the insight to understand better the topic and goal of the thesis. The eNodeB (eNB, basestation) determines the downlink transmit *energy per resource element* (EPRE). For downlink power allocation (or control), this section shows parameters which are provided from higher layers, the roles that these parameters play and the values they can take. Also the purpose of downlink power control as well as other restrictions and requirements according to the specification are introduced. In the following, the parameters which define power levels of different components of downlink signal within a subframe are introduced in more detail.

There are three parameters which are signaled by higher layers, namely *referenceSignalPower, P_a* and P_b. The values they can take are defined in Section 6.3.2 of [4] and also presented in Table 3. In the following, these parameters are defined.

Table 3: Parameters of downlink power allocation and the values they take.

Parameter	**Possible values**
referenceSignalPower	Integer(-60..50) dBm
P_a	Enumerated{-6, -4.77, -3, -1.77, 0, 1, 2, 3} dB
P_b	Integer(0, 1, 2, 3)

referenceSignalPower

The downlink reference-signal transmit power is defined as the linear average over the power contributions (in [W]) of all resource elements that carry CRS within the operating system bandwidth. The parameter *referenceSignalPower* is provided by higher layers and a UE may assume that the parameter is constant across the downlink system bandwidth and constant across all subframes until different value is received. [3, Section 5.2]

P_a and P_b

P_a defines the power level of PDSCH in OFDM symbols where CRS are not present and it is UE specific. As P_a is UE specific, it can change on a millisecond basis, that is, for

every TTI (or subframe). In the case of simultaneous frequency-separated transmission to different UEs within one TTI, P_a can, in principle, change on a resource block basis, based on the UEs resource block allocation[6]. Whereas, P_b defines the power level of PDSCH in OFDM symbols where CRS are present, it is cell-specific and it cannot be changed dynamically. P_a is mapped to power ratio denoted by ρ_a and P_b is mapped to power ratio denoted by ρ_b. The ratio of PDSCH EPRE to CRS EPRE among PDSCH REs for each OFDM symbol is denoted by either ρ_a or ρ_b according to the OFDM symbol index as given by Table 4. In addition, ρ_a and ρ_b are UE-specific and they are not applicable to PDSCH REs with zero EPRE. [3, Section 5.2]

Table 4: OFDM symbol indices within a slot of non-MBSFN subframe where the ratio of the corresponding PDSCH EPRE to the CRS EPRE is denoted by ρ_a or ρ_b. Also normal cyclic prefix is assumed.

Number of antenna ports	**OFDM symbol indices within a slot where the ratio of the corresponding PDSCH EPRE to CRS EPRE is denoted by ρ_a**	**OFDM symbol indices within a slot where the ratio of the corresponding PDSCH EPRE to CRS EPRE is denoted by ρ_b**
One or two	1, 2, 3, 5, 6	0, 4
Four	2, 3, 5, 6	0, 1, 4

Mapping of P_a to ρ_a is as follows. For transmission modes 1-7, the UE may assume that for 16QAM, 64QAM, spatial multiplexing with more than one layer or for PDSCH transmissions associated with multi-user MIMO transmission scheme,

- ρ_a is equal to $\delta_{power-offset} + P_a + 10log_{10}(2)$ dB when the UE receives a PDSCH data transmission using precoding for transmit diversity with 4 cell-specific antenna ports, i.e., transmission mode 2 with 4 antenna ports;
- ρ_a is equal to $\delta_{power-offset} + P_a$ dB otherwise,

where $\delta_{power-offset}$ is 0 dB for all PDSCH transmission schemes except multi-user MIMO and where P_a is a UE specific parameter provided by higher layers. Parameter $\delta_{power-offset}$ is not defined for multi-user MIMO by specification [3]. Determining the parameter ρ_b requires information about the cell-specific parameter P_b (signaled by higher layers), the number of configured eNB cell-specific antenna ports and the parameter ρ_a. Based on these parameters, ρ_b can be calculated using Table 5. [3, Section 5.2]

Table 5: The cell-specific ratio ρ_b/ρ_a for 1, 2, or 4 cell specific antenna ports.

P_b	ρ_b/ρ_a	
	One Antenna Port	**Two and Four Antenna Ports**
0	1	5/4
1	4/5	1
2	3/5	3/4
3	2/5	1/2

[6]In this case, it might be hard to select such P_a values to different UEs that the power of all OFDM symbols within a subframe remains constant enough.

As described in the above, for the majority of cases ρ_a corresponds directly to the parameter P_a and the simulation setup in this thesis is selected so that this condition is fulfilled. Thus for clarity and convenience, we talk about blind detection of P_a instead of blind detection of ρ_a in this thesis.

Purpose of downlink power control

The overall goal of downlink power control and the parameters defined for it is to have a constant power for all OFDM symbols to avoid power fluctuations within a subframe. As already described in Section 2.6, cell-specific reference signals are embedded into the overall signal bandwidth. As also mentioned earlier in this section, the power level of CRS must be constant over the entire bandwidth as the power level of other signal components, as control signals and data signal, is set relative to the power of CRS. Due to the importance of CRS, they are often the highest powered components within the downlink signal. However, just by boosting the power of CRS leads to a situation where the overall power of OFDM symbols where CRS are present may exceed the maximum allowed output power of the basestation. In addition, power levels within a subframe will fluctuate, which is undesirable. The purpose of parameter P_b is to reduce power of PDSCH in OFDM symbols where boosted CRS are present. In other words, when the power of CRS is boosted, by parameter P_b it is possible to reduce power of PDSCH in OFDM symbols where CRS are present. Consequently, by parameters P_a and P_b it can be ensured that the overall OFDM symbol power within a subframe remains constant enough. In the following, the usage of P_a and P_b is illustrated by an example where CRS power is boosted by 3 dB.

Example of downlink power allocation

To acquire better insight about downlink power control, a simple example is carried out. In this example, it is assumed that higher layers have provided the following parameters and their values:

- P_a= -3 dB and P_b= 2,
- Maximum output power of basestation is 43 dBm.
- CRS power (parameter *referenceSignalPower*) is set to 18.22 dBm, which corresponds to CRS boosting of 3 dB.
- The system bandwidth is 10 MHz.
- For simplicity, one transmit antenna port is considered. In this case, the mapping of CRS into a subframe is illustrated in Figure 13.

In this case, $\rho_a = P_a = -3\,\text{dB}$ and according to Table 5,

$$\frac{\rho_b}{\rho_a} = \frac{3}{5} \rightarrow \rho_b = -5.23\,\text{dB}.$$

Consequently, according to Table 4, the ratio of PDSCH EPRE to CRS EPRE is $\rho_a = -3\,\text{dB}$ in OFDM symbols 1, 2, 3, 5 and 6 within a slot and the ratio of PDSCH EPRE to CRS EPRE is $\rho_b = -5.23\,\text{dB}$ in OFDM symbols 0 and 4 within a slot. Now the power

level of PDSCH in OFDM symbols indices of 1, 2, 3, 5 and 6 is 15.22 dBm and in OFDM symbols indices of 0 and 4 it is 12.99 dBm, while CRS EPRE is 18.22 dBm.

Consequently, the total transmit power needed for OFDM symbols where CRS are present and for OFDM symbols where only PDSCH is present is 42.20 dBm and 43 dBm, respectively. This is illustrated in Figure 15, in which one PRB pair is shown and three first OFDM symbols are allocated to control signaling.

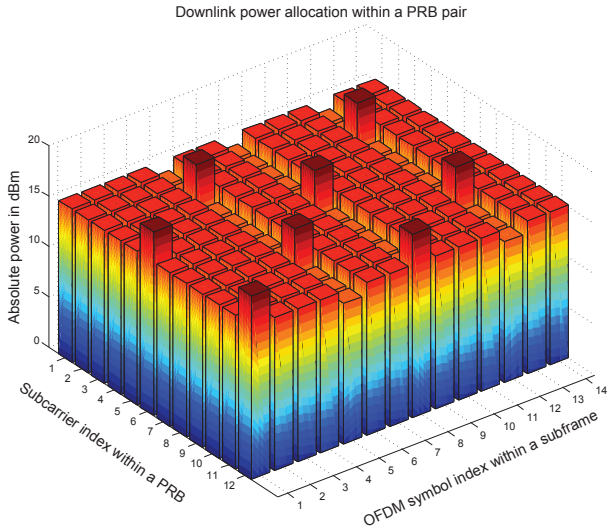

Figure 15: An illustration of downlink power allocation. One PRB pair is shown. Three first OFDM symbols are assigned for control signaling. Parameters are P_a= -3 dB, P_b= 2 and CRS power is set to 18.22 dBm while the total transmit power is 43 dBm. System bandwidth is 10 MHz.

From Figure 15 it can be seen how the power level of PDSCH is reduced by parameter P_b for OFDM symbols where CRS present. Exception is the first OFDM symbol as it consist of control signaling instead of PDSCH. In the Figure it seems like the first OFDM symbol would require more than the allowed maximum transmit power of 43 dBm. It is good to bear in mind that the Figure shows only one PRB pair and in real the first OFDM symbols, which consist of control signaling, are never (or very rarely) fully allocated within the whole bandwidth. Thus the first OFDM symbols will also include REs with zero power.

3 System Model and Receivers

In this chapter, the system model as well as the signal model of a MIMO system used in this thesis are introduced. Secondly, concepts related to channel estimation are examined especially from CRS point of view. Then interference plus noise power estimation as well as interference covariance estimation are described. Finally some common linear receivers as well as the SLIC receiver are introduced. Note that in the following, the physical layer of LTE-Advanced downlink is considered in the case of FDD operation.

3.1 NAICS system and signal model

In general, system model in NAICS studies consist of one serving cell and two interfering cells. Simplified NAICS system model is illustrated in Figure 16. Reasons for considering only two interfering cells are, among other things, that usually other interfering cells are so far from the NAICS UE that they can be treated as additional noise sources and also considering more than two interfering cells in NAICS UE would significantly increase complexity.

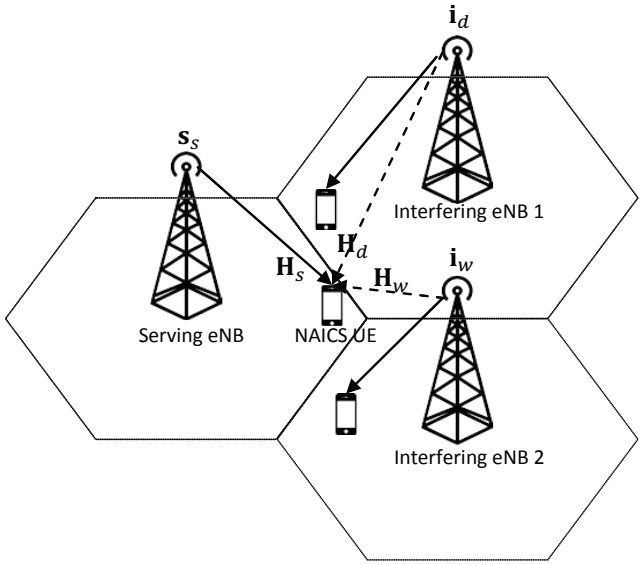

Figure 16: Simplified illustration of system model in NAICS. Signals $\mathbf{s}_\mathrm{s}$, $\mathbf{i}_\mathrm{d}$, and $\mathbf{i}_\mathrm{w}$ are intended for served UEs in serving cell, dominant interfering cell and weaker interfering cell, respectively. Channels $\mathbf{H}_\mathrm{s}$, $\mathbf{H}_\mathrm{d}$ and $\mathbf{H}_\mathrm{w}$ are between the serving basestation and NAICS UE, dominant interfering basestation and NAICS UE and weaker interfering basestation and NAICS UE, respectively.

As the focus in NAICS studies is on interference cancellation and suppression techniques, the UE under observation can be seen as a cell edge user. At the cell edge, the power level of desired signal can be relatively low compared to power of interfering signals. Therefore advanced receiver algorithms like CRS-IC, network assisted covariance estimation and non-linear receivers are needed in the NAICS UE so that it can overcome these challenging conditions, that is, it can cancel and/or suppress the inter cell interference.

In many cases, network assistance is required so that advanced receiver algorithms can perform efficiently. Network assistance, in general, means that network provides necessary and useful information about parameters used in interfering cells. This signaling can cause additional complexity to the network and to NAICS UE as well as it can be prone to harmful delay, that is, NAICS UE cannot adapt to changing conditions fast enough. Due to these facts, instead of adding all the complexity to the network, some of it can be added to the NAICS UE in form of blind detectors, whose purpose is to blindly estimate parameters of interfering cells without or with low network assistance.

System model, as illustrated in Figure 16, is considered in the following. Each eNB is having N_t transmit antennas and each UE is having N_r receive antennas. In this case, the received signal, $\mathbf{y}$, by the NAICS UE can be written as

$$\underset{N_\mathrm{r}\times 1}{\mathbf{y}} = \underset{N_\mathrm{r}\times N_\mathrm{t,s}}{\mathbf{H}_\mathrm{s}} \; \underset{N_\mathrm{t,s}\times r_\mathrm{s}}{\mathbf{B}_\mathrm{s}} \; \underset{r_\mathrm{s}\times 1}{\mathbf{s}_\mathrm{s}} + \underset{N_\mathrm{r}\times N_\mathrm{t,d}}{\mathbf{H}_\mathrm{d}} \; \underset{N_\mathrm{t,d}\times r_\mathrm{d}}{\mathbf{B}_\mathrm{d}} \; \underset{r_\mathrm{d}\times 1}{\mathbf{i}_\mathrm{d}} + \underset{N_\mathrm{r}\times N_\mathrm{t,w}}{\mathbf{H}_\mathrm{w}} \; \underset{N_\mathrm{t,w}\times r_\mathrm{w}}{\mathbf{B}_\mathrm{w}} \; \underset{r_\mathrm{w}\times 1}{\mathbf{i}_\mathrm{w}} + \underset{N_\mathrm{r}\times 1}{\mathbf{n}}, \tag{3.1}$$

where $\mathbf{H}_\mathrm{s}$ is the $N_\mathrm{r} \times N_\mathrm{t,s}$ MIMO channel between the serving eNB and NAICS UE. The applied precoding matrix $\mathbf{B}_\mathrm{s}$ for the NAICS UE is size of $N_\mathrm{t,s} \times r_\mathrm{s}$, where r_s denotes the transmission rank in serving cell. The $\mathbf{s}_\mathrm{s}$ is the transmitted signal for the NAICS UE with length of $r_\mathrm{s} \times 1$. Precoding matrices $\mathbf{B}_\mathrm{d}$ and $\mathbf{B}_\mathrm{w}$ and transmitted signals $\mathbf{i}_\mathrm{d}$ and $\mathbf{i}_\mathrm{w}$ are used by dominant interferer and weaker interferer and intended to the users they are currently serving, respectively. Transmission ranks of dominant and weaker interferers are denoted by r_d and r_w, respectively. The channel matrices $\mathbf{H}_\mathrm{d}$ and $\mathbf{H}_\mathrm{w}$ are $N_\mathrm{r} \times N_\mathrm{t,d}$ and $N_\mathrm{r} \times N_\mathrm{t,w}$ MIMO channels between the dominant interferer and NAICS UE and the weaker interferer and NAICS UE, respectively. The $\mathbf{n}$ is the noise vector.

Simulation parameters and assumptions will be described in detail in Section 4.4, but at this point it is sufficient to highlight that all eNBs are using the same number of transmit antennas and only the dominant interferer will be considered in the interference cancellation logic and therefore the weaker interferer can be seen as as co-channel interference source, which is however not targeted by the interference cancellation loop of NAICS UE receiver but treated as additional noise source. With these additional assumptions, the signal model shown in Equation (3.1) can be simplified as follows:

$$\underset{N_\mathrm{r}\times 1}{\mathbf{y}} = \underset{N_\mathrm{r}\times N_\mathrm{t}}{\mathbf{H}_\mathrm{s}} \; \underset{N_\mathrm{t}\times r_\mathrm{s}}{\mathbf{B}_\mathrm{s}} \; \underset{r_\mathrm{s}\times 1}{\mathbf{s}_\mathrm{s}} + \underset{N_\mathrm{r}\times N_\mathrm{t}}{\mathbf{H}_\mathrm{d}} \; \underset{N_\mathrm{t}\times r_\mathrm{d}}{\mathbf{B}_\mathrm{d}} \; \underset{r_\mathrm{d}\times 1}{\mathbf{i}_\mathrm{d}} + \underset{N_\mathrm{r}\times 1}{\mathbf{z}}, \tag{3.2}$$

where $\mathbf{z}$ is

$$\underset{N_\mathrm{r}\times 1}{\mathbf{z}} = \underset{N_\mathrm{r}\times N_\mathrm{t}}{\mathbf{H}_\mathrm{w}} \; \underset{N_t\times r_w}{\mathbf{B}_\mathrm{w}} \; \underset{r_\mathrm{w}\times 1}{\mathbf{i}_\mathrm{w}} + \underset{N_\mathrm{r}\times 1}{\mathbf{n}}. \tag{3.3}$$

Thus $\mathbf{z}$ contains interference from the weaker interferer as well as the noise component and consequently represents residual interference plus noise.

3.2 Channel estimation

As already mentioned in Section 2.6, the receiver can estimate the channel response (or frequency response), $\mathbf{H}$, based on the knowledge about reference signals. In general, reference signals consist of reference symbols (or pilot symbols) of predefined values inserted in predefined resource elements. In this section, a common and efficient method to estimate the frequency response of the channel is described and this method is also applicable for CRS, which was already described in Section 2.6. First, we start examining

the general concept of channel estimation by a simple example. After that, a practical channel estimation method is introduced, that is, Wiener filtering. Then we have a brief look on CRS-IC. Finally, common equalization methods are introduced to get better insight about the usage of channel estimates. This can be also seen as a good introduction for Section 3.5, where common liner receivers are studied in more detail.

As a starting point, a simple example of the usage of one reference symbol is carried out, where only one transmit and receive antenna are considered. A known reference symbol, s_{ref}, is transmitted on a predefined resource element. Then the received signal, y_{ref} at subcarrier f can be expressed as

$$y_{\text{ref}}(f) = h(f)s_{\text{ref}}(f) + n(f), \tag{3.4}$$

where $h(f)$ is the channel frequency response of a pilot subcarrier, i.e., one complex-valued number and $n(f)$ is a noise component. The receiver knows that the transmitted reference symbol is s_{ref}, so it is possible to obtain the frequency response estimate $\hat{h}_{\text{raw}}(f)$, also referred to as raw channel estimate, in that time-frequency location by a simple operation:

$$\hat{h}_{\text{raw}}(f) = \frac{y_{\text{ref}}(f)}{s_{\text{ref}}(f)} + \frac{n(f)}{s_{\text{ref}}(f)}. \tag{3.5}$$

It can be seen that the noise component distorts the raw channel estimate. Now if several resource elements are allocated for the reference signals, it is possible to determine from which time-frequency locations the receiver can obtain the channel estimates and further determine the accuracy of channel estimation. Based on Figures 13 and 14, it can be seen that CRS have relatively high density in both time and frequency directions and thus it is possible to obtain sufficiently accurate channel estimates for the whole time-frequency grid.

When the receiver has obtained all the raw channel estimates, it can estimate the frequency response between the reference symbol locations in the time and frequency direction, i.e., at non-pilot subcarriers. There are several more or less advanced algorithms that can be used for the channel estimation, ranging from simple linear interpolation to estimation relying on more detailed knowledge of the channel characteristics, for example Wiener filtering.

For the simulation results presented in this thesis, Wiener filter is used to estimate the channel response for the whole received subframe. Therefore, only basics of Wiener filtering is described in this section. Wiener filter needs assumptions about the correlation properties of the propagation channel and about the additive noise component to calculate the weights for the filter. In other words, so that the estimator can perform optimally, these properties are assumed to be known at the receiver. The Wiener filter tries to minimize the expected mean squared error between the actual and estimated data [17, p. 49]. The filter takes the raw channel estimates as an input and generates a contiguous estimate of the frequency response as an output.

One practical implementation using the Wiener filter is so called *concatenated frequency and time one dimensional filtering,* which means that at first it is possible to estimate the channel response in frequency direction, that is, for those OFDM symbols where CRS are present. After the channel estimates have been obtained for the first, fifth, eighth and twelfth OFDM symbols, it is possible to interpolate in time direction in order to obtain channel estimates also for the OFDM symbols where CRS are not present. With this approach, it is possible to avert two dimensional filtering and reduce the computational

complexity. The usage of the Wiener filtering in frequency direction is described in more detail in the following.

The raw channel estimates, i.e., the measurements taken from pilot positions, can be expressed as

$$\hat{\mathbf{h}}_{\text{raw}} = \begin{bmatrix} \hat{h}_{\text{raw},0} \\ \vdots \\ \hat{h}_{\text{raw},M-1} \end{bmatrix}$$

from which the Wiener filter generates contiguous channel estimates expressed as

$$\hat{\mathbf{h}} = \begin{bmatrix} \hat{h} \\ \vdots \\ \hat{h}_{L-1} \end{bmatrix}$$

with linear estimation matrix $\mathbf{Q}$ of size $L \times M$, where M denotes the number of pilot subcarriers and L denotes the number of subcarriers to which the channel coefficients are wanted to be estimated. Hence, the estimator is given by

$$\hat{\mathbf{h}} = \mathbf{Q}\hat{\mathbf{h}}_{\text{raw}}. \tag{3.6}$$

Wiener estimator minimizes the mean squared error for each sample and in [17] it is shown that the estimation matrix can be solved as

$$\mathbf{Q} = \mathbf{R}_{\hat{\text{h}}_{\text{raw}}\text{h}}\mathbf{R}_{\text{h}}^{-1}, \tag{3.7}$$

where $\mathbf{R}_{\text{h}}$ is the channel auto-correlation matrix and $\mathbf{R}_{\hat{\text{h}}_{\text{raw}}\text{h}}$ is the cross-correlation matrix between raw channel estimates and the channel, which both depend on the frequency auto-correlation function. The frequency auto-correlation function is a Fourier transform of the power delay spectrum. In addition, the auto-correlation matrix uses an estimate of the noise component [4, p. 76].

As an example, if one resource block during the fifth OFDM symbol is considered, there are two pilot subcarriers and ten data subcarriers per CRS port. Also estimation operation is based on a pilot window of one PRB in width. Channel estimates $\hat{\mathbf{h}}$ are wanted to be calculated for these twelve subcarriers using the Wiener filter. At first, the channel measurements, i.e., the raw channel estimates are taken from the two pilot subcarries so that

$$\hat{\mathbf{h}}_{\text{raw}} = \begin{bmatrix} \hat{h}_{\text{raw},1} \\ \hat{h}_{\text{raw},2} \end{bmatrix}.$$

Hence, the estimation matrix $\mathbf{Q}$ is of the size 12×2. It is assumed that the estimation matrix, $\mathbf{Q}$, has been solved, so the channel estimates $\hat{\mathbf{h}}$ can be calculated as

$$\begin{bmatrix} \hat{h}_1 \\ \vdots \\ \hat{h}_{12} \end{bmatrix} = \begin{bmatrix} q_{1,1} & q_{1,2} \\ \vdots & \vdots \\ q_{12,1} & q_{12,2} \end{bmatrix} \times \begin{bmatrix} \hat{h}_{\text{raw},1} \\ \hat{h}_{\text{raw},2} \end{bmatrix}.$$

This is illustrated in Figure 17. The interpolation coefficients do not depend on absolute positions of channel measurements. Therefore, it is possible to calculate channel estimates for the whole frequency band by using the same estimation matrix $\mathbf{Q}$ and sliding

the filter window over the whole frequency band. In general it can be said that the larger the filter window is, the more accurate channel estimates can be obtained as more channel measurements have been taken into account. On the other hand, larger **Q** requires more computation. It is also good to bear in mind that the filter window size should be properly dimensioned with the coherence bandwidth of the channel. This means that the filter window size should be smaller or equal than the coherence bandwidth. However, more detailed derivation and description of the Wiener filtering are out of the scope of this thesis.

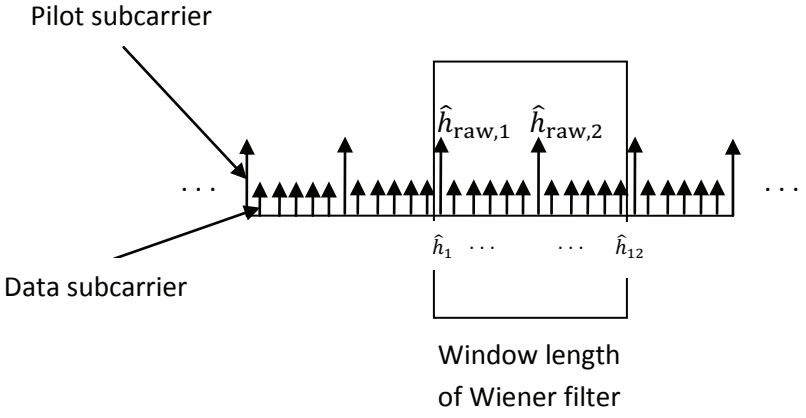

Figure 17: *Wiener filter calculates channel estimates for twelve subcarriers from two raw channel estimates.*

After the channel estimates have been obtained in frequency direction for those OFDM symbols where CRS are present, the next step is to interpolate in time direction over those OFDM symbols where CRS are not present by using the same Wiener filter principle. In the case of MIMO, when CRS is transmitted in specific resource elements from a certain antenna port, nothing is transmitted in these resource elements from other antenna ports. Hence this same processing can be performed between all the transmit and receive antenna pairs in order to obtain channel estimates also in spatial domain. Finally the physical channel matrix **H** can be constructed for each subcarrier within a subframe. For instance in the case of two transmit and two receive antennas, the channel matrix **H** is size of 2×2 as illustrated in Figure 11.

The concept of effective channel estimate

In principle, an effective channel estimate means that the precoding has been taken into account in the channel estimate. The receiver needs the knowledge about the precoding matrix used by the transmitter in order to calculate the effective channel estimate. In the following we assume that the receiver knows the precoding matrix used by the transmitter.

To clarify the usage and calculation of the effective channel estimate, Equation (3.1) can be considered as a starting point. However, for simplicity and convenience, only single link model is considered in the following. Basically this means excluding interferers' contribution from the Equation and thus the Equation can be rewritten as follows:

$$\underset{N_\mathrm{r}\times 1}{\mathbf{y}} = \underset{N_\mathrm{r}\times N_\mathrm{t}}{\mathbf{H}_\mathrm{S}} \; \underset{N_\mathrm{t}\times r_\mathrm{s}}{\mathbf{B}_\mathrm{S}} \; \underset{r_\mathrm{s}\times 1}{\mathbf{s}_\mathrm{S}} + \underset{N_\mathrm{r}\times 1}{\mathbf{n}}, \tag{3.8}$$

where notations are the same as in Equation (3.1). In order to obtain the effective channel matrix, precoding matrix $\mathbf{B}_\mathrm{s}$ is multiplied by the physical channel matrix $\mathbf{H}_\mathrm{s}$ as follows:

$$\underset{N_r \times r_s}{\mathbf{H}_{\mathrm{s,eff}}} = \underset{N_r \times N_t}{\mathbf{H}_\mathrm{s}} \quad \underset{N_t \times r_s}{\mathbf{B}_\mathrm{s}} \; . \tag{3.9}$$

Thus Equation (3.8) can be rewritten in the form of:

$$\underset{N_\mathrm{r} \times 1}{\mathbf{y}} = \underset{N_\mathrm{r} \times r_\mathrm{s}}{\mathbf{H}_{\mathrm{s,eff}}} \quad \underset{r_\mathrm{s} \times 1}{\mathbf{s}_\mathrm{s}} + \underset{N_\mathrm{r} \times 1}{\mathbf{n}}, \tag{3.10}$$

For convenience, from now on the effective channel estimate is used in equations instead of physical channel estimate and precoding matrix. Effective channel estimate is needed and used in equalization as well as in interference covariance estimation, which are described in more detail later in this chapter.

CRS Interference Cancellation

From NAICS system perspective, there are two different scenarios where CRS interference cancellation (CRS-IC) can be used to improve overall system performance, namely colliding and non-colliding CRS scenarios. In the case of colliding CRS, at least CRS transmitted from the dominant interfering eNB collides with CRS of the serving eNB. In other words, interfering and serving eNBs transmit CRS on the same time-frequency positions, that is, on the same resource elements. Whereas in the case of non-colliding CRS, at least CRS transmitted from the dominant interfering eNB collides with PDSCH of the serving eNB and consequently CRS of the interfering eNB distorts some of the PDSCH resource elements of the serving eNB. Naturally, these two scenarios have different kind of impact on the overall system performance and thus they need to be taken explicitly into account in the receiver. In the case of colliding CRS, CRS-IC can be used to improve the quality of channel estimates by cleaning the interfering CRS from the desired CRS. Whereas in the case of non-colliding CRS, CRS-IC can be used to clean those PDSCH REs, which contains CRS from the interfering eNB and consequently it can improve the performance of detection and demodulation of PDSCH. Note that CRS-IC can also be used in the same way to improve the interfering links' channel estimation and PDSCH demodulation performance in the case of colliding CRS and non-colliding CRS, respectively.

In practice, only interfering CRS above a certain minimum power level can be detected and subtracted from the desired signal. The rest can be treated as noise [19]. In this thesis, simulation setup is chosen so that the dominant interferer has colliding CRS while the weaker interferer has non-colliding CRS as shown in simulation assumptions in Table 9. However, the power level of weaker interferer is so low that it has not been considered in any IC logic and consequently it can be seen as additional noise.

The actual algorithm for CRS-IC is implementation specific but in principle it requires the following steps in the case of colliding CRS. At first, CRS of the interfering eNBs are received in addition to CRS of the serving eNB and based on the received CRS from different eNBs, SINR for each eNB's signal at NAICS UE can be estimated as described in more detail in the next section. Based on these SINR estimates, it can be decided which interferers can be canceled. In order to perform CRS-IC, channel estimation is required for all links, that is, CRS based channel estimation is performed also for interferers. So that UE in serving cell can estimate links (or channels) from interfering cells, UE needs

knowledge also about the reference signals used in interfering cells. Thus network assistance is needed, that is, serving cell has the knowledge about the used reference signals in interfering cells and signals this information to the served UE, which then performs the CRS-IC based on this knowledge.

The CRS-IC flow could be as follows. First, channel estimation is performed for the serving cell. Secondly, based on the serving cell channel estimation, CRS-IC can be performed for the interfering cell. Then channel estimation can be performed for the interfering cell and based on that, CRS-IC can be performed for the serving cell. Finally, channel estimation is performed again for the serving cell but now from the cleaned signal. Consequently the quality of the second channel estimation for the serving cell has been improved. This final channel estimation can be then passed for further processing.

In the case of non-colliding CRS, PDSCH REs can be cleaned based on the channel estimates of serving cell and interfering cell. To be more exact, contribution of CRS from interfering eNBs can be subtracted based on CRS channel estimates from those REs where PDSCH and CRS collide. Exact mathematical modeling of CRS-IC is not crucial for this thesis and thus it is skipped. At this point it is good to highlight that in this thesis, CRS-IC can be used with SLIC receiver but not with LMMSE-IRC receiver as information about interfering eNBs' CRS is not signaled for UEs with only LMMSE-IRC receiver.

3.3 Interference plus noise power estimation

Many receiver functions require knowledge about the interference plus noise power to perform optimally. Therefore, in practical systems, interference plus noise variance estimation is essential. From now on, noise plus interference power is denoted as $IoNo_{\text{est}}$, where Io and No represent the interference power and the noise power, respectively.

In principle, $IoNo_{\text{est}}$ can be estimated by using reference signals as they are known to the receiver in advance. There are several possible methods to do the estimation but in this thesis we consider only one of them, namely differential estimation method. When using the differential estimation method, it is assumed that channel estimates obtained from two consecutive pilot subcarriers are approximately the same in frequency or in time direction. In other words, the pilot subcarrier spacing in frequency or in time direction should be sufficiently small compared to the channel coherence bandwidth or to the channel coherence time, respectively. Hence the estimation can be performed either in frequency or in time direction based on the channel properties. For example, if the channel response is highly frequency selective but the UE is stationary, estimation should be performed in time domain. On the other hand, if the channel coherence bandwidth is sufficiently large but the UE is moving fast, estimation should be performed in frequency domain.

In this thesis, two transmit antennas are used with CRS based transmission mode. Hence the spacing between two CRS REs is six subcarriers, which corresponds to 90 kHz bandwidth. Especially with the channel model[7] used in this thesis, the coherence bandwidth is large enough. Therefore estimation can be performed in frequency direction.

The received reference signal y_{ref} from one antenna port at one pilot subcarrier is of the form

$$y_{\text{ref}}(f,t,N_{r,idx}) = h(f,t,N_{r,idx})s_{\text{ref}}(f,t,N_{r,idx}) + e(f,t,N_{r,idx}), \tag{3.11}$$

[7]Channel model is so called "ITU Extended Pedestrian A". This will be described in more detail in Section 4.3.

where f denotes subcarrier index, t denotes OFDM symbol index, $N_{r,idx}$ denotes receive antenna index, h is the unknown complex channel coefficient, s_{ref} is the transmitted reference symbol known to the receiver and e is unknown raw estimate of the residual interference plus noise. Using the assumption that channel estimates obtained from two consecutive pilot subcarriers are approximately the same in frequency or in time direction, raw estimate of the residual interference plus noise, e, can be calculated for every pilot subcarrier within a subframe and over all the receive antennas. Exact mathematical modeling is left out from this thesis.

In order to obtain the interference plus noise variance, all the raw estimates are first multiplied by their complex conjugate, then these are added and finally averaged by the total number of all terms. Thus the interference plus noise variance is given by

$$\sigma_{I_oN_o,avg} = \frac{1}{N_r\left(N_{PRB}*2-1\right)*4} * \sum_{N_r}\sum_{t}\sum_{f} e(f,t,N_{r,idx})e^*(f,t,N_{r,idx}), \tag{3.12}$$

where N_r is the number of receive antennas, N_{PRB} is number of physical resource blocks within downlink bandwidth, 2 denotes number of CRS REs within an OFDM symbol and 4 is the number of OFDM symbols where CRS are present in the case of two transmit antennas. Now the $IoNo_{\text{est}}$ can be simply obtained as follows:

$$IoNo_{\text{est}} = \sigma^2_{I_oN_o,avg}. \tag{3.13}$$

The $IoNo_{\text{est}}$ can be used to estimate SINR when also the receive signal power is known:

$$SINR = 10*\log_{10}\left(\frac{signalPower}{IoNo_{\text{est}}}\right) \text{dB}. \tag{3.14}$$

In real system, receive signal power can be estimated also from reference signals. However, especially in link-level simulations signal power of the serving cell is normalized to one, thus SINR can be calculated as follows:

$$SINR = 10*\log_{10}\left(\frac{1}{IoNo_{\text{est}}}\right) \text{dB}. \tag{3.15}$$

It is good to point out here that this differential estimation method can be used also for interference covariance estimation as shown in the next section.

3.4 Covariance estimation

Covariance matrix of received signal is needed in interference-suppressing demodulation, that is, in interference-aware receivers, which will be described in Section 3.5. There are several methods to do the covariance estimation with different degrees of precision. The precision depends on the assumptions of the interference behavior, the complexity of the estimation algorithm and the available information about channels of interfering links. The more precise is the interference estimate in covariance matrix, the better the interference can be suppressed, which in turn improves the post-processing SINR of the receiver.

The general form of covariance matrix of the receive signal $\mathbf{y}$ can be derived as follows:

$$\mathbf{C}_{\mathbf{y}} = E\left[\mathbf{y}\mathbf{y}^{\text{H}}\right], \tag{3.16}$$

where $\mathbf{y}$ is the form of:

$$\mathbf{y} = \mathbf{H}_{\text{eff}}\mathbf{s} + \mathbf{r}, \tag{3.17}$$

Where $\mathbf{r}$ represents total interference plus noise. Now the derivation of covariance matrix is the following:

$$\mathbf{C}_{\mathbf{y}} = E\left[\mathbf{H}_{\text{eff}}\mathbf{s}\left(\mathbf{H}_{\text{eff}}\mathbf{s}\right)^{\text{H}}\right] + \mathbf{R}_{\mathbf{r}} = E\left[\mathbf{H}_{\text{eff}}\mathbf{s}\mathbf{s}^{\text{H}}\mathbf{H}_{\text{eff}}^{\text{H}}\right] + \mathbf{R}_{\mathbf{r}}, \tag{3.18}$$

where $\mathbf{R}_{\mathbf{r}} = E[\mathbf{r}\mathbf{r}^{\text{H}}]$ is the covariance matrix of interference plus noise vector $\mathbf{r}$. Effective channel matrix $\mathbf{H}_{\text{eff}}$ can be seen as a constant with respect to the transmitted vector $\mathbf{s}$. In addition, transmitted vector $\mathbf{s}$ can be assumed to be fully uncorrelated with its hermitian transpose, thus

$$E\left[\mathbf{s}\mathbf{s}^{\text{H}}\right] = \begin{bmatrix} \sigma_{\text{s}}^2 & 0 \\ 0 & \sigma_{\text{s}}^2 \end{bmatrix} = \sigma_{\mathbf{s}}^2\mathbf{I},$$

where $\sigma_{\mathbf{s}}^2$ is the power of signal $\mathbf{s}$. Consequently, covariance matrix of the receive vector $\mathbf{y}$ can be written as follows:

$$\mathbf{C}_{\mathbf{y}} = E\left[\mathbf{y}\mathbf{y}^{\text{H}}\right] = \sigma_{\mathbf{s}}^2\mathbf{H}_{\text{eff}}\mathbf{H}_{\text{eff}}^{\text{H}} + \mathbf{R}_{\mathbf{r}}. \tag{3.19}$$

At first, the simplest form of interference plus noise covariance is considered, that is, the interference is assumed to be both spatially and spectrally white. This means that the interference power level is assumed to be the same at each receive antenna and at each subcarrier of the system. Furthermore, interference is assumed to be fully uncorrelated between the receive antennas. Thus it can be presented as a single positive scalar. This single positive scalar is in fact the $IoNo_{\text{est}}$, which was derived in the previous Section 3.3. In this case, the covariance matrix of interference plus noise $\mathbf{R}_{\mathbf{r}}$ is of the form:

$$\mathbf{R}_{\mathbf{r}} = IoNo_{\text{est}}\mathbf{I}_{N_r}, \tag{3.20}$$

where $IoNo_{\text{est}}$ can be estimated as shown in previous Section 3.3 and $\mathbf{I}_{N_r}$ is an identity matrix with N_r diagonal elements. So although $\mathbf{C}_{\mathbf{y}}$ is calculated for each subcarrier, the same averaged interference estimate is applied throughout the subcarriers. However, an assumption about spatially and spectrally white interference may be too restrictive so that advanced interference-aware receivers can perform optimally. Consequently better performance should be achieved when interference covariance matrices are estimated on per-subcarrier basis by including also proper off-diagonal elements. In the following, two of such methods are described in more detail.

Differential covariance estimation

In differential covariance estimation, the UE does not have knowledge about the effective channel of interfering links. Thus estimation relies fully on knowledge obtained from own reference signals. The algorithm flow in principle is the same as in differential interference plus noise power estimation, that is, the channel estimates obtained from two consecutive pilot subcarriers are assumed to be approximately the same in frequency or in time direction. However, now also spatial properties of the interference plus noise are estimated. This means that instead of treating each receive antenna separately, spatial properties of the received reference signal is taken into account. Consequently the received reference signal at one pilot subcarrier is of the form:

$$\underset{N_r \times 1}{\mathbf{y}_{\text{ref}}(f,t)} = \underset{N_r \times 1}{\mathbf{H}(f,t)} \ \underset{1 \times 1}{x_{\text{ref}}(f,t)} \ + \ \underset{N_r \times 1}{\mathbf{e}(f,t)}, \tag{3.21}$$

where notations are the same as in Equation (3.11). The exact mathematical modeling is left out and it is sufficient to state that the raw interference plus noise covariance estimate for one pilot subcarrier, $\mathbf{e}(f,t)$, can be calculated using the assumption that channel estimates obtained from two consecutive pilot subcarriers are assumed to be approximately the same.

Now the raw interference plus noise covariance estimate for one pilot subcarrier can be obtained as

$$\mathbf{R}_{\mathbf{r},\text{raw}}(f,t) = \mathbf{e}(f,t)\mathbf{e}^{\text{H}}(f,t). \tag{3.22}$$

Above raw interference plus noise covariance estimate can be calculated naturally only for pilot subcarriers similarly to raw channel estimates as described in Section 3.2. Thus interpolation in time and frequency is needed to obtain estimates also for subcarriers between the pilot subcarriers. In addition, interference averaging, i.e., smoothing of raw estimates can be performed to potentially improve the estimation. With these procedures, one can obtain interference plus noise covariance estimate $\mathbf{R}_\mathbf{r}$ for all subcarriers within a subframe. However, these procedures are implementation specific. Consequently, from the perspective of this thesis, the exact description of algorithms for interpolating and smoothing raw interference plus noise covariance estimates are not as important as the fact that there are such methods. Because of this, it is assumed that with the differential estimation method, one can obtain interference plus noise covariance estimates for all subcarriers within a subframe.

The actual covariance matrix used for demodulation can be now written as follows

$$\mathbf{C}_\mathbf{y} = \sigma_\mathbf{s}^2 \mathbf{H}_{\text{eff}} \mathbf{H}_{\text{eff}}^{\text{H}} + \mathbf{R}_\mathbf{r}. \tag{3.23}$$

Differential estimation method is a useful way to estimate interference covariance matrices with off-diagonal elements on per-subcarrier basis in situations when UE does not have more explicit knowledge about interfering links. In other words, with such interference covariance matrix estimate, interference-aware receivers can perform more optimally compared to previous situation where interference level was assumed to be both spatially and spectrally white. However, even better interference estimation can be performed if additional knowledge about interfering links is available as shown in the next subsection.

Network Assisted Covariance Estimation

In network assisted (NA) covariance estimation, the most fundamental fact is that the serving cell has knowledge about reference signals and precoding matrices used in neighbouring cells. This information is then signaled to the served UE. Consequently UE has the capability to estimate also the effective channel of interfering links. To be more exact, UE receives also reference signals of interfering cells, estimates physical channel of interfering links similarly to its own channel and finally, by using the knowledge about precoding matrix used in interfering links, UE can also calculate the effective channel for interfering links. However, it is good to point out that the precoding matrix (or PMI) used in interfering cells is one of the parameters that can be blindly detected in UE. Thus

dynamic signaling of interferer's PMI is not necessity if UE has blind PMI detector as well.

Based on the above description, it can be assumed that UE has estimated the effective channel at least for the dominant interferer in addition to its own effective channel. Thus the interference plus noise covariance matrix for the serving cell can be derived similarly to Equation (3.19) as follows:

$$\mathbf{R}_{\mathbf{r}}^{(\mathrm{s})} = \sigma_{\mathbf{i}_{\mathrm{d}}}^2 \mathbf{H}_{\mathrm{d,eff}} \mathbf{H}_{\mathrm{d,eff}}^{\mathrm{H}} + \sigma_{\mathrm{No}}^2 \mathbf{I}, \tag{3.24}$$

where $\mathbf{H}_{\mathrm{d,eff}}$ is the effective channel estimate of dominant interferer, $\sigma_{\mathbf{i}_{\mathrm{d}}}^2$is the power of the dominant interfering signal, σ_{No}^2 is the noise power and $(.)^{(s)}$ denotes serving cell. Next the interference covariance matrix for the dominant interferer can be derived similarly to serving cell's:

$$\mathbf{R}_{\mathbf{r}}^{(\mathrm{d})} = \sigma_{\mathbf{s}_{\mathrm{s}}}^2 \mathbf{H}_{\mathrm{s,eff}} \mathbf{H}_{\mathrm{s,eff}}^{\mathrm{H}} + \sigma_{\mathrm{No}}^2 \mathbf{I}, \tag{3.25}$$

where $\mathbf{H}_{\mathrm{s,eff}}$ is now the effective channel estimate of serving cell and $\sigma_{\mathbf{s}_{\mathbf{s}}}^2$is the power of the serving cell (desired) signal. Note that the interference covariance matrix can consist of several interference covariance matrices, that is, if UE has estimated effective channels of multiple interfering links, interference covariance matrix in the general case is of the form:

$$\mathbf{R}_{\mathbf{r}} = \sum_{\mathrm{i}=1}^{N} \sigma_{\mathrm{i}}^2 \mathbf{H}_{\mathrm{i,eff}} \mathbf{H}_{\mathrm{i,eff}}^{\mathrm{H}} + \sigma_{No}^2 \mathbf{I}, \tag{3.26}$$

where N is the number of interferers.

Now the actual covariance matrix used for demodulation of the desired signal can be written similarly to Equation (3.23) as

$$\mathbf{C}_{\mathbf{y}}^{(\mathrm{s})} = \sigma_{\mathbf{s}_{\mathrm{s}}}^2 \mathbf{H}_{\mathbf{s},\mathrm{eff}} \mathbf{H}_{\mathbf{s},\mathrm{eff}}^{\mathrm{H}} + \mathbf{R}_{\mathbf{r}}^{(\mathrm{s})}. \tag{3.27}$$

And the covariance matrix used for demodulating the dominant interfering signal can be written as

$$\mathbf{C}_{\mathbf{y}}^{(\mathrm{d})} = \sigma_{\mathbf{i}_{\mathrm{d}}}^2 \mathbf{H}_{\mathrm{d,eff}} \mathbf{H}_{\mathrm{d,eff}}^{\mathrm{H}} + \mathbf{R}_{\mathbf{r}}^{(\mathrm{d})}. \tag{3.28}$$

It is good to highlight here that $\mathbf{R}_{\mathbf{r}}^{(\mathrm{d})}$ will be needed also for blind PDSCH to CRS power ratio detection (P_a detection) as will be shown in Section 5, where algorithm for P_a detection is described. Note that only the dominant interferer and noise variance have been taken into account in NA covariance estimate and the weaker interferer is left out. This is due to the fact that weaker interferer is not targeted by the interference cancellation loop of NAICS UE receiver.

3.5 User equipment receivers

In this section, we start by briefly describing the purpose of equalization in a receiver. Then the following linear receivers are introduced: Maximal Ratio Combining (MRC), Linear Minimum Mean Squared Error (LMMSE) combining and Interference Rejection Combining (IRC). These receivers use different assumptions about the radio environment, e.g., about inter-stream and inter-cell interference. Finally, one non-linear receiver is introduced, namely Symbol Level Interference Cancellation (SLIC).

Purpose of equalization

Channel modeling and characteristics are described in more detail in Section 4.3 but at this point it is sufficient to highlight that usually there is delay dispersion in wireless channels, i.e., multi-path components arrive to the receiver with different delays and amplitudes. Delay dispersion can cause ISI, which disturbs the transmitted signal and can lead to a considerable bit error rate (BER) degradation [14]. Delay dispersion corresponds to frequency selectivity in the frequency domain, i.e., the transfer function is not constant over the system bandwidth.

In general, equalization can be implemented either in the time domain or in the frequency domain but in the case of an OFDM system, frequency domain equalization is more suitable. Furthermore, most of other receiver processing in OFDM systems is carried out in the frequency domain, because it reduces the complexity compared to the time domain processing [2].

In general, equalizers can be seen as receiver structures which reduce or eliminate ISI, meaning that they try to restore the original signal shape, at least to some extent. However, in most cases there is no ISI in OFDM systems due to usage of cyclic-prefix, as described in Section 2.1. Therefore the ultimate goal of an equalizer in an OFDM system is to minimize the bit error rate caused by the frequency selective channel, noise and interference. Interference can consist of inter-cell interference, intra-cell interference and multi-stream interference. Multi-stream interference can occur in MIMO systems in the case of spatial multiplexing, i.e., when multiple parallel communication channels are used over the radio interface. There are many possible methods to do the equalization and they have different level of complexity and performance. Thus it is crucial to use proper equalization method for different situations.

To properly compensate the effects caused by the channel, noise and interference to the transmitted symbol vector, the receiver should multiply the received signal by receive filter $\mathbf{W}$, per subcarrier, to obtain an estimate from the transmitted symbol vector as shown below:

$$\underset{r_s \times 1}{\hat{\mathbf{s}}} = \underset{r_s \times N_r}{\mathbf{W}^{\mathrm{H}}} \underset{N_r \times 1}{\mathbf{y}}, \tag{3.29}$$

where r_s denotes the number of transmission layers, i.e., the transmission rank and N_r is the number of receive antennas. In the case of MIMO and multi-layer transmission, that is, $r_s > 1$, the purpose of receive filter $\mathbf{W}$ is also spatial separation of received multiple parallel data streams in addition to equalization.

After the equalization, an estimate of the transmitted signal can be forwarded for further processing, for example, to data demodulation and channel decoding. In Section 2.5, the most simple equalization method was introduced in the context of MIMO channel, namely Zero-Forcing criterion. Zero-Forcing equalizer does not use any knowledge about noise nor interference. It may minimize ISI but it also amplifies noise and interference especially at frequencies where channel transfer function attains small values. Thus Zero-Forcing criterion is only applicable for situations where channel transfer function is relatively constant over the whole bandwidth and in such environments where are no intra-cell nor inter-cell interference.

There are receivers which construct the receive filter $\mathbf{W}$ in a more sophisticated way while utilizing more detailed assumptions about the radio environment. In the following, some of these equalization methods are introduced in more detail in a general case, where MIMO channel and precoding are considered.

Maximum Ratio Combining- MRC

In maximum ratio combining, interference is considered as white noise and thus only knowledge about the own effective channel is required. The receive filter for MRC is as follows [22]

$$\mathbf{W}_{\mathrm{MRC}}^{\mathrm{H}} = \mathbf{H}_{\mathrm{eff}}^{\mathrm{H}} = (\mathbf{HB})^{\mathrm{H}}. \tag{3.30}$$

In the case of fully orthogonal effective channel, MRC is able to maximize the SNR for each data stream separately, which results in the SNR-optimal total solution [21]. However, in practice the effective channel is not fully orthogonal due to imperfect precoding and channel estimation error. Consequently, the effective channel causes intra-stream interference and hence MRC is not able to optimize the overall SINR.

Linear Minimum Mean Squared Error - LMMSE

Linear Minimum Mean Squared Error combining takes into account multi-stream interference. In addition, LMMSE can take into account spatial properties of received interference plus noise [23]. LMMSE is able to minimize this multi-stream interference and thus LMMSE solution is more optimal solution than MRC in the case of non-orthogonal effective channel. The receive filter for LMMSE in general form is solved in the following.

By assuming the following linear signal model

$$\mathbf{y} = \mathbf{H}_{\mathrm{eff}}\mathbf{s} + \mathbf{r},$$

the LMMSE estimator can be written as

$$E[\mathbf{y}\mathbf{y}^{\mathrm{H}}]\mathbf{W}_{\mathrm{LMMSE}} = E[\mathbf{y}\mathbf{s}^{\mathrm{H}}], \tag{3.31}$$

where $E[\mathbf{y}\mathbf{y}^{\mathrm{H}}] = \mathbf{C}_{\mathbf{y}}$, namely the covariance of receive signal $\mathbf{y}$, and $E[\mathbf{y}\mathbf{s}^{\mathrm{H}}] = \mathbf{C}_{\mathbf{ys}}$, namely the covariance of the received signal $\mathbf{y}$ and the original data symbol vector $\mathbf{s}$. $\mathbf{C}_{\mathbf{y}}$ has been solved already in Equation (3.19) and is of the form:

$$\mathbf{C}_{\mathbf{y}} = E\left[\mathbf{y}\mathbf{y}^{\mathrm{H}}\right] = \sigma_{\mathbf{s}}^2\mathbf{H}_{\mathrm{eff}}\mathbf{H}_{\mathrm{eff}}^{\mathrm{H}} + \mathbf{R}_{\mathbf{r}}. \tag{3.32}$$

where $\mathbf{R}_{\mathbf{r}} = E[\mathbf{r}\mathbf{r}^{\mathrm{H}}]$ denotes the interference plus noise covariance matrix. Next the $\mathbf{C}_{\mathbf{ys}}$ can be solved as follows

$$\mathbf{C}_{\mathbf{ys}} = E[\mathbf{H}_{\mathrm{eff}}\mathbf{s}\mathbf{s}^{\mathrm{H}} + \mathbf{n}\mathbf{s}^{\mathrm{H}}] = \sigma_{\mathbf{s}}^2\mathbf{H}_{\mathrm{eff}}. \tag{3.33}$$

Finally the receive filter for LMMSE combiner can be written as

$$\mathbf{W}_{\mathrm{LMMSE}} = \mathbf{C}_{\mathbf{y}}^{-\mathbf{1}}\mathbf{C}_{\mathbf{ys}} = (\sigma_{\mathbf{s}}^2\mathbf{H}_{\mathrm{eff}}\mathbf{H}_{\mathrm{eff}}^{\mathrm{H}} + \mathbf{R}_{\mathbf{r}})^{-1}\sigma_{\mathbf{s}}^2\mathbf{H}_{\mathrm{eff}}. \tag{3.34}$$

In Equation (3.34), the first component, $\mathbf{H}_{\mathrm{eff}}\mathbf{H}_{\mathrm{eff}}^{\mathrm{H}}$, describes the multi-stream interference, whereas the the second component, $\mathbf{R}_{\mathbf{r}}$, describes the spatial properties of received interference plus noise.

The capability of LMMSE receiver to suppress inter-cell interference depends heavily on the accuracy of interference plus noise covariance estimation, that is, properties of $\mathbf{R}_{\mathbf{r}}$. In Section 3.4, three different interference plus noise covariance estimation methods

were introduced. These three methods do the interference plus noise covariance estimation with different degrees of precision. The precision depends on the assumptions of the interference behavior, the complexity of the estimation algorithm and the available information about channels of interfering links. The more precise the interference plus noise covariance $\mathbf{R_r}$ is, the better the interference can be suppressed, which in turn improves the post-processing SINR of LMMSE receiver, or in other words, results in better performing LMMSE receiver.

If only a scalar estimate of interference plus noise can be obtained as described in Section 3.3, the $\mathbf{R_r}$ is of the form:

$$\mathbf{R_r} = IoNo_{\text{est}}\mathbf{I}_{N_r}.$$

Herein we will refer to the LMMSE combiner with only a scalar estimate of interference plus noise as LMMSE-White. The receive filter for LMMSE-White can be written as:

$$\mathbf{W}_{\text{LMMSE-White}} = (\sigma_{\mathbf{s}}^2\mathbf{H}_{\text{eff}}\mathbf{H}_{\text{eff}}^{\text{H}} + IoNo_{\text{est}}\mathbf{I}_{\mathbf{N_r}})^{-1}\sigma_{\mathbf{s}}^2\mathbf{H}_{\text{eff}}. \tag{3.35}$$

From NAICS system point of view, an assumption about spatially and spectrally white interference is too restrictive. Consequently better performance is achieved when interference covariance matrices are estimated on per-subcarrier basis by including also proper off-diagonal elements as described in Section 3.4. In the following, three of such receivers are described in more detail.

Interference Rejection Combining - IRC

If interference plus noise is not spatially white, that is, $\mathbf{R_r}$ contains proper off-diagonals in addition to antenna port specific interference plus noise power in diagonal, LMMSE solution is often called as LMMSE - Interference Rejection Combiner, i.e., LMMSE-IRC. Note that the general LMMSE solution in Equation (3.34) is the same also for LMMSE-IRC but the structure of $\mathbf{R_r}$ is specific.

LMMSE-IRC receiver requires interference plus noise covariance estimation which describes spatial properties of received inter-cell interference plus noise. The performance of LMMSE-IRC receiver, or in other words, the capability of LMMSE-IRC receiver to suppress inter-cell interference depends heavily on the accuracy of interference plus noise covariance estimation.

If UE does not have knowledge about the effective channel of interfering links, the interference plus noise covariance estimation relies fully on knowledge obtained from own reference signals. As described in Section 3.4, differential covariance estimation method can be used to obtain such $\mathbf{R_r}$. Hence the receive filter for LMMSE-IRC can be written similarly as in Equation (3.34):

$$\mathbf{W}_{\text{LMMSE-IRC}} = (\sigma_{\mathbf{s}}^2\mathbf{H}_{\text{eff}}\mathbf{H}_{\text{eff}}^{\text{H}} + \mathbf{R_r})^{-1}\sigma_{\mathbf{s}}^2\mathbf{H}_{\text{eff}}. \tag{3.36}$$

where $\mathbf{R_r}$ now consist of proper off-diagonal elements, that is, $\mathbf{R_r}$ has now spatial properties. From now on, LMMSE-IRC is called just IRC for convenience.

If UE has the capability to estimate also effective channel of interfering links via network assistance, network assisted covariance estimation can be performed to obtain even more accurate interference plus noise covariance estimate as described in Section 3.4. In this case, LMMSE solution is often called as Enhanced-IRC (E-IRC) and $\mathbf{R_r}$ is of the form:

$$\mathbf{R_r} = \sum_{\mathrm{i}=1}^{N} \sigma_{\mathrm{i}}^2 \mathbf{H}_{\mathrm{i,eff}} \mathbf{H}_{\mathrm{i,eff}}^{\mathrm{H}} + \sigma_{No}^2 \mathbf{I}, \tag{3.37}$$

where N is the number of interfering cells. Hence the receive filter for E-IRC can be written as

$$\mathbf{W}_{\mathrm{E-IRC}} = (\sigma_{\mathbf{s}}^2 \mathbf{H}_{\mathrm{eff}} \mathbf{H}_{\mathrm{eff}}^{\mathrm{H}} + \sum_{\mathrm{i}=1}^{N} \sigma_{\mathbf{i}}^2 \mathbf{H}_{\mathrm{i,eff}} \mathbf{H}_{\mathrm{i,eff}}^{\mathrm{H}} + \sigma_{\mathrm{No}}^2 \mathbf{I})^{-1} \sigma_{\mathbf{s}}^2 \mathbf{H}_{\mathrm{eff}}. \tag{3.38}$$

In this theses, the baseline receiver is IRC with differential covariance estimation.

Symbol Level Interference Cancellation - SLIC

SLIC receiver can be described as a successive interference cancellation receiver which operates by successively applying linear detection, reconstruction and cancellation of interferer(s) signal at symbol level. Thus, the performance of the SLIC receiver is depending on how good estimate of the interfering signal can be reconstructed. In order to reconstruct the interfering signal, SLIC needs the knowledge of specific parameters of the interfering cell. For reconstruction of interfering signal, UE needs knowledge about PMI, modulation order and P_a used in the interfering cell. In addition, in order to obtain effective channel of interfering link for interference plus noise covariance estimation as well as for reconstruction, UE needs knowledge about reference signals used in the interfering cell. This knowledge is also provided by the network. In the following, SLIC receiver is described in more detail with the assumption that all the above mentioned necessary information is available.

In simulations used in this thesis, only the dominant interferer is treated by the SLIC receiver while the weaker interferer can be seen as as co-channel interference source, which is however not targeted by the SLIC receiver but treated as additional noise source. Thus the following description is considering only the dominant interferer for simplicity. However, extending the description for arbitrary number of interfering signals is straightforward. As shown already in Equation (3.2), the received signal is of the form:

$$\mathbf{y} = \mathbf{H}_{\mathrm{s,eff}} \mathbf{s}_{\mathrm{s}} + \mathbf{H}_{\mathrm{d,eff}} \mathbf{i}_{\mathrm{d}} + \mathbf{z}, \tag{3.39}$$

where $\mathbf{H}_{\mathrm{s,eff}}$ and $\mathbf{H}_{\mathrm{d,eff}}$ are the effective channels of serving cell and dominant interfering cell, respectively, $\mathbf{s}_{\mathrm{s}}$ and $\mathbf{i}_{\mathrm{d}}$ are the transmitted symbol vectors of serving cell and dominant interfering cell, respectively, and $\mathbf{z}$ is the residual interference plus noise vector. At first, E-IRC linear detection is applied to the dominant interfering signal to obtain E-IRC estimate of $\mathbf{i}_{\mathrm{d}}$:

$$\hat{\mathbf{i}}_{\mathrm{d}} = \mathbf{W}_{\mathrm{E-IRC,d}}^{\mathrm{H}} \mathbf{y}, \tag{3.40}$$

where the receive filter for E-IRC is

$$\mathbf{W}_{\mathrm{E-IRC,d}} = (\sigma_{\mathbf{i}_{\mathrm{d}}}^2 \mathbf{H}_{\mathrm{d,eff}} \mathbf{H}_{\mathrm{d,eff}}^{\mathrm{H}} + \sigma_{\mathbf{s}_{\mathrm{s}}}^2 \mathbf{H}_{\mathrm{s,eff}} \mathbf{H}_{\mathrm{s,eff}}^{\mathrm{H}} + \sigma_{\mathrm{No}}^2 \mathbf{I})^{-1} \sigma_{\mathbf{i}_{\mathrm{d}}}^2 \mathbf{H}_{\mathrm{d,eff}}, \tag{3.41}$$

where $\sigma_{\mathbf{i}_{\mathrm{d}}}^2$, $\sigma_{\mathbf{s}_{\mathrm{s}}}^2$ and σ_{No}^2 are powers of dominant interfering signal, desired signal and noise, respectively. Next the E-IRC estimate of the interfering signal is reconstructed by applying either soft or hard demodulation, depending on the implementation. For demodulation, modulation order of the interfering signal is required. After reconstruction

of the interfering signal, it is subtracted from the overall signal. Thus the received signal is now of the form:

$$\mathbf{y} = \mathbf{H}_{\mathrm{s,eff}}\mathbf{s}_{\mathrm{s}} + \hat{\mathbf{z}}, \tag{3.42}$$

where $\hat{\mathbf{z}}$ contains now also residual interference from the dominant interferer, that is, an additional error which occurs when non-ideal reconstructed interfering signal is subtracted from the overall signal. Note that the interference covariance estimate for demodulating the desired signal has to be updated, i.e., covariance matrix of the dominant interferer is subtracted from the overall interference covariance estimate. However, subtracting all the estimated interference basically implies that perfect cancellation of the interfering signal is assumed. In practice, this is not the case and thus such assumption results in an additional error in SLIC receiver. After updating the covariance matrix, E-IRC linear detection is applied to the desired signal:

$$\hat{\mathbf{s}}_{\mathrm{s}} = \mathbf{W}^{\mathrm{H}}_{\mathrm{E-IRC,s}}\mathbf{y}, \tag{3.43}$$

where the receive filter for E-IRC is

$$\mathbf{W}_{\mathrm{E-IRC,s}} = (\sigma^2_{\mathbf{s}_{\mathrm{s}}}\mathbf{H}_{\mathrm{s,eff}}\mathbf{H}^{\mathrm{H}}_{\mathrm{s,eff}} + \sigma^2_{\mathrm{No}}\mathbf{I})^{-\mathbf{1}}\sigma^2_{\mathbf{s}_{\mathrm{s}}}\mathbf{H}_{\mathrm{s,eff}}. \tag{3.44}$$

Finally E-IRC estimate of the desired signal is forwarded for demodulation and decoding.

4 Research Methods

The performance of LTE radio link is studied by numerical simulations. The simulator, which is used to provide the results for this thesis, has the capability to model LTE type of downlink transmission at link level [16]. In this chapter, more detailed description of the simulator is discussed as well as parameters and assumptions used in simulations.

4.1 Link simulation principles

A link level simulation means that the transmitted signals are modeled at symbol level and thus the baseband time-domain waveform is truly generated. The propagation through the channel is modeled by applying the radio channel model to the signal. In other words, the signal is distorted by the channel. Then the reception is modeled, meaning signal processing in order to recover the payload data in the receiver.

In link level simulations, one common result measure is the link throughput as a function of link signal-to-noise ratio or signal-to-interference-plus-noise-ratio. The reason for this is the fact that commonly only one mobile station (or user equipment) is modeled. This kind of modeling is called a *single-link model* or *single-link-with-interference model*. In the case of single-link-model, the power level of the transmitted waveform is kept constant and the desired SNR is generated by adding noise with specific variance after the radio channel modeling. The average energy of resource elements within a subframe is one and thus the normalized energy of the transmitted signal is one. For example, if the SNR of the signal is wanted to be 10 dB and it is assumed that the normalized energy of the signal is one, the noise variance should be 0.1, because $10\log_{10}(\frac{1}{0.1}) = 10$ dB.

In the case of single-link-with interference model, noise is added similarly to single-link model, but now also baseband time-domain waveform of interfering cells is truly generated and added to the overall signal with predefined interference-to-noise-ratio (INR). Therefore, the received signal is the combination of signals of the serving cell and interfering cells. Interference modeling is described in more detail in the following.

Interference modeling

INR profiles have been evaluated and agreed in 3GPP work by several companies in order to simulate with the same interference settings. These settings can be found from [12]. INR profiles can be mapped to so called DIP profiles (Dominant Interferer Proportion), which are used in the simulator. INR profile defines the signal-to-noise ratio of the explicitly modeled interferer(s) whereas DIP profile defines the power ratio(s) between the explicitly modeled interferer(s) and the overall interference plus noise power. In the link simulator, first the baseband time-domain waveforms of the serving eNB, dominant interferer and weaker interferer are generated. Then the propagation of each signal through the channel is modeled and interfering signals are scaled based on the interference model before adding them to the overall signal. Finally AWGN is added to the overall signal based on the desired SINR. This is illustrated in Figure 18, where INR3 profile is used to have example values. These values are derived in the following.

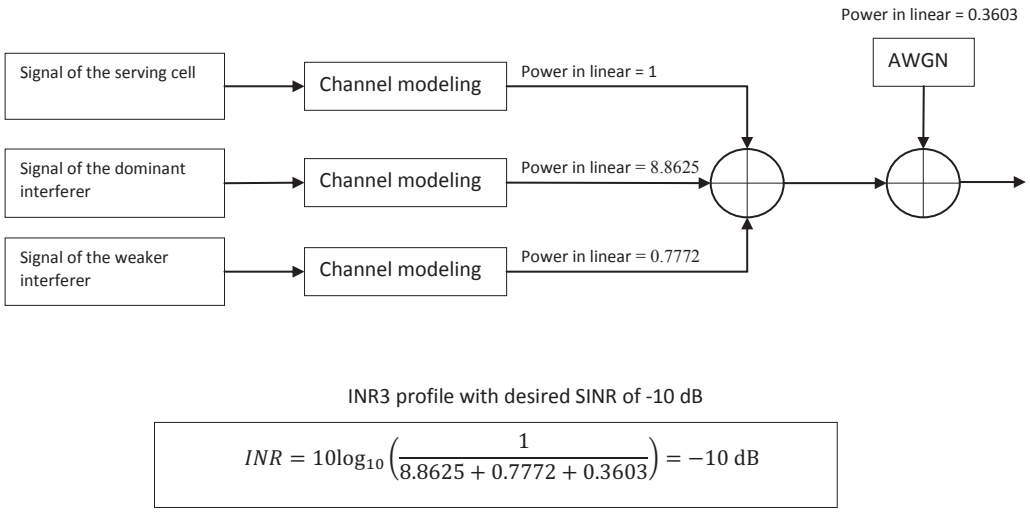

Figure 18: Illustration of interference modeling. Interfering signals are scaled based on the interference model before adding them to the overall signal. AWGN is then added to the overall signal based on the desired SINR.

In this thesis, INR3 profile is used, which corresponds to one strong interferer (dominant interferer) and one weaker interferer. To take exact values into account, INR3 profile corresponds to relative powers of [13.91, 3.34] dB, where the first value is for the dominant interferer and the second for the weaker interferer. INR3 profile corresponds to DIP profile of [-0.524416, -11.09441] dB. Explicit mapping (conversion) of INR profile to DIP profile is not relevant for this thesis and thus it is skipped.

As an example, let us assume unit signal power for the serving cell and SINR of -10 dB. This corresponds to the overall interference plus noise power of 10 (power of dominant interferer, P_d, + power of weaker interferer, P_w, + noise, n), because

$$10\log_{10}(\frac{signal\,power}{P_d + P_w + n}) = 10\log_{10}(\frac{1}{10}) = -10\,\text{dB}$$

Now the signal power of the dominant interferer can be obtained as

$$10\log_{10}(\frac{P_d}{10}) = -0.524416\,\text{dB} \rightarrow P_d \approx 8.8625$$

and the signal power of the weaker interferer can be obtained as

$$10\log_{10}(\frac{P_w}{10}) = -11.09441\,\text{dB} \rightarrow P_w \approx 0.7772$$

and thus the noise power is

$$P_d + P_w + n = 10 \rightarrow n = 0.3603$$

Values are also presented in Table 6.

Table 6: Results of an example for interference modeling when operation point (SINR) is -10 dB.

Operation point: SINR = -10 dB	**Power in linear scale**	**INR3 profile**	**DIP profile for INR3**
Serving cell	1	-	-
Dominant Interferer	8.8625	13.91 dB	-0.524416 dB
Weaker Interferer	0.7772	3.34 dB	-11.09441 dB
AWGN	0.3603	-	-

4.2 Single-link simulation flow

In order to find the average performance in a specific channel profile, multiple different channel realizations have to be created within one SNR or SINR point. In the simulator, these channel realizations are called *fast fading drops* (FFD). Thus, the number of FFDs defines how many independent channel realizations are used within one SNR or SINR point. Characteristics of the channel model, for example the frequency selectivity, have effects on demodulation performance and further to the overall performance. Thus, in order to capture the average link performance in a specific channel profile and for a specific SNR or SINR, averaging over a sufficient number of FFDs is required.

For every FFD, a predefined number of subframes are simulated. The need for multiple subframes stems from the fact that the mobile terminal is assumed to be non-stationary and thus the channel is varying over the time. The speed of the mobile terminal can be defined and consequently faster mobile speed results in faster channel variations. One simulation run consists of three loops, where each of the loops has a predefined number of iterations. This is illustrated in Figure 19.

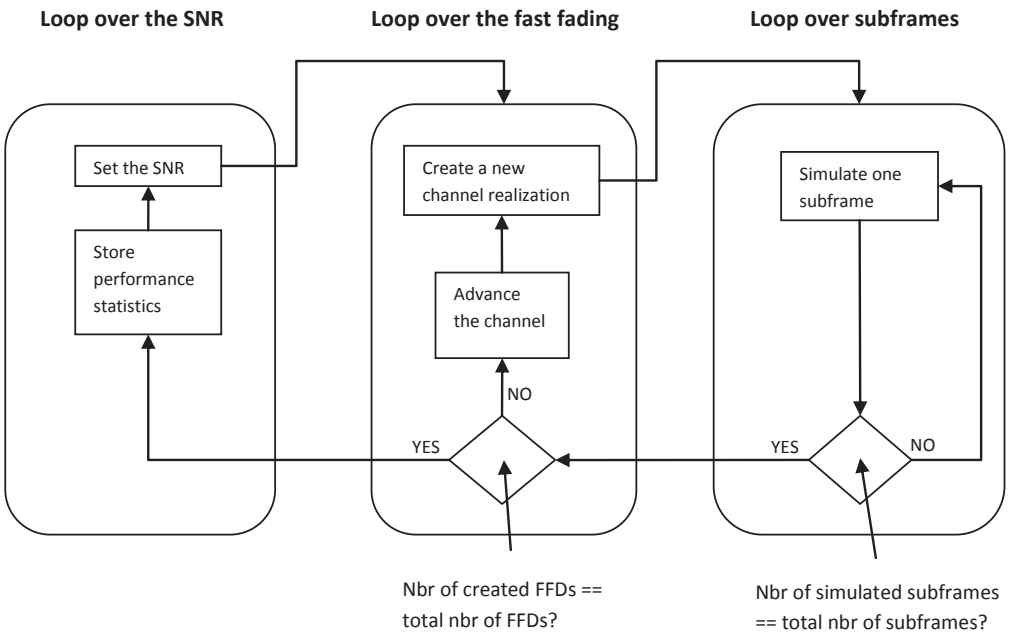

Figure 19: *Single-link simulation model. One simulation run consists of three loops.*

4.3 Channel modeling

In this section, channel model features are examined in more detail. However, before proceeding to the channel modeling used in the simulator, some background about the propagation characteristics of a radio channel is provided.

Reliable communication in wireless channels can become a difficult task because the transmitted signal is not only distorted by noise, but it can also suffer from inter-symbol interference, fading and interference from other users. In general, the fading in radio propagation can be categorized into large-scale and small-scale fading. In wireless communications, large-scale fading illustrates the path-loss, which depends on the environment and shadowing, and hence provides understanding about the radio propagation over large areas. However, in most practical systems, like in LTE, radio communications is far more complex than just plain path-loss and therefore small-scale fading models are needed to explain the radio communications better.

In practical wireless communications, the transmitted signal usually suffers refractions, shadowing and reflections due to objects like buildings, trees and so on. As a consequence, the signal arrives to the receiver antenna(s) over multiple paths, known as multipath propagation. Each path can be characterized by three parameters, namely delay, attenuation and phase shift. As already described in Section 2.1, cyclic-prefix can be used as a countermeasure against small-scale fading, that is, against inter-symbol-interference caused by the multipath propagation.

Small-scale fading can be expressed by time-spreading of the signal, which is also knows as delay dispersion, and by time-variant nature of the channel [17]. Delay dispersion can be manifested by channel frequency selectivity or in other words, delay dispersion is equivalent to frequency selectivity of the channel [14]. Whereas, time-variant nature of the signal can be manifested by fast fading and slow fading. Intuitively, one major factor affecting to the time-variant nature of the signal is the motion of an UE.

A commonly used measure of multipath richness is so called *Power Delay Profile* (PDP). The PDP contains information about how much power arrives to the receiver with a certain delay. Although the PDP is a function, it can be described by a single parameter. While there are a number of different parameters, the *delay spread* has obtained a special stature among all parameters. In general, delay spread can be interpreted as the difference between the time of arrival of the earliest significant multipath component and the time of arrival of the latest multipath component. Delay spread can be quantified through different metrics, but the most common one is the root mean square (rms) delay spread. It has been shown that under specific circumstances, the error probability due to delay dispersion is proportional to the rms delay spread. This means that, under specific circumstances, rms delay spread can be the only needed parameter for modeling channels. [14][18]

For channel modeling used in the simulator, channel frequency selectivity and spatial correlation properties are the most important channel model features. And as described already in this section, the channel frequency selectivity can be determined by the delay spread of the channel. Commonly, the delay spread is modeled in time domain as discrete channel taps with relative time differences and average relative power. One channel realization or fast fading drop is created by modifying the power of the taps so that the average relative power is kept constant. [1, p. 49.] Extended ITU models use this kind of channel modeling and they are given in Table 7. In this thesis, ITU Extended Pedestrian A (EPA) channel model is used as stated also in the next section. Corresponding delay spread profiles for these channel models are given in Table 8.

Instantaneous channel taps define the impulse response of a filter and the effect of

the radio channel is applied to the baseband time-domain signal by using this filter. In the case of modeling of time-variant nature of the signal, these channel tap values can be changed according to the speed of the UE. High mobility basically means that the channel tap values change rapidly. This also enables modeling of Doppler spread. [1, p. 50.].

In the case of multiantenna modeling, independent channel realizations are created between each of the transmit and receive antenna pairs, meaning that the channel fading is truly uncorrelated between the antennas. It should be noted that a real-life antenna array may have closely spaced elements, meaning that the channel fading is somewhat correlated between the transmit and receive antennas and a spatial correlation model is needed. Nevertheless, this kind of modeling is out of the scope of this thesis and the simulation setup has been selected so that channels between the antennas are spatially uncorrelated.

Table 7: Extended ITU channel models [5].

Delay Spread Category	Channel Model	Acronym	r.m.s ds [ns]	Mobility [km/h]
Short	Extended Pedestrian A	EPA	43	3
Medium	Extended Vehicular A	EVA	357	3 and 30
High Delay	Extended Typical Urban	ETU	991	30 and 130

Table 8: Power delay profiles of Extended ITU models [5].

TAP	EPA		EVA		ETU	
	Delay [ns]	Relative Power [dB]	Delay [ns]	Relative Power [dB]	Delay [ns]	Relative Power [dB]
1	0	0.0	0	0.0	0	-1.0
2	30	-1.0	30	-1.5	50	-1.0
3	70	-2.0	150	-1.4	120	-1.0
4	80	-3.0	310	-3.6	200	0.0
5	110	-8.0	370	-0.6	230	0.0
6	190	-17.2	710	-9.1	500	-0.0
7	410	-20.8	1090	-7.0	1600	-3.0
8	-		1730	-12.0	2300	-5.0
9	-		2510	-16.9	5000	-7.0

4.4 Simulation parameters

Simulations were run in order to assess the link performance. Before presenting simulations results, blind detection of P_a is firstly described and investigated analytically in Chapter 5 and the simulation results are given and analyzed in Chapter 6. The performance is examined through the link throughput which is defined as the number of successfully transferred payload bits per second. The throughput is given as a function of SINR as described in Subsection 4.1. The number of bits transferred in 1 ms subframe depends on the *modulation and coding scheme* (MCS) and the number of resource blocks assigned to the mobile terminal. In LTE, modulation and coding scheme is given as a MCS index, which corresponds to a specific modulation order and coding rate. However, calculating the exact coding rate for PDSCH based on the given MCS index is not that simple. The reason for this is the fact that the exact number of REs used for PDSCH must be known and consequently the exact number of REs used by control signaling and

reference signals must be known. Also impact of different coding rates on blind detection performance is not relevant for the evaluations and analysis in this thesis and therefore the coding rate is fixed in simulations and the calculation of exact coding rate is not essential. The detailed determination of modulation order and coding rate in LTE is given in Section 7.1.7 of [3].

The general simulation setup as well as detailed simulation parameters, which are selected for this thesis, are based on simulation setup used in RAN WG4 standardization work on NAICS. The general simulation setup in NAICS and in this thesis is as follows:

- Two interfering cells, from which the other one is the dominant interferer. So called INR profiles are used to determine the power of interfering cells. In this thesis, INR3 profile is used in simulations, which corresponds to one dominant interferer and to one weaker interferer. More detailed explanation of interference modeling is carried out in Section 4.1.
- Only the dominant interferer is canceled by SLIC receiver.
- Serving cell and the dominant interferer have overlapping (or colliding) CRS. Weaker interferer has non-colliding CRS.
- All eNBs are transmitting PDSCH on whole bandwidth, i.e., there are no unused REs.
- Channel estimation as well as covariance estimation are realistic (non-ideal).
- All eNBs have same subframe configuration, which is typically two OFDM symbols for control signaling and 12 OFDM symbols for PDSCH. This corresponds to CFI of 2 (Control Format Indicator).
- Serving cell has MCS of 5 (QPSK) and interfering cells have either MCS of 5, MCS of 14 (16QAM), or MCS of 25 (64QAM).
- Propagation channel is EPA, which is described in more detail in previous Subsection 4.3.
- UE velocity is 2.7 kmph, which corresponds to 5 Hz Dobbler shift because the carrier frequency is set to 2 GHz.
- All eNBs have two transmit antennas and a UE is equipped with two receive antennas (2x2 antenna configuration). Channel is spatially uncorrelated.
- Receiver algorithms of UE are genie-aided SLIC (all parameters are known or signaled), SLIC with blind P_a detector and IRC.
- System bandwidth is 10 MHz which corresponds to 50 PRBs.

Detailed simulation assumptions are given in Table 9.

Table 9: *Parameters for simulations.*

Parameter	**Value**
Number of channel realizations (FFDs) per one SNR point	20
Number of subframes per one channel realization	2500
Serving eNB cell ID	0
Interfering eNBs cell IDs	Dominant: 6 (colliding CRS), Weaker: 1 (non-colliding CRS)
Carrier frequency	2.0 GHz
System Bandwidth	10 MHz (50 Resource Blocks)
Interference Noise Profiles	INR3 profile = [Dominant: 13.91 dB, Weaker: 3.34 dB] Described in Section 4.1.
Antenna configuration at eNBs	2x spatially uncorrelated
DL power allocation	Total power: 43 dBm *referenceSignalPower:* 15.2185 dBm P_a: 0 dB P_b: 1
Antenna configuration at mobile station	2x spatially uncorrelated
Subframe configuration	2 symbols for control signaling, 12 PDSCH symbols (CFI = 2)
Channel model	ITU Extended Pedestrian A (EPA)
Mobile station velocity	2.7 kmph (5 Hz Doppler)
Resource allocation	50 PRBs
Transmission mode	2x2 Closed-loop codebook-based precoding limited to single layer transmission (TM6).
Modulation and coding scheme (MCS#) of serving cell	5
Modulation and coding scheme (MCS#) of interfering cells	5, 14, 25
HARQ (Retransmissions)	Maximum number of retransmissions is set to 4
Channel frequency response estimation	Realistic, Concatenated frequency and time 1D Wiener filtering
Covariance estimation	Realistic. Network assisted covariance estimation for SLIC. Differential covariance estimation for IRC.
Wiener filter bandwidth	6 RBs
SNR estimation	Realistic, Estimate from CRS
Receiver algorithms	Genie-aided SLIC with CRS-IC, SLIC with blind P_a detector with CRS-IC, IRC without CRS-IC
PMI feedback	Follow wideband PMI
Error Vector Magnitude (EVM)	In all eNBs: Tx = 6%, Rx = 0%

5 Blind Detection of Interfering Cell Data Channel Power Level

In this chapter, we will discuss the purpose of blind detection and potential blindly detected parameters in CRS based transmission modes. However, the main focus is blind detection of interfering cell's data channel power level. Estimating power level of interfering cell's CRS is straightforward because serving eNB signals all the needed information of interfering CRS to the NAICS UE. As described in Section 2.8, PDSCH-to-CRS power ratio is denoted by parameter P_a. Therefore by estimating parameter P_a, which is used in interfering cell, power level of interfering cell's PDSCH can be easily calculated. The algorithm of P_a detector is introduced and modeled and the sensitivity of SLIC receiver on incorrect PDSCH power levels is studied, that is, the impact of P_a detection error on SLIC receiver performance. Finally we will address the following:

- The impact of different P_a search spaces on P_a detection performance.
- The impact of different number of samples on P_a detection performance, that is, bandwidth used for detection.
- The impact of interfering cells' modulation order on P_a detection performance.
- Study how much complexity P_a detector adds to the SLIC logic.

The main RAN4 Work Group objective of the NAICS is to identify reference Interference Suppression (IS) and Interference Cancellation (IC) receivers with and without network assistance, and evaluate their performance and complexity trade-off and implementation feasibility [13]. Enhanced IS/IC receivers, like SLIC, require knowledge of the interference signal parameters. Then the ultimate question is that which of these parameters need to be signaled to the NAICS UE, that is, network assistance is required, and which parameters could be blindly detected in NAICS UE. In this thesis, the focus is on CRS based transmission modes, that is, transmission modes which utilize Cell-specific Reference Signals. The main parameters related to CRS based PDSCH interference signals are:

- Precoder Matrix Indicator (PMI) and Rank Indicator (RI).
- Power allocation parameters, which are P_a (Data to reference signal EPRE ratio) and presence of PDSCH signal.
- PDSCH modulation format, i.e., QPSK, 16QAM or 64QAM.

The RAN4 goal is to identify whether these parameters can be reliably and blindly detected without major impacts on the performance. In addition, impact of complexity of blind detectors on UE implementation needs to be studied. Based on these results, system level (RAN1) Work Group can make the decision on the need for dynamic parameters signaling or detection. In the following, blind detection of P_a is examined in detail.

5.1 Recent studies on blind PDSCH to CRS power ratio detection

There are companies which have recently been studying the same issue and they have somewhat different conclusions. The reason for this is the fact that companies use their

own simulators with different algorithms for blind detection. In the following, conclusions and proposals of some companies are presented.

In [8], up to 2 dB performance degradation is shown when using SLIC receiver with blind P_a detector compared to so called genie-aided SLIC receiver. Genie-aided receiver means that all the parameters are known in advance. In [8] it is proposed that the bandwidth for blind P_a detection should be at least 3 PRB pairs and the set of possible P_a values could be reduced from the full set of 8 values to 3 values (or even only 1 value) in order to improve detection performance and to reduce complexity.

In [9] it is observed that blind P_a detection results in significant performance degradation even with reduced subset of [-3, 0, 3], that is, from 1.5 dB up to 6 dB degradation. It is also shown that with different subsets of P_a, the degradation seems similar.

In [10] it is observed that restricting the possible P_a values for quantization has a beneficial impact on detection performance and assuming that P_a set is restricted to 3 values, detection error rates are deemed acceptable. However, results in terms of throughput are not shown.

In [11], it is observed that blind P_a detection can be reliable if UE has knowledge on the serving cell data to RS EPRE ratio. This is indeed the case in this thesis as P_a of serving cell is assumed to be known.

Based on these contributions of different companies, it seems that the general observation is that the set of possible P_a values used for quantization should be reduced in order to achieve better detection performance. Also blind detection of P_a may result in significant performance degradation in some scenarios, but it can be also reliable.

5.2 Blind detection of PDSCH to CRS power ratio

To perform SLIC on the data REs efficiently, that is, PDSCH interference cancellation, the NAICS UE needs to know correct power level of the interfering PDSCH signal. In particular, the UE needs to know PDSCH to CRS power ratio. This ratio is known as parameter ρ_a in OFDM symbols where CRS are *not* present. The ρ_a is UE specific, can take a finite set of possible values of [-6, -4.77, -3, -1.77, 0, 1, 2, 3] dB and can be derived from parameter P_a as described in Section 2.8. In addition, CRS power is signaled as parameter *referenceSignalPower* which is an absolute power in dBm.

Meanwhile, parameter ρ_b defines the PDSCH to CRS power ratio in OFDM symbols where CRS are present. In other words, the ρ_b defines an additional PDSCH power offset for OFDM symbols where CRS are present. The ρ_b value can be derived by using parameters ρ_a and P_b as described in Section 2.8.

For further analysis, it is assumed that the cell-specific parameter P_b is perfectly known, while UE has no information on the P_a value associated with the interference signal transmission. In addition, the simulation setup and settings are selected so that ρ_a corresponds directly to P_a and thus for clarity and convenience, we talk about blind detection of P_a instead of blind detection of ρ_a.

Mathematical modeling

In general, to estimate PDSCH to CRS power ratio of dominant interfering cell $\rho_a^{(\mathrm{d})}$, signal power of the received PDSCH signal should be compared versus the estimates obtained from CRS REs. With this method, the PDSCH to CRS power ratio estimation can be performed via comparing the measured receive signal covariance matrix on the

data REs with different reconstructed receive signal covariance matrix hypothesis. This covariance matrix hypothesis can be constructed by using different PDSCH to CRS power ratio values of interfering signal with the effective channel estimates. This method is so called covariance matching due to the fact that the covariance matrix of the received signal $\mathbf{C_y}$ is matched to reconstructed (or emulated) receive signal covariance matrix.

In the following, the algorithm for blind detection of PDSCH to CRS power ratio of dominant interfering cell $\rho_a^{(\mathrm{d})}$ is shown. The algorithm below is modified and adapted version of the algorithm for blind detection of PMI and RI presented in [11]. When the serving cell signal power, i.e., the PDSCH to CRS power ratio of serving cell, $\rho_a^{(\mathrm{s})}$, is known while PDSCH to CRS power ratio of dominant interfering cell $\rho_a^{(\mathrm{d})}$ is known to belong to a finite set of values S[8], $\rho_a^{(\mathrm{d})}$ can be estimated as:

$$\rho_a^{(\mathrm{d})} = \underset{\rho_{a,n}^{(\mathrm{d})} \varepsilon \mathrm{S}}{\arg\min} \left(\| \hat{\mathbf{C}}_{\mathbf{y}} - \tilde{\mathbf{R}}(\rho_{a,n}^{(\mathrm{d})}) \|^2 \right), \tag{5.1}$$

$$\hat{\mathbf{C}}_{\mathbf{y}} = \frac{1}{N_{\mathrm{RE}}} \sum_{k=1}^{N_{\mathrm{RE}}} \mathbf{y}_{\mathrm{k}} \mathbf{y}_{\mathrm{k}}^{\mathrm{H}} \tag{5.2}$$

where $\rho_{a,n}^{(\mathrm{d})}$ is the PDSCH to CRS power ratio hypothesis of dominant interferer, $\hat{\mathbf{C}}_{\mathbf{y}}$ is the covariance matrix of the received signal estimated on the N_{RE} PDSCH REs, $\tilde{\mathbf{R}}(\rho_{a,n}^{(\mathrm{d})})$ is the covariance matrix hypothesis of the reconstructed (or emulated) received signal for the case of using n-th $\rho_{\mathrm{a}}^{(\mathrm{d})}$ candidate from subset S, $\mathbf{y}_{\mathrm{k}}$ is receive signal vector on the k-th RE. In this thesis, blind PDSCH to CRS power ratio detection is performed for the dominant interferer, which CRS is colliding with the serving cell. In this case the covariance matrix of the reconstructed/emulated received signal can be represented as:

$$\tilde{\mathbf{R}}(\rho_{a,n}^{(\mathrm{d})}) = \left\langle \rho_a^{(\mathrm{s})} * \mathbf{H}_{\mathrm{s,eff}} * \mathbf{H}_{\mathrm{s,eff}}^{\mathrm{H}} \right\rangle + \left\langle \rho_{a,n}^{(\mathrm{d})} * \mathbf{H}_{\mathrm{d,eff}} * \mathbf{H}_{\mathrm{d,eff}}^{\mathrm{H}} \right\rangle + \hat{\mathbf{z}}, \tag{5.3}$$

where $\mathbf{H}_{\mathrm{s,eff}}$ and $\mathbf{H}_{\mathrm{d,eff}}$ are the effective channel estimates[9] of serving cell and dominant interferer, respectively and $\hat{\mathbf{z}}$ is the residual interference plus noise estimate, i.e., including contribution from the weaker interferer and noise.

From estimation accuracy point of view, the covariance matrix of the reconstructed/emulated received signal shown in Equation (5.3) would be optimal as it includes contribution also from the weaker interferer. However, in this thesis network assisted covariance estimator is able to calculate interference plus noise covariance estimate only including the dominant interferer plus noise leaving out contribution from the weaker interfering signal. From dominant interferer point of view, the serving cell is the dominant interferer and PDSCH to CRS power ratio the of serving cell, $\rho_a^{(\mathrm{s})}$, is known to the NAICS UE. Consequently, the Equation (5.3) is simplified as follows:

$$\tilde{\mathbf{R}}(\rho_{a,n}^{(\mathrm{d})}) = \left\langle \rho_{a,n}^{(\mathrm{d})} * \mathbf{H}_{\mathrm{d,eff}} * \mathbf{H}_{\mathrm{d,eff}}^{\mathrm{H}} \right\rangle + \mathbf{R}_{\mathbf{r}}^{(\mathrm{d})}, \tag{5.4}$$

where

$$\mathbf{R}_{\mathbf{r}}^{(\mathrm{d})} = \rho_a^{(\mathrm{s})} \mathbf{H}_{\mathrm{s,eff}} \mathbf{H}_{\mathrm{s,eff}}^{\mathrm{H}} + \sigma_{\mathrm{No}}^2 \mathbf{I}.$$

[8] S can be the set of [-6 -4.77, -3, -1.77, 0, 1, 2, 3] dB or any subset of these values.

[9] The concept of effective channel estimate is described in Section 3.2.

as shown already in Equation (3.25), but now signal power of desired signal is denoted as PDSCH to CRS power ratio of serving cell $\rho_a^{(s)}$. As the contribution of the weaker interferer is not taken into account in Equation (5.4), estimation accuracy will suffer. The impact of this will be revealed in the following sections where the performance of the algorithm is studied in detail.

It is also good to emphasize that as there is the lack of knowledge of the exact transmitted symbols, the receive signal average covariance matrix is analyzed. This means that the receive signal covariance matrix $\hat{\mathbf{C}}_{\mathbf{y}}$ as well as the reconstructed/emulated receive signal covariance matrix hypothesis $\tilde{\mathbf{R}}(\rho_{a,n}^{(d)})$ is averaged over all PDSCH REs used for detection. The more there are available PDSCH REs, the more accurate the estimation should be but also the complexity increases. Algorithm flow is illustrated in Figure 20. [11]

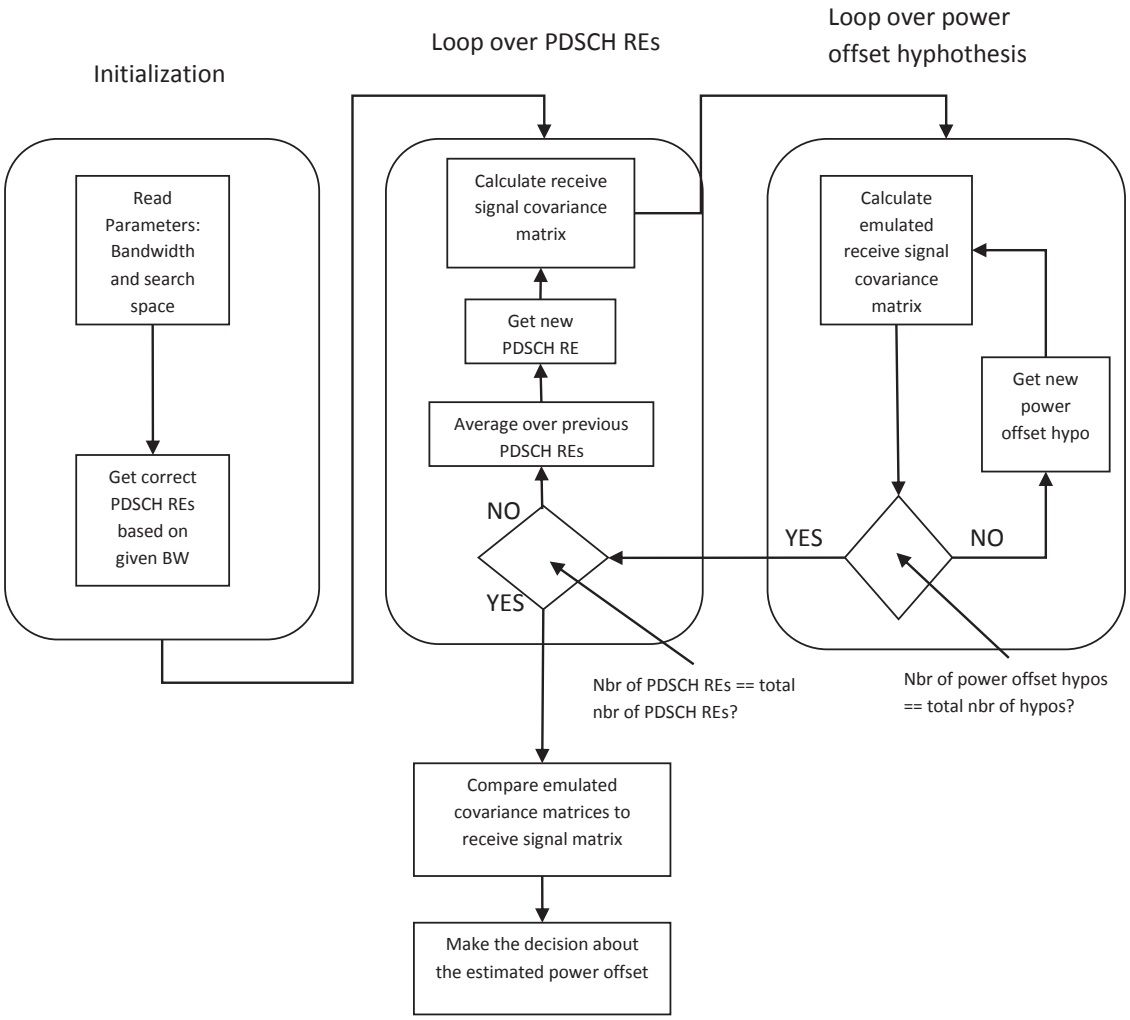

Figure 20: Illustration of the algorithm flow for blind P_a detection for the dominant interfering signal.

Usage of blind PDSCH to CRS power ratio detector in SLIC receiver

In the case of multiple interfering eNBs, usage of blind P_a detector in SLIC logic is illustrated in Figure 21. At first, necessary parameters, which are needed to perform SLIC,

are collected. Most important parameters are network assisted covariance estimate, channel estimate, precoder matrix, modulation, number of transmit and receive antennas and number of PDSCH REs. Based on the channel estimate and precoding matrix, effective channel estimate can be calculated for LMMSE equalization. Next interfering cells are put in order so that the strongest interfering signal is canceled first and the weakest last. This ordering is based on SINR estimates for each eNB. SINR estimate for each eNB can be calculated using received CRS of all eNBs. After choosing the interfering eNB to be processed, blind P_a detection is performed and the overall PDSCH signal is scaled based on the power offset estimate. Then LMMSE equalization and soft demodulation are carried out for the current interfering eNB, that is, reconstruction of interfering PDSCH signal. Finally SLIC can be performed, i.e., the current interfering PDSCH signal can canceled from the overall signal. If there are more interfering eNBs left to be canceled, the above loop is re-performed for them. When all desired interfering PDSCH signals are canceled, LMMSE equalization and soft demodulation of the desired signal can be performed.

5.3 Sensitivity of SLIC receiver on incorrect interfering cell PDSCH to CRS power ratio

In this section sensitiveness of SLIC receiver on incorrect P_a values is studied. There will be estimation errors, or estimation offsets, in blind P_a detector, i.e., detector chooses different P_a value instead of the actual one. Intuitively incorrect P_a value should result in performance degradation in SLIC receiver and therefore it is reasonable to acquire some insight about the effects of estimation errors. One straightforward way to study this issue is to force SLIC receiver to use different set of incorrect P_a values. Hence, set of simulations were run with the simulation setup described in Section 4.4, but in this case SLIC is forced to use a specific incorrect P_a value while the actual one is set to 0 dB.

As the possible P_a values are [-6, -4.77, -3, -1.77, 0, 1, 2, 3] dB , as described in Section 2.8, and in simulations P_a is set to 0 dB, reasonable values to test are the ones around 0 dB, that is, a subset of [-3, -1.77, 1, 2, 3] dB. It is unlikely that blind detector chooses values -4.7 dB or -6 dB with this setup and therefore these two values are excluded from simulations. Modulation of interferer can be either QPSK (MCS of 5), 16QAM (MCS of 14) or 64QAM (MCS of 25). These three cases are tested exclusively as sensitivity might vary substantially with different modulations. In all results throughout this thesis, IRC receiver, which is described in Section 3.5, will function as a baseline. IRC is practical and relatively low-complexity receiver, at least compared to the SLIC receiver, and thus it is also noteworthy solution for UEs as a base receiver in environments with interference. In Figures 22, 23 and 24, performance of SLIC receiver is shown when incorrect P_a values are used.

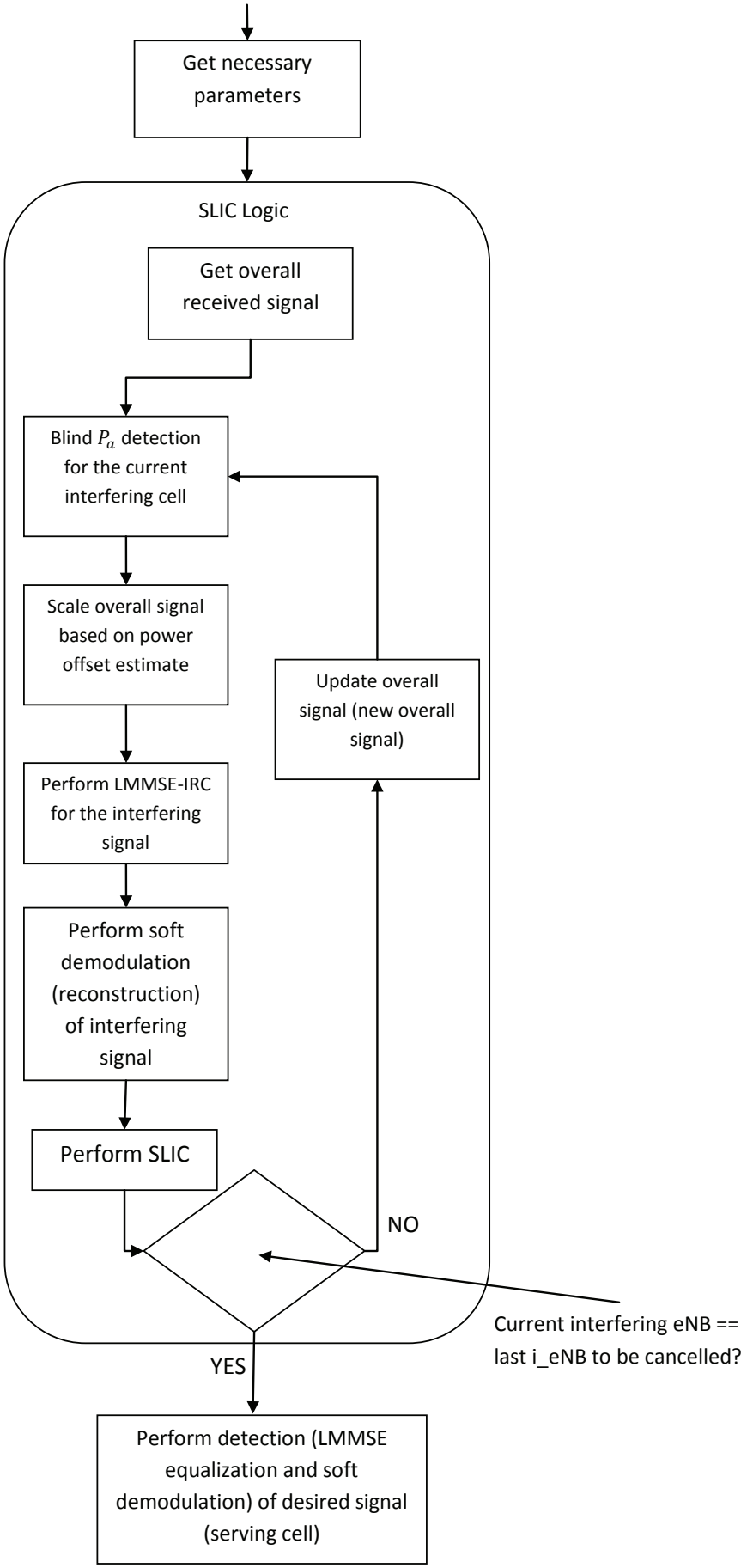

Figure 21: Usage of blind P_a detector in SLIC in the case of multiple interfering signals.

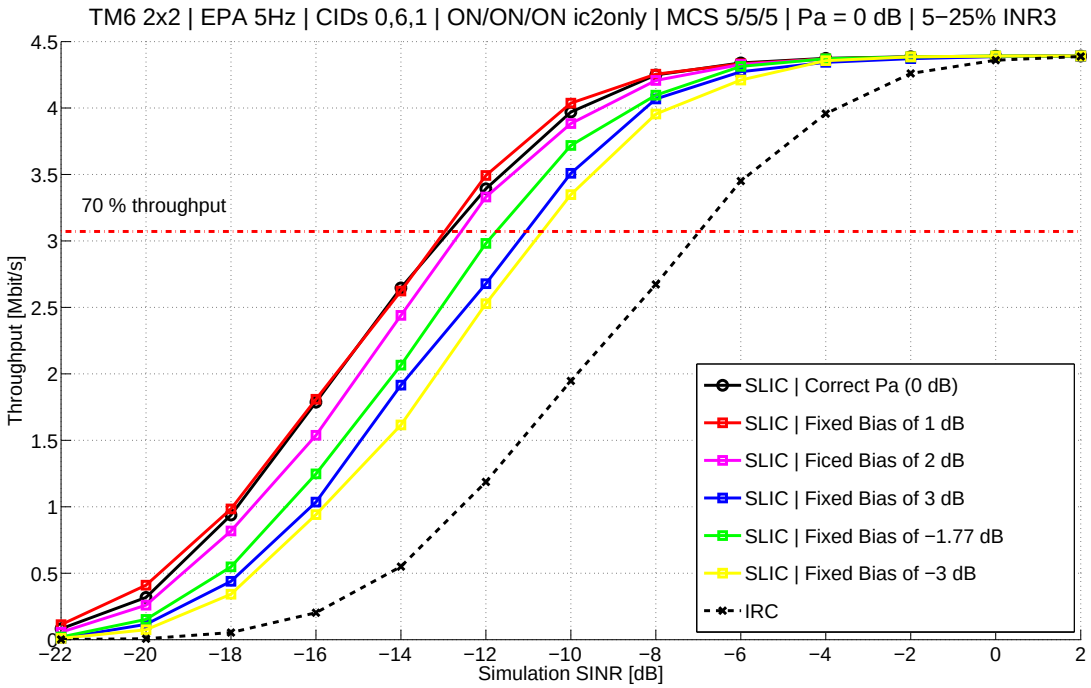

Figure 22: Sensitivity of SLIC receiver on incorrect P_a values. Serving eNB and interfering eNBs use both QPSK modulation (MCS 5/5/5). Actual P_a is set to 0 dB in all eNBs.

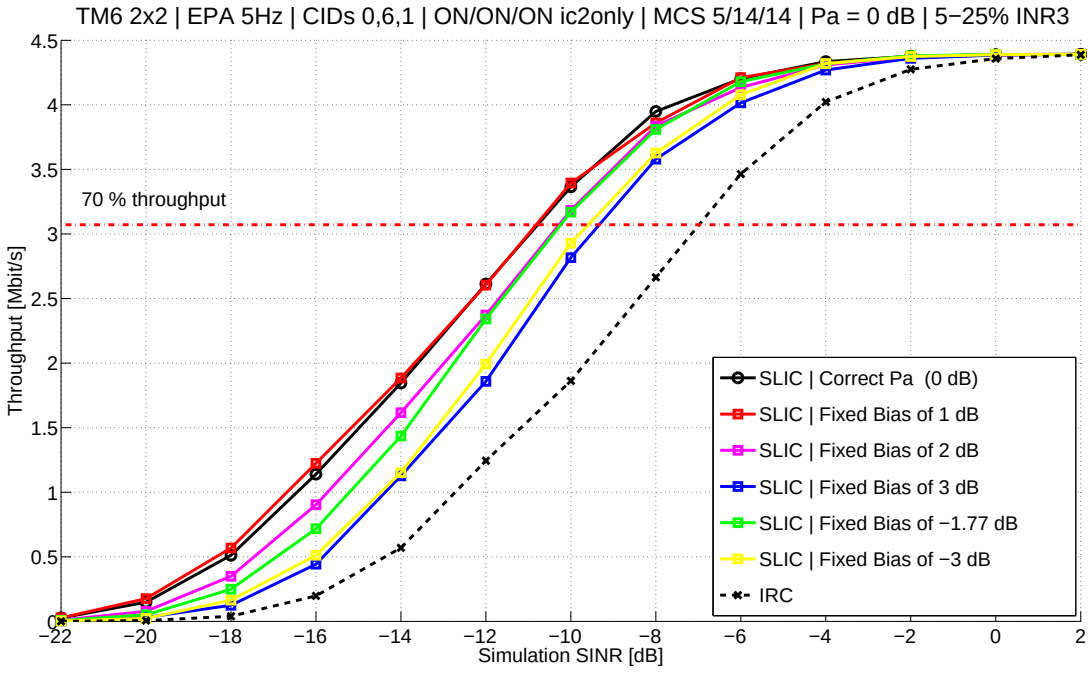

Figure 23: Sensitivity of SLIC receiver on incorrect P_a values. Serving eNB uses QPSK and interfering eNBs use 16QAM modulation (MCS 5/14/14). Actual P_a is set to 0 dB in all eNBs.

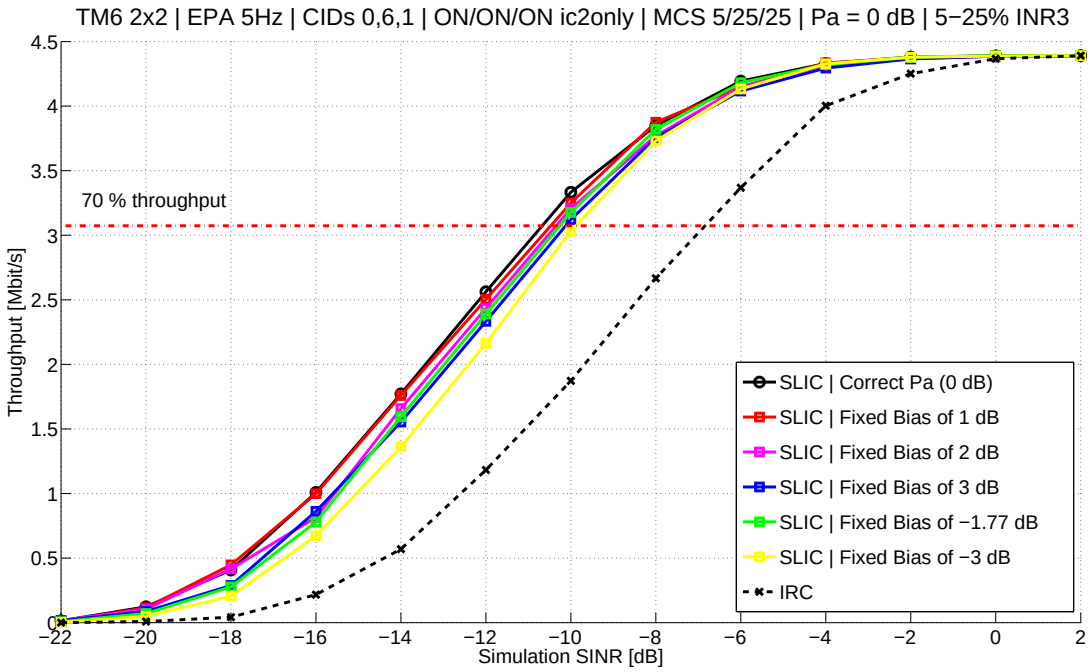

Figure 24: Sensitivity of SLIC receiver on incorrect P_a values. Serving eNB uses QPSK and interfering eNBs use 64QAM modulation (MCS 5/25/25). Actual P_a is set to 0 dB in all eNBs.

From the Figures 22, 23 and 24 it can be clearly seen that SLIC receiver is relatively sensitive to incorrect P_a values. When interfering cells use QPSK modulation, SLIC receiver achieves the best gain over IRC and when interferers use 16QAM or 64QAM, SLIC receiver achieves less gain over IRC but still the gain is significant. Reading gains (or losses) from the 70% throughput line (dashed red line), SLIC receiver achieves 6 dB gain over IRC with the correct P_a assumption (solid black curve) when interfering cells use QPSK. Similarly, SLIC receiver achieves 3.8 dB gain over IRC when interfering cells are using either 16QAM or 64QAM.

At first glance, SLIC seems to be the most sensitive to incorrect P_a values when interfering cells use QPSK and the least sensitive when they use 64QAM. However, when interfering cells use QPSK, SLIC seems to perform very well, which basically means that interfering cell's signal has been reconstructed mostly correctly, i.e., the interfering signal has been subtracted efficiently. Then if incorrect P_a value is used, SLIC either subtracts too much interference or does not subtract all the estimated interference, which both should result in a performance degradation, intuitively. However, in the case of SLIC receiver, analyzing gains and/or losses are not always straightforward due to the complexity of SLIC algorithm. As described in more detail in Section 3.5, SLIC uses soft decisions, i.e., soft demodulation and log-likelihood-ratios (LLR) in order to reconstruct the interfering cell's signal. Especially the usage of soft decisions (or soft demodulation) makes an all-encompassing analysis difficult. As an example, in some rare cases it can be seen that actually slightly incorrectly estimated power level may even improve the performance somewhat. One explanation to this is that if the reconstructed signal is mostly incorrect, it might be helpful that not all the estimated interference is subtracted.

When Figure 22 is considered, that is, interfering cells use QPSK, SLIC seems to be somewhat more sensitive to underestimation than overestimation. To be more exact, 2 dB and 3 dB overestimation results in around 0.5 dB and 2 dB degradation in performance,

respectively. Whereas, 1.77 dB and 3 dB underestimation results in 1 dB and 2.4 dB degradation in performance, respectively. Interestingly 1 dB overestimation does not degrade the performance at all. It is good to point out that even with underestimation of 3 dB, the gain over IRC is more or equal compared to the gain when interfering cells use 16QAM or 64QAM with the correct P_a.

When interfering cells use 16QAM in Figure 23, there is not so clear difference in sensitivity to underestimation and overestimation. To be more exact, 2 dB and 3 dB overestimation results in around 0.4 dB and 1.4 dB degradation in performance, respectively. Similarly, 1.77 dB and 3 dB underestimation results in 0.4 dB and 1.4 dB degradation in performance, respectively.

General observation is that incorrect P_a values definitely degrade the performance of SLIC receiver but overestimation (positive power offset) is somewhat more tolerable than underestimation (negative power offset).

Counter intuitively, when interfering cells are using 64QAM in Figure 24, SLIC is not as sensitive to incorrect P_a values as in Figures 22 and 23. The maximum loss is not more than around 1 dB when there are 3 dB underestimation or overestimation. In general, 64QAM should be rather sensitive to amplitude distortion, that is, when there are offsets in amplitudes, from 1 dB up to 3 dB, intuitively there should be more errors in reconstruction of interfering signal.

This counter intuitive behavior stems from the fact that soft demodulation is used in reconstruction of interfering signal. If hard symbols, i.e., hard demodulation had been used in reconstruction, incorrect power levels with 64QAM would definitely degrade the performance more compared to the usage of soft demodulation. One explanation to this is that reconstruction of 64QAM signal is very hard to perform perfectly anyway, that is, there will be always more or less errors. Now if Figure 21 is considered, it can be seen that scaling of the overall signal based on the selected P_a value is performed before applying linear detection and reconstruction (soft demodulation) of the interfering signal. Now scaling with a incorrect power level value could actually compensate some errors or at least scaling does not increase existing errors significantly.

However, all-encompassing explanation to this kind of behavior is very hard to provide because also the current simulation setup and interference profile have an impact on this. In other words, all-encompassing explanation would require several simulations with several different simulation setups and interference profiles. Anyway, comprehensive analysis of sensitivity of SLIC receiver on incorrect power level assumptions is not crucial for this thesis as the focus is on performance of blind P_a detection. Therefore it is sufficient to conclude that incorrect P_a values definitely degrade the performance of SLIC receiver and consequently efficient P_a detector is needed.

5.4 Impact of different parameters on PDSCH to CRS power ratio detection performance

There are parameters, which affects the P_a detection performance and swiftness. It is good to keep in mind that if P_a detector is used in practical NAICS UE, the detection needs to be performed in real time. Consequently, these parameters needs to be carefully examined and optimized in order to find the best combination. The most important parameters to be optimized are the number of samples, that is, detection bandwidth, and the search space, that is, set of possible P_a values, which is used for quantization. There are also parameters, which NAICS UE cannot affect, namely parameters of interferer, and the most essential

parameter of interferer is its modulation.

In this section, the impact of different parameters on P_a detection performance is performed through simulations. There are three parameters, which simultaneously provide information:

- *Estimation error rate.* However, in the case of blind P_a detection, it can be said that there is no truly incorrect P_a value in the terms of throughput. This is because in the case of SLIC, in some scenarios it might be beneficial to use slightly different P_a value instead of the actual one. In other words, high estimation error rate does not always imply bad performance in the terms of throughput. This is due to the soft demodulation used in SLIC receiver.

- *Average estimation offset* [dB]. This parameter shows the average power offset value used in SLIC receiver within one operation point, that is, within one SINR point. Average estimation offset within one operation point corresponds to geometric mean of all estimated power offsets.

- *Average number of selected P_a values*. This parameter shows the average number of each power offset value selected by P_a detector. Averaging is performed between the SINR points.

When analyzing performance of P_a detector, the sensitivity of SLIC receiver to incorrect P_a values is good to keep in mind, that is, the study carried out in the previous section. For example, from the previous section it can be seen that overestimation (positive power offset) is more tolerable than underestimation (negative power offset).

P_a search space

Studying the impact of different P_a search spaces is very essential as usage of different search spaces might result in substantially different performance in terms of throughput as well as in terms of detection swiftness. From network flexibility point of view, the most beneficial P_a search space would be the full set of possible values, that is, [-6, -4.77, -3, -1.77, 0, 1, 2 ,3] dB. If P_a detection could be performed using the full set, restrictions to network configurations would not be needed. On the other hand, from hardware vendor point of view, full set of P_a values might result in too heavy implementation as well as significant performance degradation due to high estimation errors.

Three different search spaces were used:

- *No predefined search space.* Meaning that the search space does not consist of possible P_a values. However, due to the implementation of P_a detection algorithm as described in Section 5.2, the power level cannot be truly arbitrary and some sort of quantization is needed. Therefore the interval of this search space has been set to 0.2 dB with minimum value of -6 dB and maximum value of 3 dB, thus the search space is [-6 : 0.2 : 3] dB. Consequently usage of this set is very exhaustive and heavy and thus not very practical. However, usage of this set provides useful information about the behavior of the algorithm as well as upper boundary from the complexity point of view.

- *Full set of possible P_a values, that is, set of [-6, -4.77, -3, -1.77, 0, 1, 2, 3] dB*. This set would be optimal from the network flexibility point of view. However, due to closely spaced values, estimation error rate might be high.

- *Reduced set of P_a values, that is, set of [-6, -3, 0, 3] dB.* This set would be the optimal from a UE point of view as it has the lowest complexity as well as the estimation error rate should be sufficient. However, usage of this set will restrict network flexibility as well as it will require signaling, because NAICS UE needs to know which subset is used. Also if an estimation error occurs, the power level offset will be significant. This subset is also recommended by some companies as discussed in Section 5.1.

In simulations, detection bandwidth was *fixed to nine PRB pairs*, which is the largest bandwidth considered in this thesis. The reason for this is that the impact of different number of samples on P_a detection performance is studied in the next subsection and for P_a search space study, we want to be sure that the bandwidth is large enough for accurate detection. In addition, simulations were run with three different modulation of interfering cells, that is, QPSK, 16QAM and 64QAM and the actual P_a value is set to 0 dB, like in all simulations in this thesis. Simulation results are shown in Figures 25, 26 and 27.

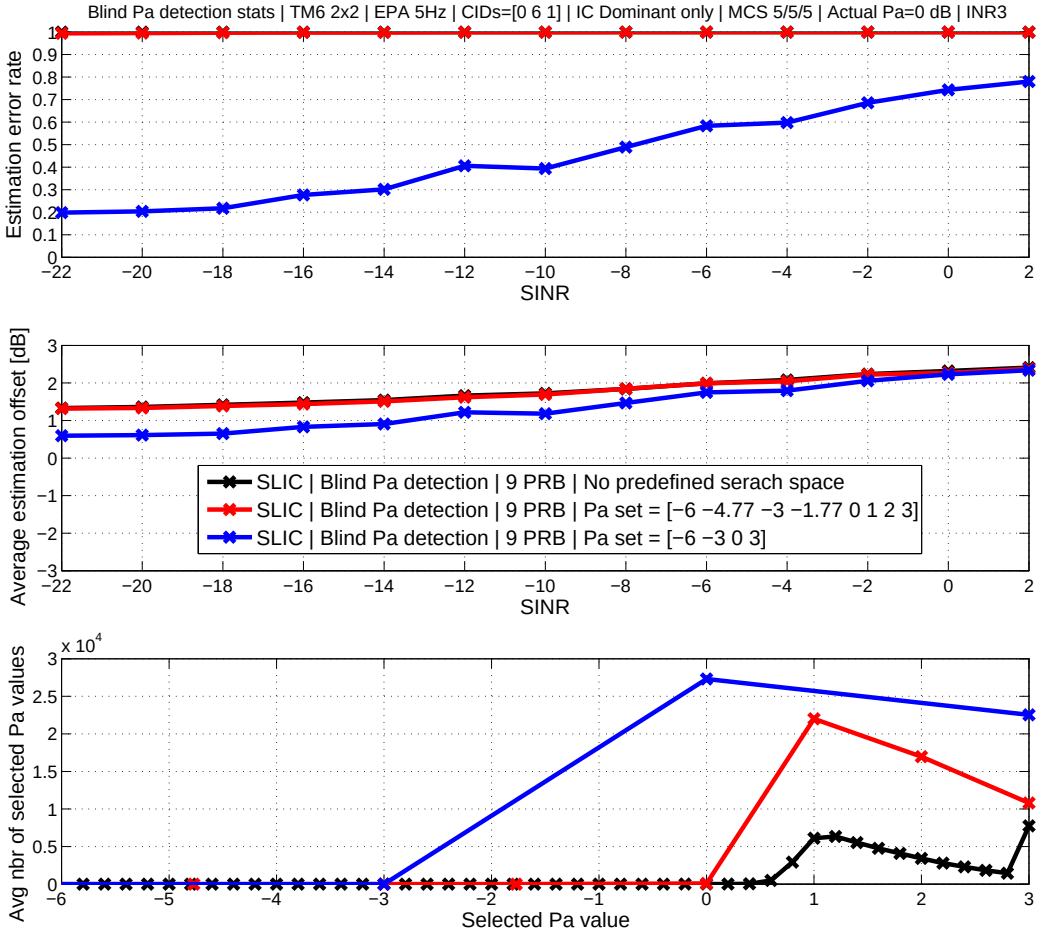

Figure 25: Effect of different P_a search spaces on P_a detection performance in the case of QPSK modulated interferer.

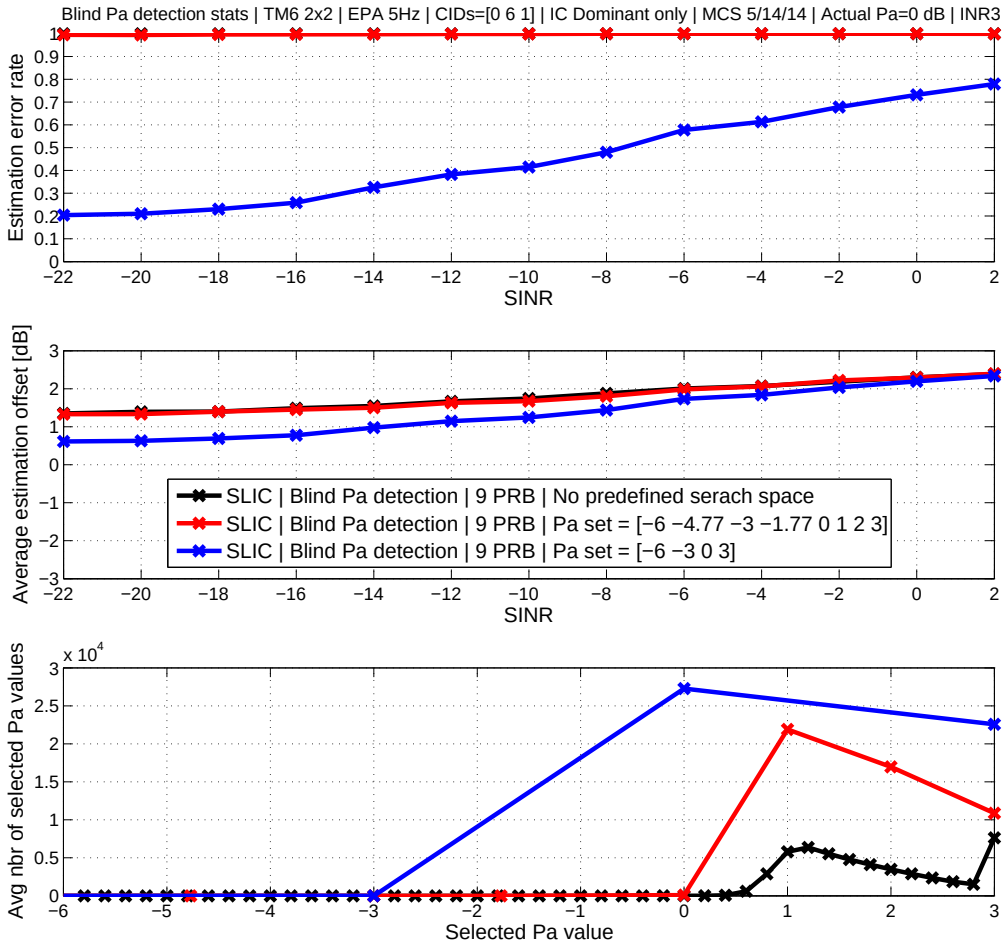

Figure 26: Effect of different P_a search spaces on P_a detection performance in the case of 16QAM modulated interferer.

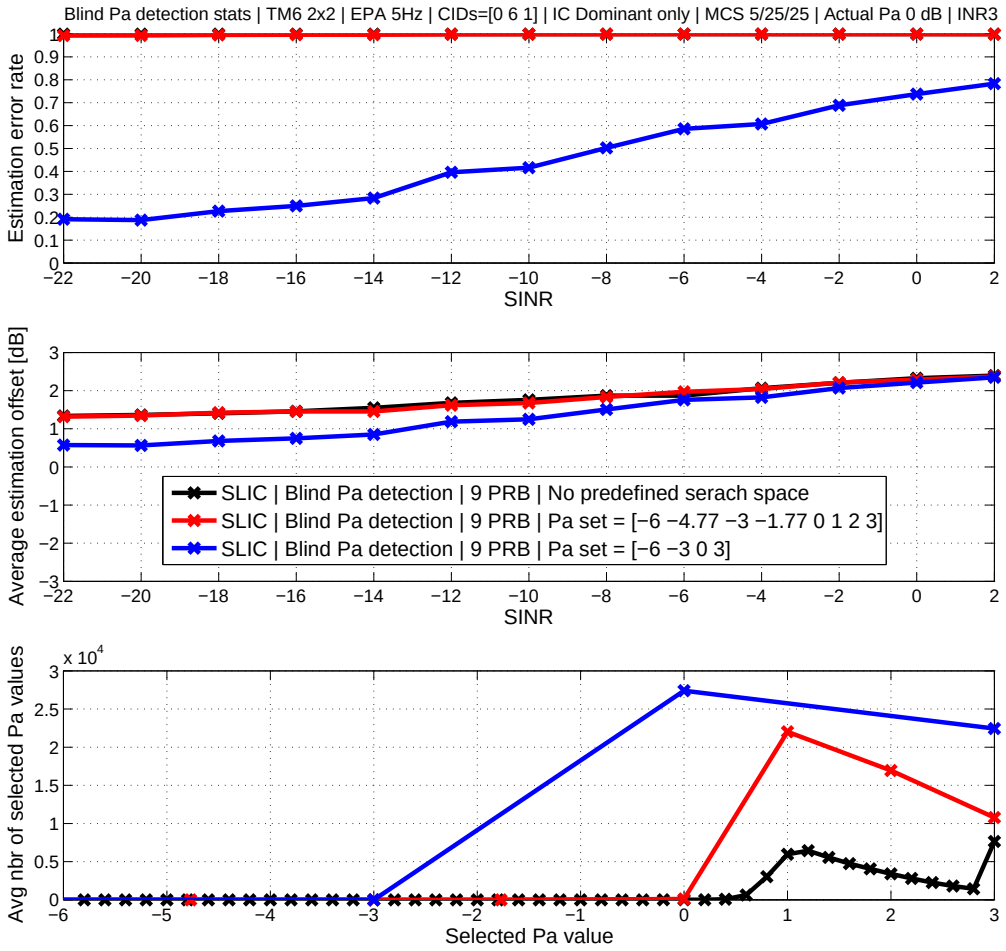

Figure 27: Effect of different P_a search spaces on P_a detection performance in the case of 64QAM modulated interferer.

From Figures 25, 26 and 27 it can be seen that the behavior of P_a detector is fairly similar in all simulated cases, i.e., modulation of interferer does not have an effect on P_a detection performance. The general behavior seems to be that P_a detector tends to overestimate, i.e, power level offset is always positive. With no search space and with full P_a set, the average power offset is almost the same. In addition, with both search spaces, the estimation error rate is one. This means that P_a detector chooses always values which differs from 0 dB and the values vary from 1.3 dB up to 2.3 dB. In the case of reduced P_a set, estimation error rate vary from 0.2 up to 0.8 and the average power offset vary from 0.6 dB up to 2.3 dB. The average power offset increases as the SINR increases. This means that when the signal power of interferers decrease, the average power offset increases. From the parameter *average number of selected P_a values* it can be also observed that with all different search spaces, P_a detector tends to overestimate. In the case of reduced P_a set, value of 3 dB is selected more than with other search spaces. This is due to the fact that reduced P_a set does not have any quantization level between 0 dB and 3 dB and when estimation error occurs, power offset is always significant.

As a conclusion:

- P_a detector tends to overestimate rather than underestimate. This behavior stems

from the fact that network assisted covariance estimator constructs interference plus noise covariance matrix so that power from the weaker interferer is left out, i.e., weaker interferer is not considered. Received covariance matrix calculated directly from the received signal naturally consist of all the signal components, that is, own signal, signal of dominant interferer, signal of weaker interferer and noise. Constructed covariance matrix does not include any power from the weaker interferer and therefore P_a detector compensates this by overestimating. However, based on sensitivity analysis in previous section, overestimation is more tolerable than underestimation.

- With full P_a set and with no P_a set, the performance is the same. Meaning that exhaustive searching of (almost) arbitrary power level is not needed and sufficient power level can be found from the full P_a set.
- Using reduced P_a set results in the lowest estimation error rate but when the error occurs, it is always 3 dB rather than -3 dB.
- Interfering cells' modulation order do not have an impact on the different search spaces.

Based on these observations, the conclusive question is, which is more beneficial in the term of throughput:

- Reduced P_a set which results in the lowest estimation error rate but when an estimation error occurs, the power offset is significant, that is, 3 dB.
- Full P_a set which results in high estimation error rate but the average power offset is smaller.

The answer to this question will be given after examining the throughput results in the next chapter.

Number of samples

Simulations were run to study the effects of different number of samples on $P_a$detection performance. In simulations as well as in practice, the number of samples are denoted by PRB pairs. One PRB pair is the smallest unit that can be assigned for downlink transmission and thus UE can receive downlink transmissions only as a group of PRB pairs. As the parameter P_a is UE specific, the maximum number of PRB pairs, which can be used for blind detection, is the number of PRB pairs assigned for the UE. Therefore, it would be beneficial to use as few PRB pairs as possible for blind detection in order to achieve more flexibility in downlink transmissions. In addition, less samples reduces the complexity as well as improves the swiftness of blind detection.

Four different number of PRB pairs were studied and the values are: 1, 3, 6 and 9 PRB pairs. It is good to highlight that in the case of multiple PRB pairs, the used bandwidth is continuous, i.e., PRB pairs are consecutive. In addition, consecutive PRB pairs are not selected from the edge of the bandwidth and neither from the middle. To calculate exact number of samples, i.e., number of REs used for detection, CRS structure of interferer needs to be known. However, this is not a problem as NAICS UE is receiving and processing also CRS of dominant interferer in order to calculate effective channel estimate

Table 10: Statistics of number of samples for blind P_a detection.

Number of PRB pairs	**PRB pair set (Whole bandwidth is 0:49)**	**Bandwidth in kHz**	**Number of samples (PDSCH REs)**
1	8	180	132
3	6:8	540	396
6	6:11	1080	792
9	6:14	1620	1188

and network assisted covariance estimate for the dominant interferer. Exact number of samples for different number of PRB pairs are calculated in Table 10.

In this study, modulation of interferers is fixed to QPSK because based on the P_a search space study performed in the previous subsection, it was shown that modulation of interferers did not have an impact on the different search spaces. However, all the search space combinations are used. Simulations results are shown in Figures 28, 29 and 30.

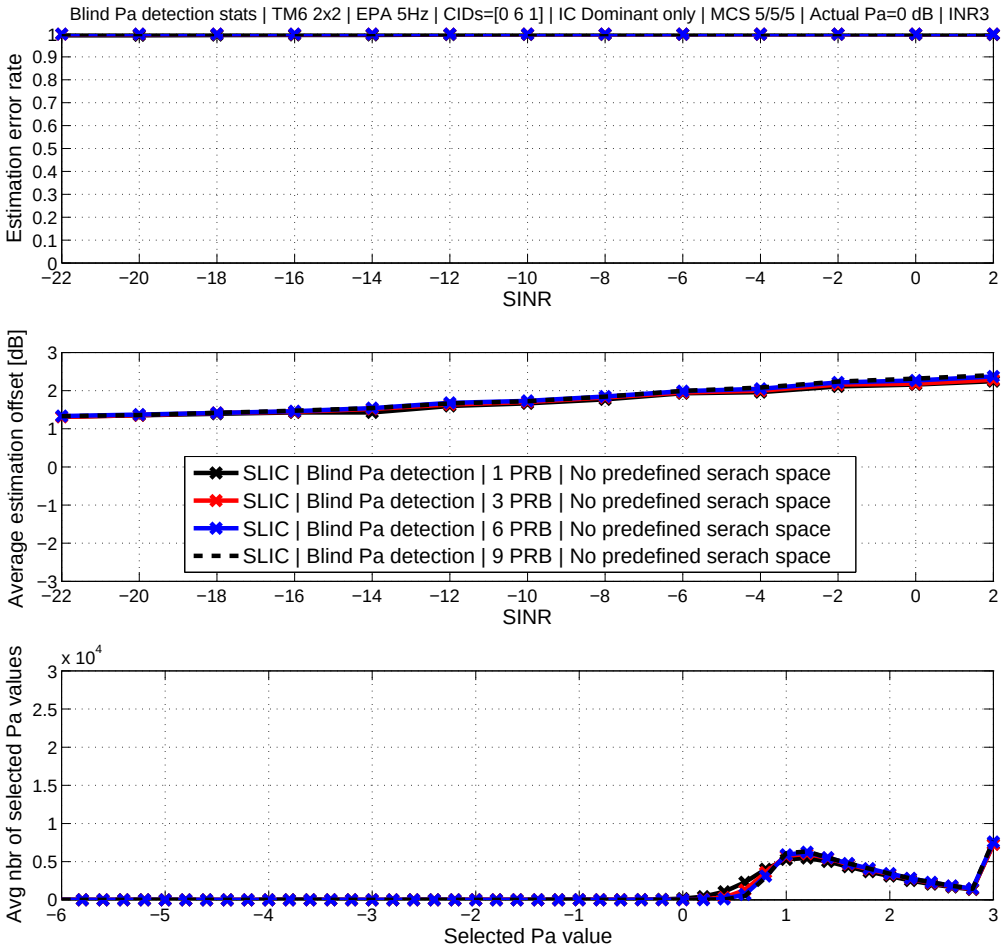

Figure 28: Impact of number of samples on P_a detection performance in the case of no predefined P_a search space.

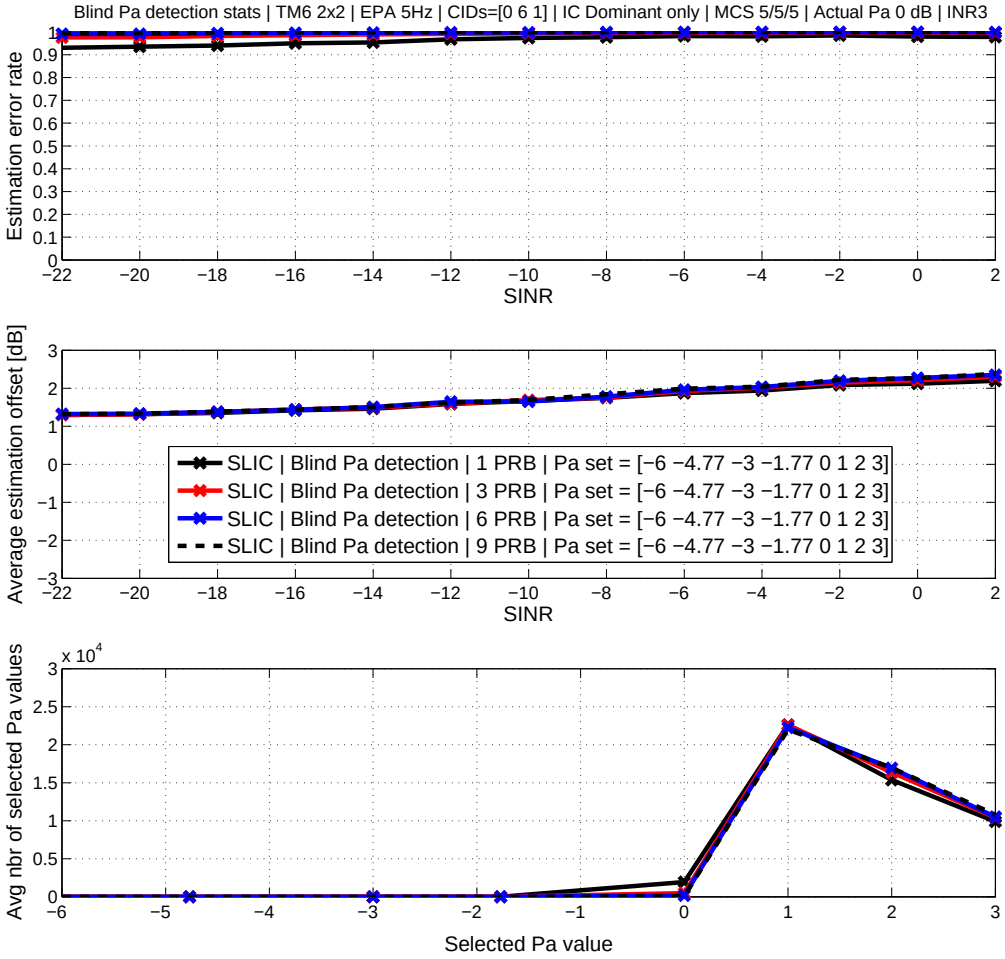

Figure 29: Impact of number of samples on P_a detection performance in the case of full P_a search space.

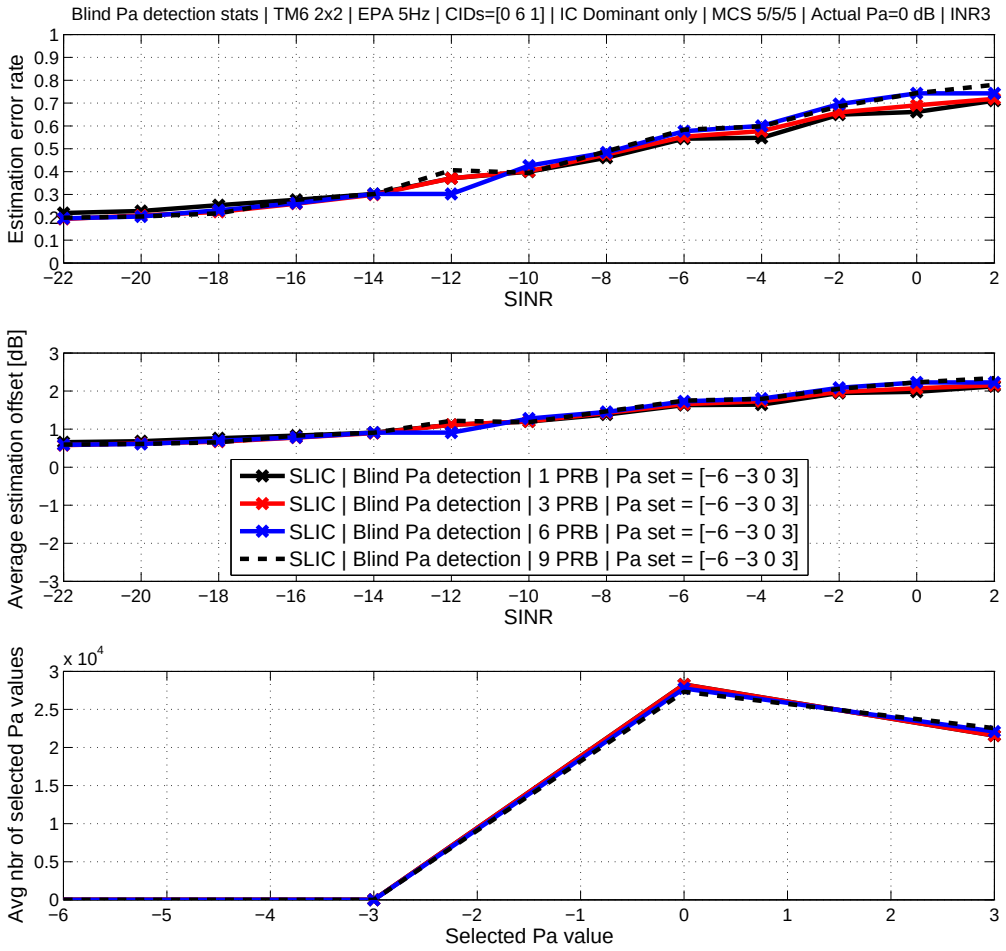

Figure 30: Impact of number of samples on P_a detection performance in the case of reduced P_a search space.

When analyzing the results shown in this section, it is good to bear in mind that the primary information is received from the difference and variation of different curves compared to each other, instead of the absolute values, which can be regarded as secondary information at this point. There are two reasons for this. The first is the fact that it is not possible to predict the exact impact of absolute values on the throughput and the second is that the goal of this study is to specifically study the impact of number of samples on P_a detector performance.

From Figures 28, 29 and 30 it can be seen that the general behavior is similar in all the simulated cases. Based on these results, it can be seen that increasing the number of PRB pairs for blind P_a detection does not have an significant impact on the detection performance. As a conclusion it can be stated that blind P_a detection can be performed using only one PRB pair. Therefore from now on, one PRB pair is used in blind P_a detector.

Modulation of interfering eNBs

In the following, impact of different interfering cell's modulation on P_a detection performance is studied. As shown is the previous subsection, namely subsection 5.4; Number of samples, P_a detection can be performed from one PRB pair and thus only one PRB pair is used for P_a detection in this study. Simulation results are shown in Figures 31, 32 and 33.

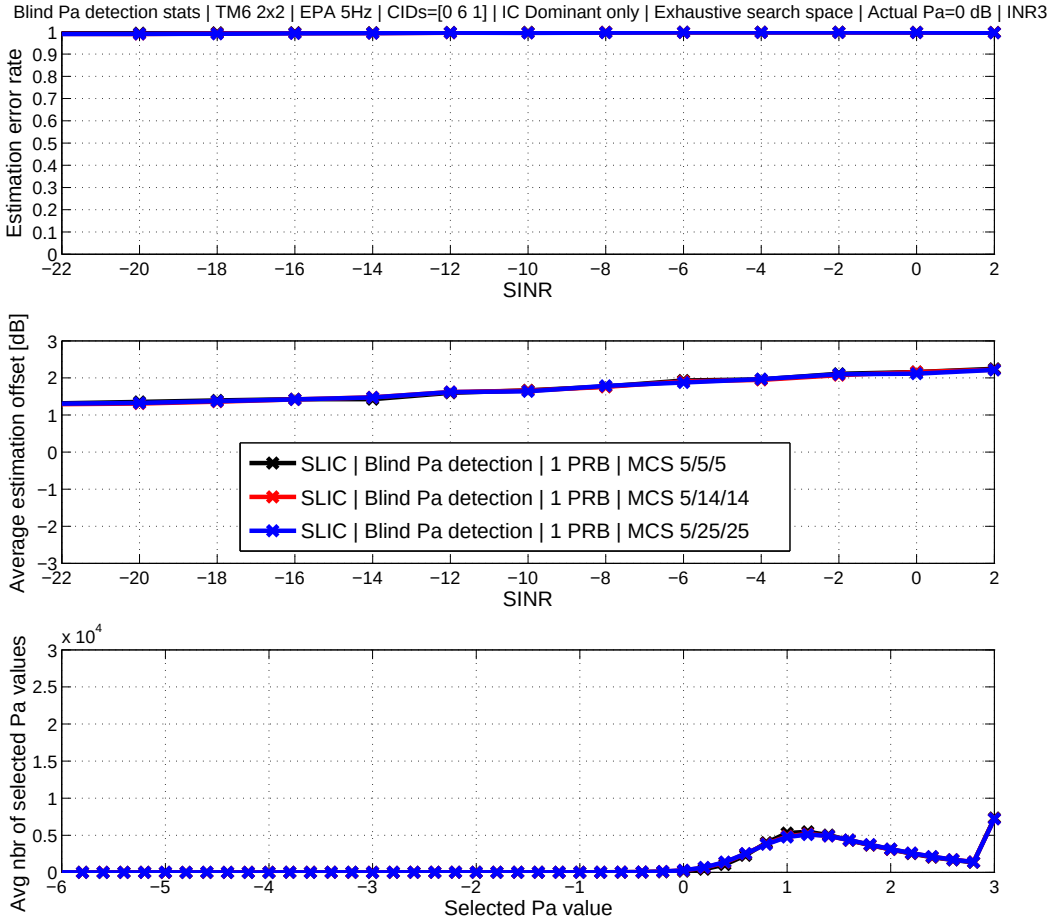

Figure 31: Impact of different interfering cell's modulation on P_a detection without P_a search space.

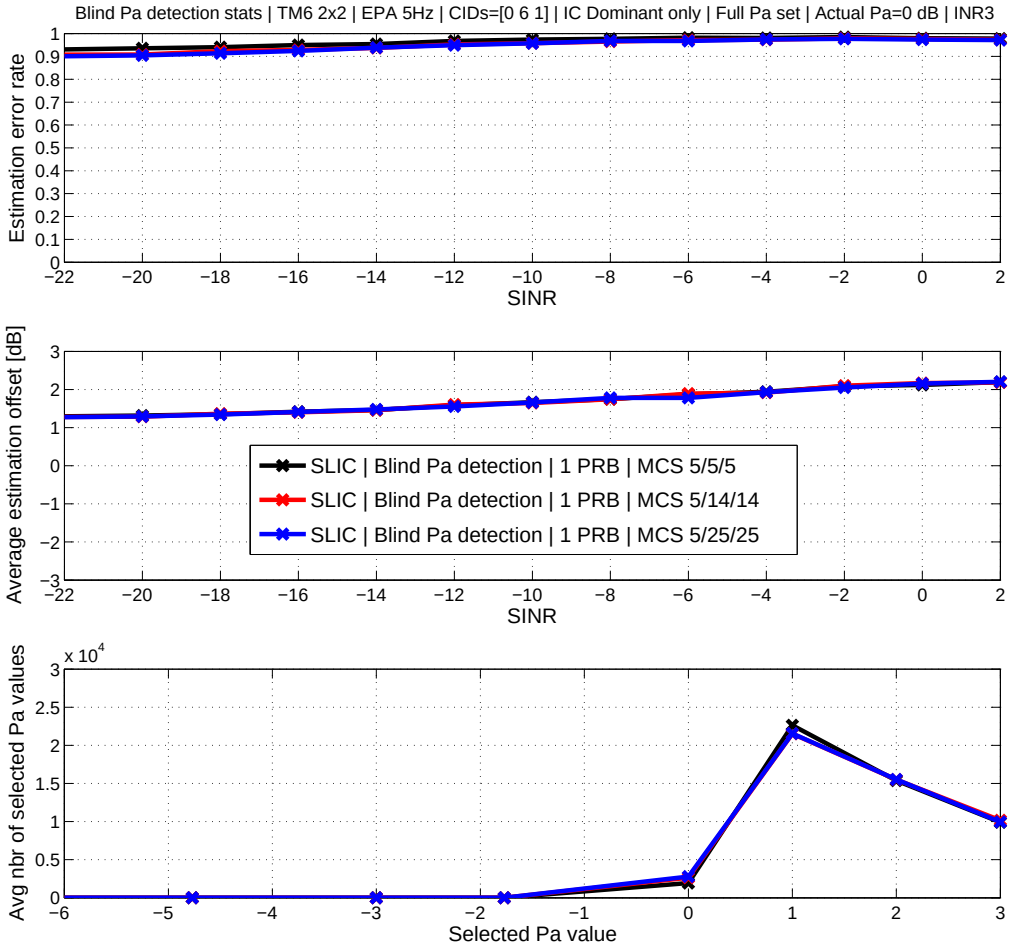

Figure 32: Impact of different interfering cell's modulation on P_a detection when full P_a set is used, that is, [-6, -4.77, -3, -1.77, 0, 1, 2, 3] dB.

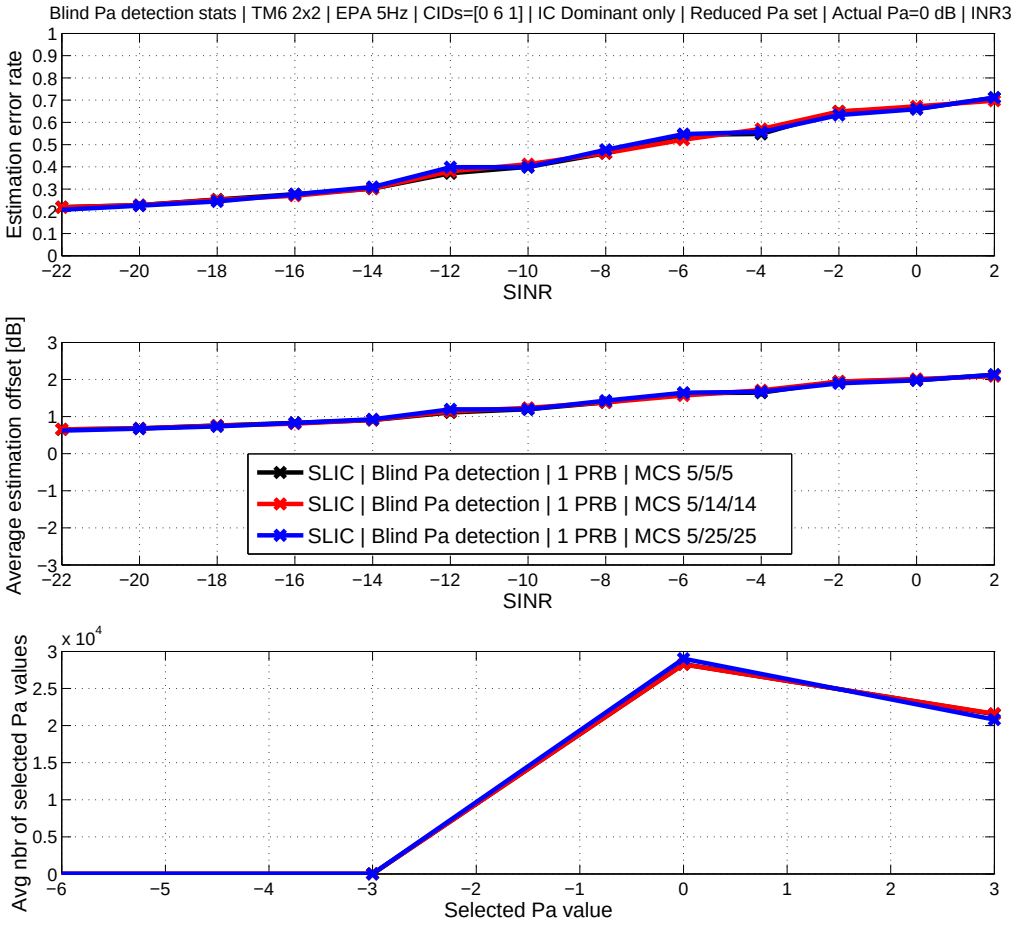

Figure 33: Impact of different interfering cell's modulation on P_a detection when P_a subset of [-6, -3, 0, 3] dB is used.

From Figures 31, 32 and 33 it can be seen that the impact of interfering cells' modulation order on P_a detection performance is negligible. In other words, with all different search spaces, the P_a detection performance remains the same when interfering cells' modulation is either QPSK, 16QAM or 64QAM.

5.5 Detection swiftness

In this section, swiftness of P_a detection is studied on a specific platform to give some insight about the P_a detection algorithm performance with certain settings. Hence the analysis here is just directional due to the fact that the used platform might bias the comparison somewhat. The general simulation setup is fixed and only parameters affecting P_a detector are altered. In addition, random number generator is fixed, that is, all seeds take the same values and consequently channel models, AWGN and so on will be exactly the same in all simulations. With these settings, it is possible to approximate the time taken to detect P_a with different P_a detection parameters like detection bandwidth and search space. Baseline will be the so called genie-aided SLIC receiver where P_a parameter of the interferer is completely known and thus blind detection is not needed. However, it is good to bear in mind that the intention of this study is just to give some insight about the

complexity of P_a detection algorithm and these results won't apply in the real hardware implementation. The results are presented in Table 11 in percentage, that is, the extra time taken compared to the genie-aided SLIC.

Table 11: Swiftness of P_a detection compared to the genie-aided SLIC receiver. Simulation time on a same platform.

Baseline: Genie-Aided SLIC receiver. Compared to IRC: -40 %.	**Search Space**		
Bandwidth	**Exhaustive search space [-6:0.2:3] dB**	**Full P_a search space [-6, -4.77, -3, -1.77, 0, 1, 2, 3] dB**	**Reduced P_a search space [-6, -3, 0, 3] dB**
1 PRB pair	+13.7 %	+2.1 %	+1.5 %
3 PRB pairs	+41.0 %	+6.8 %	+3.0 %
6 PRB pairs	+81.3 %	+14.6 %	+6.0 %
9 PRB pairs	+122.5 %	+21.9 %	+11.1 %

From Table 11 it can be seen that with exhaustive search space the time taken to detect P_a is significantly greater compared to full and reduced P_a search spaces. However, as concluded in Subsection 5.4; P_a search space, exhaustive search space results in the same performance compared to full P_a search space and thus due to its additional complexity, there is no usage for it in practical implementation. The difference between full and reduced P_a search space is not significant and thus it can be said that both cases can be practical and P_a detector does not add too much complexity to the receiver. And as concluded in Subsection 5.4; Number of samples, P_a detection can be performed reliably from one PRB pair and in this case the additional time taken is only from 1.5 % up to 2.1 %. In addition, when comparing the genie-aided SLIC receiver to the IRC receiver, the additional time taken is increased by 40% and in general it can be said that SLIC receiver is much more complex that IRC receiver, which is intuitive.

5.6 Summary and Settings of blind PDSCH to CRS power offset detector for throughput simulations

In this chapter, P_a detector and parameters affecting P_a detection performance were studied in detail. For throughput results, the following conclusions can be drawn:

- SLIC receiver is more sensitive to power level underestimation than overestimation. Significant offsets in power level will degrade the performance of SLIC receiver.
- Using exhaustive search space for estimation results in the same P_a detection performance compared to full P_a search space. Full P_a search space results in high estimation error rate but the average power offset is rather small, whereas reduced P_a search space results in lower estimation error rate but when an error occurs, the power offset is significant.

- P_a detection can be performed from one PRB pair.
- Modulation of interfering cells does not have an impact on P_a detection performance.
- When full or reduced P_a search space is used, P_a detector does not add significant complexity to SLIC receiver from execution speed point of view.

Based on these observations, throughput results are simulated with the following P_a detector settings:

- P_a detection is performed from one PRB pair.
- Only full and reduced P_a search spaces are used.

6 Throughput Results and Analysis

In this chapter, the simulation results are presented and analyzed. The simulation assumptions are described in Section 4.4, and link-simulation principles are described in Section 4.1. The simulation setup used in this thesis is based on the simulation setup used by 3GPP RAN4 Work Group on NAICS. Therefore results presented in this chapter are comparable with results published by RAN4 Work Group on NAICS.

In the previous chapter, we started by explaining the purpose of blind detection and also potential blindly detected parameters in NAICS UE. Next the algorithm of P_a detector was introduced and also its usage in SLIC receiver. Then we studied the sensitivity of SLIC receiver on incorrect P_a values to have some insight how significant performance degradation incorrectly detected P_a could cause. Finally, effects of different parameters on P_a detection performance were studied, that is, optimization of those parameters. Based on these results, settings of blind P_a detector for throughput simulations were selected and presented in Section 5.6. Using the simulation assumptions and settings of blind P_a detector described in Sections 4.4 and 5.6, respectively, comprehensive link simulations were carried out and evaluated to obtain throughput performance. These results are presented in the following.

6.1 Performance of SLIC receiver with PDSCH to CRS power ratio detector

In order to analyze the performance of SLIC receiver with P_a detector, baseline and upper boundary of throughput are needed. In all results, IRC receiver, which is described in Section 3.5, will function as a baseline. IRC is a practical and relatively low-complexity receiver, at least compared to the SLIC receiver, and thus it is also noteworthy solution for UEs as a base receiver. IRC receiver is also used as a baseline by RAN4 Work Group on NAICS. The so called genie-aided SLIC receiver will function as an upper boundary of throughput. In genie-aided SLIC receiver, all parameters, including P_a of interfering cells, are known in advance and thus blind detection is not needed. This can be also seen as a situation where P_a is always detected perfectly.

For throughput results, P_a detection is performed using one PRB pair, that is, from 132 PDSCH REs as shown in Table 10. Two different P_a search spaces are used, namely full P_a set and reduced P_a set. Summary of settings for throughput simulations in addition to the simulation assumptions are collected in Table 12.

There are three different cases to be analyzed, that is, interfering signals are QPSK, 16QAM and 64QAM modulated. In the following, these three cases are presented and analyzed separately. It is good to highlight that the performance of different receivers are compared using 70 % throughput line, which is the dashed red line in presented Figures.

Table 12: Summary of settings for throughput simulations in addition to simulation assumptions presented in Section 4.4.

Fact under observation	**Describtion**
P_a detection bandwidth	1 PRB pair = 132 PDSCH REs = 180 kHz
P_a search space	Full P_a set of [-6, -4.77, -3, -1.77, 0, 1, 2, 3] dB and reduced P_a set of [-6, -3, 0, 3] dB
Actual P_a of all eNBs	0 dB
Modulation of interfering signals	QPSK, 16QAM and 64 QAM
Modulation of desired signal	Always QPSK
Baseline	Interference Rejection Combining (IRC) receiver without CRS-IC
Upper boundary of throughput	Genie-aided SLIC receiver with CRS-IC
Metric to compare performance	70 % throughput line (dashed red line)
SLIC Logic flow	Only dominant interferer is canceled

QPSK modulated interfering signals

In Figure 34, performance of genie-aided SLIC receiver, SLIC receiver with blind P_a detector and IRC receiver are shown in the case of QPSK modulated interfering signals. It can be observed that genie-aided SLIC receiver achieves 5.89 dB gain over IRC receiver. When SLIC receiver is using the blind P_a detector with P_a search space of [-6, -4.77, -3, -1.77, 0, 1, 2, 3] dB, the loss compared to the genie-aided SLIC receiver is 0.18 dB and the gain over IRC receiver is 5.71 dB. When SLIC receiver is using the blind P_a detector with reduced P_a search space of [-6, -3, 0, 3] dB, the loss compared to the genie-aided SLIC receiver is 0.57 dB and the gain over IRC receiver is 5.32. These results are summarized in Table 13.

Table 13: Results in the case of QPSK modulated interfering signals.

Receiver	**Gain over IRC receiver (Loss compared to genie-aided SLIC) [dB]**
Genie-aided SLIC	5.89 (-)
SLIC with full P_a search space	5.71 (0.18)
SLIC with reduced P_a search space	5.32 (0.57)

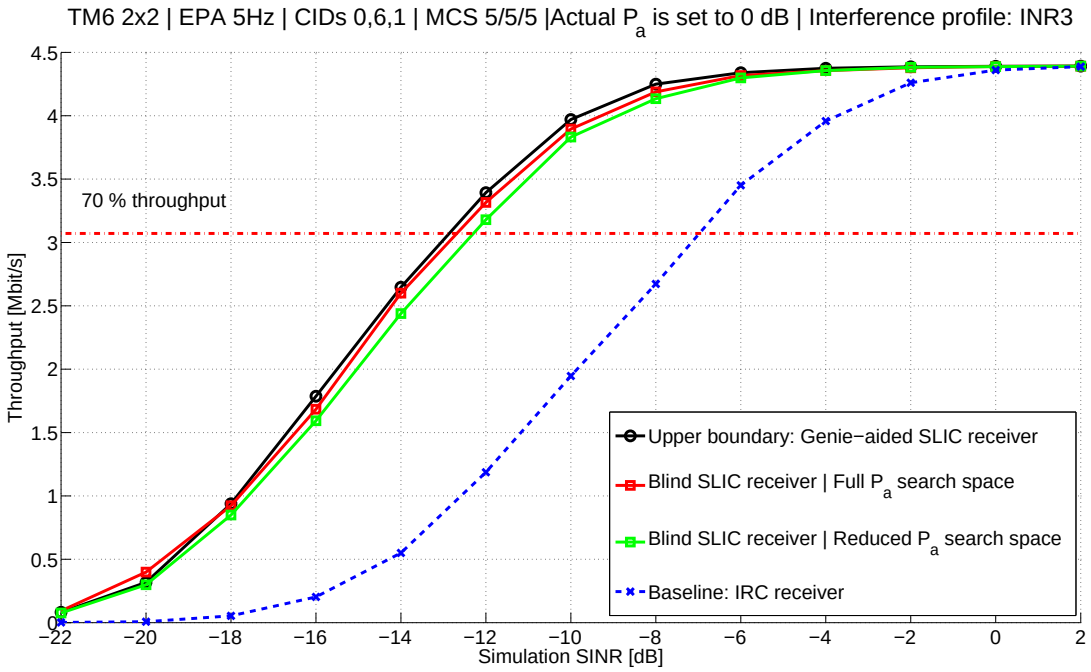

Figure 34: Performance of SLIC receiver with blind P_a detector in the case of QPSK modulated interfering signals. IRC receiver functions as a baseline while genie-aided SLIC receiver functions as an upper boundary. Two different P_a search spaces are used.

16QAM modulated interfering signals

In Figure 35, performance of genie-aided SLIC receiver, SLIC receiver with blind P_a detector and IRC receiver are shown in the case of 16QAM modulated interfering signals.

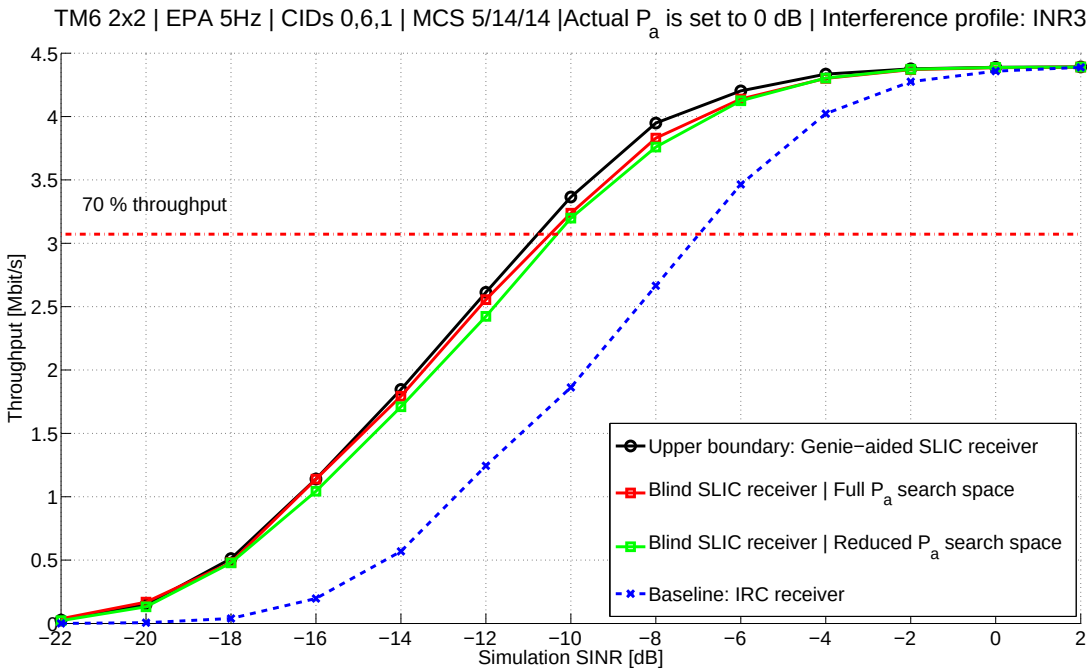

Figure 35: Performance of SLIC receiver with blind P_a detector in the case of 16QAM modulated interfering signals.. IRC receiver functions as a baseline while genie-aided SLIC receiver functions as an upper boundary. Two different P_a search spaces are used.

It can be observed that genie-aided SLIC receiver achieves 3.81 dB gain over IRC receiver. When SLIC receiver is using the blind P_a detector with P_a search space of [-6, -4.77, -3, -1.77, 0, 1, 2, 3] dB, the loss compared to the genie-aided SLIC receiver is 0.30 dB and the gain over IRC receiver is 3.51 dB. When SLIC receiver is using the blind P_a detector with P_a search space of [-6, -3, 0, 3] dB, the loss compared to the genie-aided SLIC receiver is 0.45 dB and the gain over IRC receiver is 3.36 dB. These results are summarized in Table 14.

Table 14: Results in the case of 16QAM modulated interfering signals.

Receiver	**Gain over IRC (Loss compared to genie-aided SLIC) [dB]**
Genie-aided SLIC	3.81 (-)
SLIC with full P_a search space	3.51 (0.30)
SLIC with reduced P_a search space	3.36 (0.45)

64QAM modulated interfering signals

In Figure 36, performance of genie-aided SLIC receiver, SLIC receiver with blind P_a detector and IRC receiver are shown in the case of 64QAM modulated interfering signals.

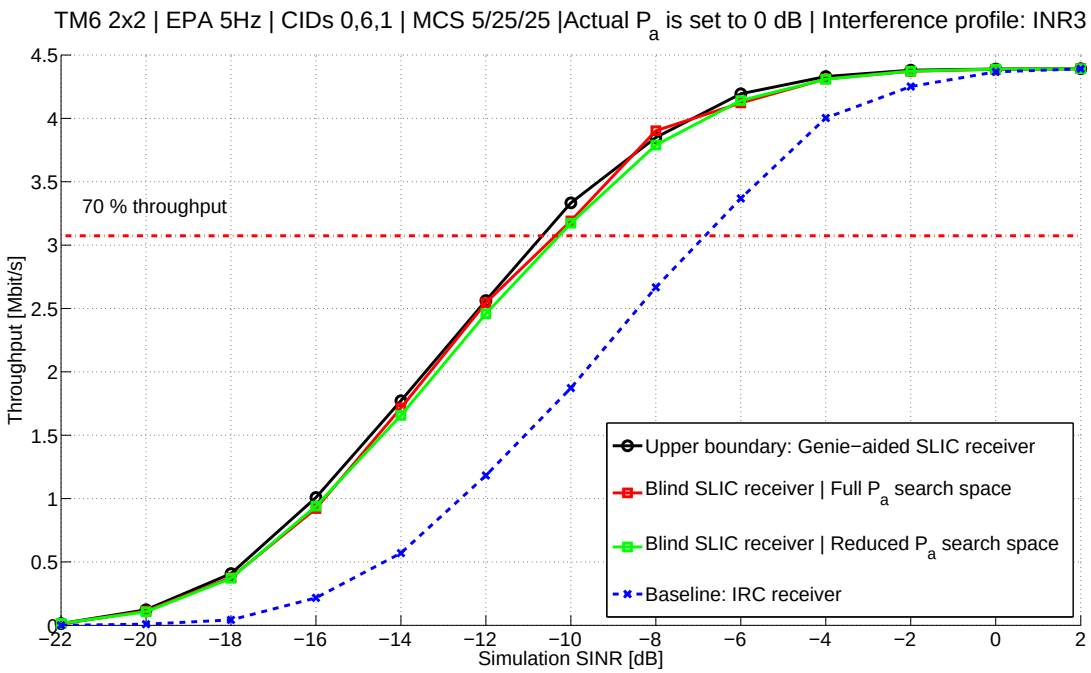

Figure 36: Performance of SLIC receiver with blind P_a detector in the case of 64QAM modulated interfering signals. IRC receiver functions as a baseline while genie-aided SLIC receiver functions as an upper boundary. Two different P_a search spaces are used.

It can be observed that genie-aided SLIC receiver achieves 3.84 dB gain over IRC receiver. When SLIC receiver is using the blind P_a detector with P_a search space of [-6, -4.77, -3, -1.77, 0, 1, 2, 3] dB, the loss compared to the genie-aided SLIC receiver is 0.30 dB and the gain over IRC receicer is 3.54 dB. When SLIC receiver is using the blind P_a detector with P_a search space of [-6, -3, 0, 3] dB, the loss compared to the genie-aided SLIC receiver is 0.40 dB and the gain over IRC receiver is 3.44 dB. These results are summarized in Table 15.

Table 15: Results in the case of 64QAM modulated interfering signals.

Receiver	**Gain over IRC (Loss compared to genie-aided SLIC) [dB]**
Genie-aided SLIC	3.84 (-)
SLIC with full P_a search space	3.54 (0.30)
SLIC with reduced P_a search space	3.44 (0.40)

6.2 Analysis of throughput results

Based on the results shown in Tables 13, 14 and 15, it can be observed that the genie-aided SLIC receiver as well as SLIC receivers with blind P_a detectors perform roughly 2 dB better when interfering signals are QPSK modulated compared to cases when interfering signals are either 16QAM or 64QAM modulated. In addition, when interfering signals are 16QAM and 64QAM modulated, the performance of the SLIC receivers are similar. This kind of behavior is rather intuitive due to the fact that it is easier to apply linear detection and reconstruction to QPSK modulated interfering signal compared to 16QAM and 64QAM modulated interfering signals. However, the main objective was to study the feasibility of blind P_a detection and thus the performance of blind SLIC receiver with two different P_a search spaces is analyzed in more detail in the following.

When taking all the three cases into account, i.e., when interfering signals are either QPSK, 16QAM or 64QAM modulated, SLIC receiver with blind P_a detector degrades the performance from 0.18 dB up to 0.57 dB compared to the genie-aided SLIC receiver. In the case of blind P_a detector with the full P_a search space, there is slightly less degradation in performance compared to blind P_a detector with the reduced P_a search space. As already indicated in Section 5.4; P_a search space, the full P_a search space is better also from the network flexibility point of view. In addition, when comparing the complexity of these two options based on the Table 11, the full P_a search space does not add significant complexity to the SLIC logic compared to the reduced P_a search space. Consequently, it can be said that the blind P_a detector utilizing the full P_a search space is better option.

When the blind SLIC receiver with the full P_a search space is analyzed exclusively, the performance degradation compared to the genie-aided SLIC receiver is from 0.18 dB up to 0.30 dB depending on the modulation of interfering signals. As the gain over IRC receiver with genie-aided SLIC receiver is from 3.81 dB up to 5.89 dB, the loss of utilizing the blind SLIC receiver in percentage is from 3.1 % up to 7.9 %. Hence the degradation

in performance is tolerable, especially when considering that the other option is to use network assistance to signal P_a values to the NAICS UE.

7 Conclusions

As stated in the introduction, the focus and objective of this thesis is to study feasibility of blind P_a detector in NAICS UEs. The ultimate objective is to decide whether it is possible to detect interfering cell data channel power level blindly without signaling, that is, without network assistance. The most important criteria is that adding the blind P_a detector to the SLIC receiver should not result in significant degradation in the link performance. In addition, blind P_a detector should not add too much complexity to the SLIC logic, that is, the receiver processing should be possible to perform without significant delay also when utilizing the blind P_a detector. In the following, important observations from Chapters 5 and 6 are collected as well as further studies on this topic are proposed.

7.1 Observations

In Section 5.3, sensitivity of SLIC receiver on incorrect power level of interfering signals, that is, on incorrectly detected P_a values of interfering cells was studied. It was concluded that incorrect power level of interfering signals will degrade the performance of SLIC receiver significantly in most of the cases. The performance degradation depends on the significance of power offsets and on the modulation used in interfering cells. In addition, SLIC receiver is more sensitive to underestimation than overestimation, that is, positive power offset is more tolerable than negative. Based on the sensitivity study, it can be concluded that well-performing blind P_a detector is definitely needed if this parameter is not part of the network assistance, that is, it is not signaled to the NAICS UE.

In Section 5.4, impact of different parameters on P_a detection performance was studied. These parameters are P_a search space, bandwidth used for the detection and modulation of interfering signals. Using the full P_a search space, that is, P_a values of [-6, -4.77, -3, -1.77, 0, 1, 2, 3] dB, results in high estimation error rate but rather low average power offsets. Whereas using the reduced P_a search space, that is P_a values of [-6, -3, 0, 3] dB, estimation error rate is rather low but when an error occurs, the power offset is significant. Based on the simulations it can be observed that by increasing bandwidth used for the P_a detection from one PRB pair up to nine PRB pairs, the P_a detection performance remains roughly the same. Thus only one PRB pair, which corresponds to around 132 PDSCH REs, is sufficient for P_a detection. Also differently modulated interfering signals did not have an impact on P_a detection performance. In addition, based on Table 11, P_a detector does not add significant complexity to the receiver from execution speed point of view. General observation is that blind P_a detector tends to overestimate rather than underestimate. In other words, P_a detectors tends to choose positive power offset values. This behavior stems from the fact that network assisted covariance estimator constructs interference plus noise covariance matrix so that the contribution of the weaker interferer is left out. Received covariance matrix calculated directly from the received signal naturally consist of all the signal components, that is, the own signal, the signal of dominant interferer, the signal of weaker interferer and noise. Constructed covariance matrix does not include any power from the weaker interferer. As the P_a detector is basically comparing the received covariance matrix to the constructed, or emulated, covariance matrix to find the most suitable P_a estimate, the estimated P_a value tends to be higher than the actual P_a value. Thus it can be said that the P_a detector compensates the absence of the weaker interferer's signal in the constructed covariance matrix by overestimating.

Based on the observations, comprehensive link simulations were carried out and eval-

uated to obtain throughput performance. Throughput results were presented in Section 6. In these simulations, one PRB pair as well as full and reduced P_a search spaces are used in blind P_a detector, interfering signals are either QPSK, 16QAM or 64QAM modulated and IRC receiver operates as the baseline while the performance of genie-aided SLIC receiver forms the upper boundary. Based on the simulation results, genie-aided SLIC receiver performs significantly better compared to IRC receiver. Depending on the modulation of interfering signals, the gain over IRC receiver is from 3.8 dB up to 5.9 dB. The minimum gain is obtained when interfering signals are either 16QAM or 64QAM modulated whereas the maximum gain is obtained when interfering signals are QPSK modulated.

Next, SLIC receiver with blind P_a detector was considered. From the simulation results it can be observed that the performance of the blind SLIC receiver is similar regardless of the differently modulated interfering signals. In addition, the blind P_a detector does not degrade the SLIC performance significantly and using the full P_a search space results in slightly better performance compared to the reduced P_a search space. To be more exact, blind SLIC receiver with the full P_a search space degrades the SLIC performance from 0.18 dB (3.1 %) up to 0.30 dB (7.9 %) depending on the modulation of interfering signals. When considering that the worst case scenario corresponds to 0.30 dB (7.9 %) degradation in the link throughput, it can be said that the blind P_a detector performs relatively well.

The following conclusions can be drawn. It is possible to blindly detect interfering cell data channel power level without significant degradation in the link throughput. Consequently network assistance for interfering cell's P_a parameter is not necessarily needed. In addition, only one PRB pair is sufficient bandwidth for blind P_a detection as well as all the P_a values defined in LTE specification can be used directly for quantization. This implies that using the blind P_a detector maintains the full flexibility of the network. Also blind P_a detector does not add significant complexity to the receiver. All in all, blind P_a detector presented in this thesis is a noteworthy solution for cell edge UEs, which have to utilize advanced non-linear receivers for suppressing, mitigating or canceling strong inter-cell interference.

7.2 Further study

Determining the feasibility of blind P_a detector for different channel models, UE velocities, transmission modes and interference profiles was out of the scope of this thesis. Also the the network assisted covariance estimator could be updated so that interference from all interfering cells are taken into account when constructing, or emulating, the interference plus noise covariance. This should improve the performance of blind detectors that are using the covariance matching method as well as the performance of non-linear advanced receivers.

There are also other potential blindly detected parameters in addition to the P_a, such as precoding matrix and modulation order. Consequently the next step to continue this study could be the simulation of the additional cases, improving network assisted covariance estimator as well as implementing new blind detectors for different parameters, which are required in advanced non-linear receivers.

3GPP has started a study on downlink Multiuser Superposition Transmission (MUST) for LTE [26]. This technique is also also know as Non-Orthogonal Multiple Access (NOMA). It's a single cell technique where two users are multiplexed in the same time-frequency and also spatial resources. Thus this technique differs from regular single-cell

MU-MIMO in the sense that orthogonalization of the different spatially multiplexed signals is not explicitly pursued, through multiantenna processing. In order to separate signals of these two users, they must have sufficiently different operation point, that is, their SINR must be sufficiently different. This is why the two users are referred to as a near user and a far user. Near user has better SINR than far user. Therefore near user is relatively close to the serving eNB while the far user is at cell edge. Fraction of the total transmission power intended to the far user is given to the near user transmission. For example 10% of the total transmission power is allocated to the near user signal while the rest is allocated to the far user signal. Near user must have a non-linear advanced receiver, for example the SLIC receiver described in this thesis, for canceling the strong far user signal. Far user treats the near user signal as an additional white noise and thus it can use, e.g., LMMSE-IRC receiver. For canceling the far user signal, near user must have knowledge of far user transmission parameters, including power level of the far user PDSCH. These parameters can be either signaled to the near UE by its serving eNB or blindly detected similarly to the NAICS scenario. Thus the power level of the far user PDSCH can be blindly detected using the power level detection algorithm presented in this thesis. However, as both users are served by the same eNB and also the far UE signal is very strong compared to the near UE signal, blind detection could be more reliable and accurate. Also constructing the interference plus noise covariance for the detection algorithm can be more accurate and straightforward as the near user and far user use the same CRS for channel estimation in CRS based transmission modes.

References

[1] Tero Kuosmanen, *"Tracking of radio channel state in LTE and LTE-A Downlink"*, Master of Science Thesis, Tampere University of Techology, 8th of Septemper 2010.

[2] Erik Dahlman, Stefan Parkvall, Johan Sköld, *"LTE / LTE-Advanced for Mobile Broadband*", Oxford 2011, Elsevier, Academic Press, 431 p.

[3] 3GPP, Technical Specification 36.213, *"Evolved Universal Terrestrial Radio Access (E-UTRA) ; Physical layer procedures",* www.3gpp.org/specification-numbering, version 11.3.0 Release 11.

[4] 3GPP, Technical Specification 36.331, *"Evolved Universal Terrestrial Radio Access (E-UTRA) ; Radio Resource Control (RRC); Protocol spesification",* www.3gpp.org/specification-numbering, version 11.7.0 Release 11.

[5] Radio propagation in wireless networks, *"Mobile radio channel and fading models*", Tampere University of Technology. Limited availability

[6] James F. Kurose, Keith W. Ross. *"Computer networking, A Top-Down Approach"*, Fifth edition. Boston: Pearson Education 2010.

[7] About 3GPP RAN4, "*RAN4 - Radio performance and protocol aspects*", www.3gpp.org/specifications-groups/ran-plenary/ran4-radio-performance-and-protocol-aspects.

[8] LG Electronics, *"Blind detection under CRS based transmission mode*", RAN4 contribution R4-143207.

[9] MediaTek, "*Blind detection of P_a",* RAN4 contribution R4-143616.

[10] NVIDIA, *"Further results on blind detection of dynamic interference parameters*", RAN4 contribution R4-143206.

[11] Intel Corporation, "*Discussion on PDSCH interference signal parameters detection for NAICS",* RAN4 contribution R4-140609.

[12] MediaTek Inc., *"Text Proposal for TR36.863 for NAICS (Section 8)"* RAN4 contribution R4-134458.

[13] MediaTek, Renesas Mobile Europe, Broadcom Corporation, *"Study on Network Assisted Interference Cancellation and Suppression for LTE",* RP-130404, March 2013.

[14] Andreas F. Molisch, *"Wireless Communications*", Second Edition, United Kindom 2011, John Wiley & Sons Ltd, 827 p.

[15] 3GPP, *"Revised Work Item Description for network assistance interference cancellation and suppression for LTE*", RP-141634, September 2014.

[16] Panayiotis Papadimitriou, Tero Ihalainen, Heikki Berg and Klaus Hugl, *"Link-level Performance of an LTE UE Receiver in Synchronous and Asynchronous Networks, IEEE Wireless Communications and Networking Conference (WCNC)*", April 7-10, 2013, Shanghai, China.

[17] Muhammad Saad Akram, *"Pilot-based Channel Estimation in OFDM Systems*", Master of Science Thesis, 6th of August 2007.

[18] Goldsmith, Andrea, *"Wireless Communications*", Cambridge University Press 2005, p. 86

[19] Beatriz Soret, Yuanye Wang, Klaus I. Pedersen, *"CRS Interference Cancellation in Heterogeneous Networks for LTE-Advanced Downlink*" Aalborg University, Nokia Siemens Networks, Denmark 2012.

[20] Harri Niemeläinen, *"System Level Studies For Single and Multi User Interference Alignment in LTE-Advanced Downlink",* Master of Science Thesis, Tampere University of Techology, November 2013.

[21] A.A. Hutter et al., "Receive Diversity for Mobile OFDM Systems", in Proc. of the IEEE Wireless Communications and Networking Conference (WCNC. 2000), 2000.

[22] A. Ghosh, J. Zhang, J. G. Andrews, and R. Muhamed. Fundamentals of LTE. Prentice Hall, August 2010.

[23] A.B. Gershman & N.D. Sidiropoulos, "Space-time Processing for MIMO Communications", 2005, John Wiley & Sons, ISBN: 978-0-470-01002-0, pages 283-284.

[24] Mikko Mäenpää, "*Power boosting of cell-specific reference signals in 3GPP LTE mobile cellular radio downlink*", Bachelor's Thesis, Tampere University of Technology, December 2013.

[25] 3GPP, Technical Specification 36.211, *"Evolved Universal Terrestrial Radio Access (E-UTRA) ; Physical channels and modulation",* www.3gpp.org/specification-numbering, version 10.0.0 Release 10.

[26] 3GPP, Technical Report 36.859, *"Study on Downlink Multiuser Superposition Transmission (MUST) for LTE",* www.3gpp.org/ftp/specs/archive/36_series/36.859, version 0.2.0 Release 13.

[27] Neal Gompa, *"ITU designates LTE-Advanced as "True 4G"",* ExtremeTech, January 2012.

[28] Eiko Seidel, "*Overview LTE PHY: Part 1 – Principles and numerology etc*", Nomor 3GPP Newsletter, June 2007.